Development of Novel Herbal Compound Combinations Targeting Neuroinflammation: Network Pharmacology, Molecular Docking and Experimental Verification

Yang Liu

WESTERN SYDNEY
UNIVERSITY

A thesis submitted in partial fulfilment of the requirement for the degree of

Master of Research

The National Institute of Complementary Medicine Health Research Institute (NICM)

Western Sydney University, NSW, Australia

February 2023

Dedication

I would like to dedicate this thesis to my parents, Mr Wenzhong Liu and Mrs Gaifeng Song, and my elder sister Ms Jing Liu, for all of their encouragement along my research journey.

I also dedicate this dissertation to my principal supervisor Dr Xian (Phoebe) Zhou, for her guidance and patience during my Master stage.

Also, I sincerely appreciate my partner, Mr Haitao Zheng, for his emotional support and encouragement.

Acknowledgements

I would like to express my deepest gratitude to my principal supervisor, Dr Xian (Phoebe) Zhou. For all her support, patience and encouragement throughout the MRes years. Without her guidance and help, this thesis would not have been possible.

I also would like to express my grateful to my co-supervisors, Professor Dennis Chang and Dr Michelle (Tianqing) Liu, for their continued advice and guidance during the course of my degree.

I would also like to thank all administrative staff and researchers at NICM, especially Mr Dinakaran Vadassery, Dr Mitchell low, Dr Deep Bhuyan, Mr John Bulaong, Ms Deborah Blackmore, Ms Gemma Deakin, Ms Jule Forti, Ms Shitu Mathew, Ms Simi Singh, Ms Seungyeon Yeon, Ms Katerina Chritofides, Ms Kayla Jaye, Mr Ali Butt, Ms Jolle Metri, Ms Indeewarie Dissanayake and Ms Radwa Eladwy, for their assistances. And I want to express my deepest thanks to all my family members, for their support and encouragement throughout my life.

Declaration

Unless where due acknowledgement has been given, the work contained in this thesis is the result of original investigations by the author carried out in the NICM Health Research Institute, Western Sydney University, New South Wales, Australia, under the primary supervision of Dr Xian (Phoebe) Zhou, co-supervision of Professor Dennis Chang and Dr Michelle (Tianqing) Liu. I hereby declare that this thesis has not been previously submitted to any university or institution for a higher degree.

_____

Yang Liu

February, 2023

Table of Contents

List of Tables

List of Figures

List of Peer-reviewed Publications During MRes Candidature

1. **Liu, Y.,** Chang, D., Liu, T., & Zhou, X. (2023). Natural product-based bioactive agents in combination attenuate neuroinflammation in a tri-culture model. Frontiers in Pharmacology Neuropharmacology (**Q1**), 14. Doi: 10.3389/fphar.2023.1135934

2. Yousaf, M.; Chang, D.; **Liu, Y.;** Liu, T.; Zhou, X. (2022). Neuroprotection of Cannabidiol, Its Synthetic Derivatives and Combination Preparations against Microglia-Mediated Neuroinflammation in Neurological Disorders. Molecules (**Q1**), 27, 4961. Doi: 10.3390/molecules27154961

3. Wang, C., Sun, Y., Liu, W., **Liu, Y.,** Afzal, S., Grover, J., *et al.* (2022). Protective effect of the curcumin-baicalein combination against macrovascular changes in diabetic angiopathy. Frontiers in Endocrinology (**Q1**), 13. Doi: 10.3389/fendo.2022.953305.

4. Hossain, S., Yousaf, M., **Liu, Y.,** Chang, D. and Zhou, X. (2022). An Overview of the Evidence and Mechanism of Drug–Herb Interactions Between Propolis and Pharmaceutical Drugs. Frontiers in Pharmacology (**Q1**), 13. Doi: 10.3389/fphar.2022.876183

5. **Liu, Y.,** Chang, D. and Zhou, X. (2022). Development of a Novel Herbal Compound-Formula Targeting Neuroinflammation: Network Pharmacology, Molecular Docking and Experimental Verification. Evidence-Based Complementary and Alternative Medicine (**Q2**), Under review.

List of Conference Presentations During MRes Candidature

1. **Liu Y,** Chang D, Münch G, Zhou X. Illustrating synergistic effect of herbal compound-formula in targeting neuroinflammation. ISN-APSN 2022 Meeting, August 28 – September 1, 2022, Honolulu, USA (Poster)

2. **Liu Y,** Chang D, Zhou X. Development of Synergistic Herbal Compound-Formula Targeting Neuroinflammation. Australasian Neuroscience Society 40th Annual Scientific Meeting, 5-7 December, 2022, Melbourne, Australia. (Poster)

3. **Liu Y,** Chang D, Zhou X. Development of Novel Herbal Compound Combinations Targeting Neuroinflammation: Network Pharmacology, Molecular Docking and Experimental Verification. Neuroimmunology Australia 9th Workshop, 17 February, 2023, Sydney, Australia. (Oral)

List of Abbreviations

6-SG: 6-shogaol

AN: Andrographolide

AD: Alzheimer's disease

APP/PS1:   Amyloid precursor protein / presenilin 1

AKT: Protein kinase B

ANOVA: Analysis of variance

BA: Baicalein

BBB: Blood-brain barrier

BP: Biological pathways

CI: Combination index

CU: Curcumin

COX-2:   Cyclooxygenase-2

CC: Cellular content

DMEM: Dulbecco's Modified Eagle Medium

DMSO: Dimethyl sulfoxide

DAVID: Database for Annotation, Visualization and Integrated Discovery

DL: Drug-likeness

ERK: Extracellular signal regulated kinase

ELISA: Enzyme-linked immunosorbent assay

FBS: Fetal bovine serum

Fa: Fraction affected

GLY: Glycyrrhizin

GO:	Gene Ontology
HES:	Hesperidin
iNOS:	Inducible nitric oxide synthase
IL:	Interleukin
IκBα:	Inhibitor κB
JNK:	Jun N-terminus kinase
KEGG:	Kyoto Encyclopedia of Genes and Genomes
LPS:	Lipopolysaccharide
LU:	Luteolin
MAPK:	Mitogen-activated protein kinase
MPTP:	N-methyl-4-phenyl-1,2,3,6-tetrahydropyridine
MF:	Molecular function
MTT:	3-(4,5-Dimethylthiazol-2-yl)-2,5-Diphenyltetrazolium Bromide
NO:	Nitric oxide
NVU:	Neurovascular unit
NLRP3:	Nucleotide-binding oligomerization domain-like receptor protein three
N2A:	Mouse neuroblastoma Nuro2A cell lines
NF-κB:	Nuclear factor kappa light chain-enhancer of activated B cells
N11:	Mouse microglia N-11
NOS:	Nitric oxide synthase
OB:	Oral bioavailability
OMIM:	Online Mendelian Inheritance in Man
P-tau:	Phosphorylated tau

PD: Parkinson's disease

PDB: Protein Data Bank

PBS: Phosphate-buffered saline

SD: Sprague-Dawley

STRING: Search Tool for the Retrieval of Interacting Genes/Proteins

SEM: Standard error of the mean

TEER: Transepithelial/endothelial electrical resistance

TE: Tetrandrine

TCM: Traditional Chinese Medicine

TNF-α: Tumor necrosis factor-alpha

TLR4:   Toll-like receptor 4

TCMSP: Traditional Chinese Medicine Systems Pharmacology Database and Analysis

Platform

ZO-1:   Zonula occludens-1

Abstract

Neuroinflammation plays an important role in the onset and progression of neurodegenerative diseases. The hyperactivation of microglia triggers the release of excessive proinflammatory mediators that lead to the leaky blood-brain barrier and impaired neuronal survival. The multi-component and multi-target approach of natural products may provide a practical strategy to address the complex pathological mechanisms of neuroinflammation. This study aimed to develop a novel herbal compound combination to attenuate neuroinflammation with a synergistic approach *in vitro* (Chapter 1).

Eight phytochemicals derived from natural products with anti-neuroinflammatory potential were selected in the present study, including luteolin (LU), baicalein (BA), andrographolide (AN), 6-shogaol (6-SG), curcumin (CU), hesperidin (HE), tetrandrine (TE) and glycyrrhizin (GLY). In Chapter 2, network pharmacology analysis was first conducted to predict the key gene and protein targets of the eight phytochemicals. The analyses also help to illustrate the possible interactions of the phytochemicals and the associated hub genes and protein targets. A compound-gene target-signaling pathway network was constructed to predict the mechanisms of action of each phytochemical and their interactions at the molecular level. Molecular docking was performed to verify the binding affinity of each phytochemical to its key protein targets. An experimental study was followed to identify synergistic/antagonistic interactions among the eight phytochemicals using lipopolysaccharides (LPS) induced-microglia N11 cells model. The combination index (CI) model, which is commonly used to identify and quantify the synergistic/antagonistic interaction among agents in a mixture, was applied to determine the plausible synergistic interaction among tested phytochemicals. The associated molecular mechanisms were examined by immunoblotting based on the findings from the network pharmacology study. A tri-culture model with microglial N11 cells, microvascular endothelial MVEC cells, and neuroblastoma N2A cells was established in a 24-well transwell system. The tri-culture model was stimulated by LPS to induce neuroinflammation, and the synergistic phytochemical combinations were subjected to the tri-culture model for their anti-neuroinflammatory and neuroprotective activity. Immunofluorescence staining was applied to investigate

the nuclear translocation of nuclear factor kappa B p65 (NF-κB p65) on N11 cells, expressions of protein zonula occludens-1 (ZO-1) on MVEC cells and phosphorylated tau (p-tau) on N2A cells, respectively. The endothelial barrier permeability of MVEC cells was assessed by the Evans blue dye, and the resistance from the endothelial barrier was measured by transepithelial/endothelial electrical resistance (TEER) value. Neuronal survival of N2A cells was determined by Alamar blue and 3-(4,5-Dimethylthiazol-2-yl)-2,5-Diphenyltetrazolium Bromide (MTT) assays.

Network pharmacology analysis in Chapter 3 suggested that MAPK14, MAPK8, NOS3, EGFR and SRC were the top five hub genes for the eight phytochemicals against neuroinflammation, and molecular docking confirmed strong binding affinities of each phytochemical to their coded protein MAPK and NOS3. This illustration lays the foundation for the synergy mechanism studies described in Chapters 4 and 5.

The results in Chapter 4 demonstrated the synergistic anti-neuroinflammatory activities of two pair-wised combinations on LPS-induced N11 cells. Among all the individual phytochemicals, andrographolide (AN), baicalein (BA), 6-shogaol (6-SG) were found to be effective in inhibiting LPS-induced nitric oxide (NO), tumour necrosis factor-α (TNF-α) and interleukin-6 (IL-6) productions in N11 cells. Among all the paired combinations, only AN-SG and BA-SG resulted in more potent and synergistic interaction (CI<1 representing synergy) in inhibiting NO, TNF-α and IL-6. Based on the results from Chapter 3, MAPK14 and NOS3 were the key hub molecular targets that maybe responsible for the observed synergistic anti-neuroinflammatory activities of AN-SG and BA-SG. Immunoblotting analysis suggested that the AN-SG combination exhibited greater inhibitions of the protein expressions of inducible nitric oxide synthase (iNOS) ($p<0.05$ *vs*. individual component). However, no significant difference was observed for iNOS expression in BA-SG compared with the individual component, as well as the phosphorylated MAPKp38/MAPK p38 expression compared between the combination and the individual components.

Results in Chapter 5 further tested the anti-neuroinflammatory and neuroprotective effects of AN-SG and BA-SG on an established neuroinflammatory tri-culture model. AN, BA and 6-SG used alone (25 µM) or

in pair-wised combinations (12.5 µM +12.5 µM) were subjected to the tri-culture system. AN-SG and BA-SG continued to show advanced inhibitory effects in general on NO, TNF-α and IL-6 compared with their individual components. The molecular mechanism of attenuated neuroinflammation was likely to be mediated by downregulated NF-κB p65 translocation ($p<0.0001$ *vs.* LPS stimulation) on N11 cells. In the MVEC cells, both AN-SG and BA-SG significantly restored TEER values, ZO-1 expression and reduced permeability. Furthermore, AN-SG and BA-SG significantly improved neuronal survival and reduced expressions of p-tau on N2A cells. Remarkably, the protective effects on the endothelial tight junction and neuronal survival by AN-SG and BA-SG were superior to their individual components.

Taken together, two novel herbal compound combinations were identified *in vitro* that were effective in reducing microglia-mediated neuroinflammation, as evidenced by synergistically reduced proinflammatory mediators including NO, TNF-α and IL-6. Subsequently, the combinations protected endothelial tight junction and neuronal survival in a tri-culture system. The synergistic mechanisms were associated with further reduced iNOS expression and downregulated NF-κB p65 translocation, which were in line with findings in the network pharmacology analysis. Our study has provided an integrative approach to explore synergistic combinations of phytochemicals by network pharmacology, molecular docking and experimental validation. Furthermore, we have identified two synergistic combinations as potential therapeutic agents in targeting neuroinflammation and neurodegenerative diseases with a multi-component and multi-target approach. The study also further validated the application of the tri-culture model as a practical neuroinflammatory drug screening tool prior to animal studies.

Chapter 1: Introduction

1.1 Neuroinflammation and neurodegenerative diseases

1.1.1 Background

Neurodegenerative diseases, including Alzheimer's disease (AD) and Parkinson's disease (PD), are disorders characterised by the progressive loss of neurons associated with the deposition of proteins showing altered physicochemical properties in the brain and peripheral organs (Kovacs, 2018). It is a group of major diseases in older adults, which have significantly affected families, communities, and healthcare systems around the world. According to the World Health Organization, there are more than 55 million people suffering from dementia worldwide (World, 2022). In Australia, there is a strong concern about the growing population of dementia, which is expected to have one new case diagnosed every 6 minutes by 2050 (Elizabeth, 2017).

Neuroinflammation refers to the activation of the brain's innate immune system and abnormal secretion of proinflammatory cytokines in response to an inflammatory challenge (DiSabato, 2016). Emerging evidence has shown that neuroinflammation is associated with the onset and development of many neurodegenerative diseases, such as AD, PD, and amyotrophic lateral sclerosis (Kwon & Koh, 2020).

1.1.2 Pathological role of microglia-mediated neuroinflammation in neurodegenerative diseases

Neuroinflammation involves multiple mediators released from microglia and astrocyte cells and their interactions within the neurovascular unit (NVU) (De la Fuente, 2008; Fernández, et al., 2008; Maccioni, et al., 2009; Maccioni, et al., 2018). The neurovascular unit comprises neurons, neural supporting cells like microglia, and vascular cells such as cerebral endothelial cells (Adriani, et al., 2017). Microglia are the resident immune cells in the central nervous system (CNS) that play a crucial role in normal brain function and neuroinflammation-mediated neuronal pathology (Block and Hong, 2005). Under pathological conditions, the activated microglia secrete excessive neuroinflammatory mediators such as NO, TNF-α, reactive oxygen species and IL-6 in CNS (Ha et al., 2012; Milatovic, et al., 2017). It has been implicated

as a pathological contributor to several neurodegenerative diseases (Schain & Kreisl, 2017). The released cytokines can directly impair the blood-brain barrier (BBB) and result in higher permeability of toxins that worsen neuroinflammation and the NVU environment (Q. Li & Barres, 2018). In addition, neuroinflammation mediated by activated microglia has shown a strong link in neurodegeneration by inducing phosphorylation of tau, tauopathies and neuronal injury (Guzman-Martinez et al., 2019). Thus, neuroinflammation has been considered an important therapeutic target for preventing and treating neurodegenerative diseases (Schain & Kreisl, 2017).

As the first defence, the breakdown of the BBB allows further immune cell recruitment, which then attacks the myelin around nerves and results in nerve damage leading to escalated neuroinflammation (Kempuraj et al., 2016). In addition, emerging evidence has shown that the crosstalk among various groups of glial cells, and between microglia and neuron within the NVU are important in the pathogenesis of neuroimmunomodulation in CNS (De la Fuente, 2008; Fernández, et al., 2008; R. B. Maccioni et al., 2018; R. B. Maccioni, et al., 2009). In an observational clinical study, Zotova *et al.* (2013) suggested that phospho-tau correlated directly with all microglial markers. In addition, IgG, C1q and the number of T cells and amyloid-β immunotherapy resulted in the downregulation of microglial activation and may potentially decrease the inflammation-mediated component in patients with AD (Zotova et al., 2013). Although the understanding of how microglia-neuron cellular interaction occurs in CNS neuroinflammation remains limited, a recent study has shown that microglia-mediated neuroinflammation is linked with neuronal injury and phosphorylation of tau and tauopathies (Guzman-Martinez et al., 2019). The physiological function of the tau protein can be altered by the chronic stimulation of glial cells, which leads to the activation of enzymes that phosphorylate tau, then reduced neuronal capacity (Wyss-Coray & Mucke, 2002). All these interactions and the positive feedback loop between the tau pathology and the activation of glial cells cause continuous neuroinflammatory cycles eventually leading to neurodegeneration (Morales, et al., 2014).

Robust *in vitro* and *in vivo* models that can measure the multifaceted interactions are key to the understanding of the complex pathophysiology of neuroinflammation and to the development of therapeutic

interventions. Research has been devoted to establishing co- and tri-culture models as practical *in vitro* tools for screening brain-targeted drug candidates before animal testing. For example, Park *et al.* (2018) study, a neuron, astrocyte and microglia tri-culture system that can induce microglial recruitment, release pro-inflammatory cytokines and chemokines, and cause the death of neurons and astrocytes (Park et al., 2018). Our previous study has established a tri-culture model incorporating microglial, endothelial and neuronal cells to stimulate the NVU environment under neuroinflammation. It was observed that the activated microglia directly provoked the damage of the endothelial tight junction and triggered neuronal loss (Zheng, et al., 2021).

1.1.3 Conventional therapies

The current treatment of neurodegenerative diseases largely focuses on symptomatic relief. Cholinesterase enzyme inhibitors such as galantamine, donepezil, rivastigmine, and N-methyl d-aspartate antagonists (i.e. memantine) have been shown to improve memory, thinking, judgment and other thought processes. However, none of these treatments could prevent or stop the progression of those diseases (Van Bulck, et al., 2019). Furthermore, most conventional medicines exhibit mono-compound and mono-target behaviour, which makes their effects limited when combatting complex pathological mechanisms (Liu et al., 2017). The challenge is the complex pathological progress involved in neurodegenerative diseases. The etiologic and underlying pathophysiology of neurodegenerative diseases is variable and includes different factors (Leroi, et al., 2006). Numerous recent studies have demonstrated that neuroinflammation is an emerging and important therapeutic target for neurodegenerative diseases (Craft et al., 2005; Gordon & Woodruff, 2017; Guzman-Martinez et al., 2019; Liu, et al., 2022). Thus, it is worth to identify effective anti-neuroinflammatory agents which may help to prevent the onset of the disease and slow down the progression.

1.2 Natural products

1.2.1 Phytochemicals derived from natural products

Natural products have been extensively explored regarding their biological activities and potential therapeutic benefits for neurodegenerative disorders (Mohd Sairazi & Sirajudeen, 2020). Increasing evidence has shown that natural products in combination can achieve synergistic and multi-target behaviours (Liebner et al., 2018). For instance, quercetin and sesamin mixture exhibited a higher potential to block pro-inflammatory cytokines (IL-6, IL-1, and TNF-α) to safeguard neuronal survival than those used alone on the microglial-neuronal co-culture system (Bournival, 2012). Yang *et al.* (2021) study demonstrated that Chinese herb pair, Fuzi (*Aconitum carmichaelii* Debx.) and Ganjiang (*Zingiber officinale* Rosc.) exhibited a multi-target behaviour against neuroinflammation as evidenced by reduced productions of IL-6, TNF-α, reactive oxygen species, NO, and prostaglandins E2 in microglia BV2 cells which were likely to be attributed to the interactions of their bioactive components (Yang et al., 2021).

1.2.2 Anti-neuroinflammatory potential of selected phytochemicals
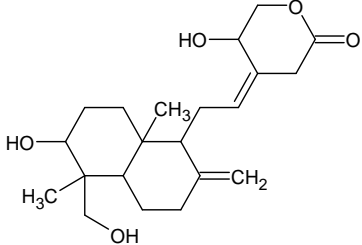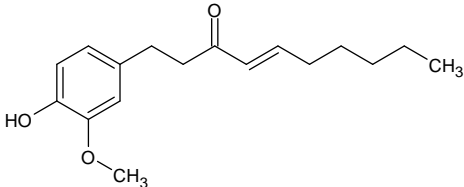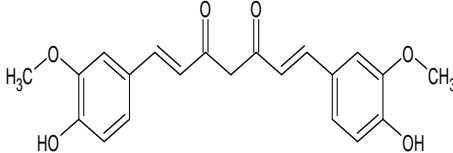
Literature review was conducted to search and identify phytochemicals with promising anti-neuroinflammatory activities. Eight phytochemicals were selected from a thorough review in literature as shown below. Luteolin (LU), a flavonoid found in vegetables, medicinal plants and fruits, possesses anti-inflammatory, antioxidant, neuroprotective, neurotrophic and neurogenesis activities (Zhu L.-H, et al., 2011). LU alleviates neuroinflammation *via* downregulating the toll-like receptor 4 (TLR4)/TRAF6/NF-κB pathway after intracerebral haemorrhage in rats (Yang Y, et al., 2020). Baicalein (BA) is a main bioactive ingredient from the root of *Scutellaria baicalensis* Georgi. This phytochemical has been shown to possess various biological characteristics, including anti-bacterial, anti-hypertensive, and anti-neuroinflammatory effects (Yang, et al., 2019; Zhang, et al., 2017; Hashimoto et al., 2017). BA can lower the levels of a broad range of pro-inflammatory cytokines, such as IL-1, TNF-α, and IL-6, which were associated with inhibited the NF-κB signaling pathway (Zhang, et al., 2017). Andrographolide (AN) is a
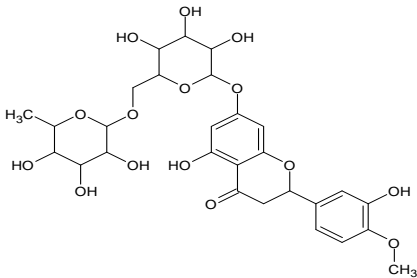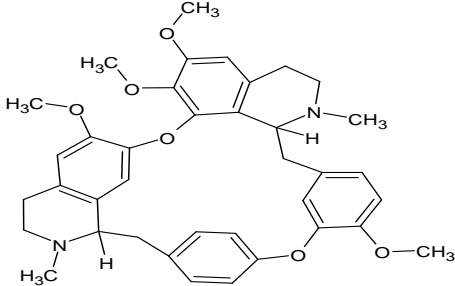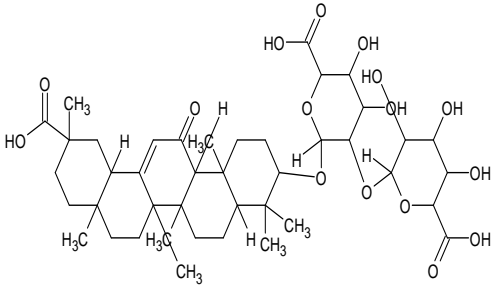
major active constituent of *Andrographis paniculate* Burm. f., that has been shown to have a wide range of biological actions, including anti-inflammatory, antioxidant, anti-neuroinflammatory, and neuroprotective effects (Zhang, et al., 2021). The mechanism of AN against neuroinflammation was found to be associated with inhibited NF-κB signaling and nucleotide-binding oligomerization domain-like receptor protein three (NLRP3) inflammasome activation (Li, et al., 2018). 6-shogaol (6-SG), a bioactive ingredient in dried ginger *Zingiber officinale* Rosc., possesses strong anti-neuroinflammation properties (Park, et al., 2013; Moon, et al., 2014; Pan, et al., 2008) and has been shown to improve memory function in animal models of cognitive disorders (Ha et al., 2012). 6-SG was shown to significantly suppress TNF-α and NO levels, and the mechanism was associated with downregulated COX-2, p38 mitogen-activated protein kinase (MAPK), and NF-κB signaling pathways in the LPS-induced microglia BV2 cells and neuroinflammatory mouse model (Ha et al., 2012). Curcumin (CU) has been shown to exert anti-aging, anti-cancer, anti-microbial, anti-neuroinflammatory and antioxidant characteristics (Tiwari, V., & Chopra, K. 2012). In addition, CU is an effective phytochemical against neurodegeneration and neuroinflammation as observed in AD (Yang, et al., 2014). The anti-neuroinflammatory role of CU is primarily through inhibition of the p38 MAPK and NF-κB signaling pathways, and induction of HO-1 by the Nrf2/antioxidant response element (ARE) signaling pathway, thereby decreasing the production of inflammatory mediators in the Pam3CysSerLys4 (Pam3CSK4)-stimulated BV-2 microglial cells (Jin et al., 2018). Hesperidin (HES) is a flavanoglycone abundantly present in citrus fruits, which exerts neuroprotective effects against PD and Huntington's disease by virtue of its antioxidant, anti-inflammatory, neuroprotective and anti-apoptotic actions (Justin Thenmozhi et al., 2018). HES improves motor disability in rat spinal cord injury through anti-inflammatory *via* Nrf-2 and HO-1 signal pathways (Heo et al., 2020). Tetrandrine (TE) is a bis-benzylisoquinoline alkaloid that is extracted from the roots of *Stephania tetrandra* S. Moore. TE possesses a diverse array of biological actions, including anti-neuroinflammatory and antioxidative activities (Bao, et al., 2016; He, et al., 2011). In an amyloid-β (1-42) induced Alzheimer's disease rat model, TE reduced spatial memory impairment and hippocampus neuroinflammation *via* suppressing NF-κB activation (He, et al., 2011). Glycyrrhizin (GLY), a triterpenoid saponin phytochemical, is the main bioactive constituent of

Glycyrrhiza glabra L., and has been shown to possess anti-neuroinflammatory and neuroprotective properties (Song et al., 2013). GLY treatment suppressed over-expressions of pro-inflammatory cytokines of IL-1β and TNF-α in the LPS-induced Alzheimer's mouse model by inhibiting TLR4 signaling pathway activation (Liu, et al., 2019). A summarised information of these selected phytochemicals against neuroinflammation is shown in **Table 1**. From the literature, each of the phytochemicals appeared to exhibit versatile pharmacological actions that are associated with neuroinflammation and neuroprotection. It was worth noticing that the scientific evidence to support the use of these phytochemicals was mostly from cellular and animal studies (Li, et al., 2016; Moon et al., 2014; Serrano et al., 2014; Yang S, et al., 2019). However, clinical trials for their individual use in treating neurodegenerative diseases are lacking, which maybe partly attributed to their relatively high dose in animal studies (see Table 1.1).
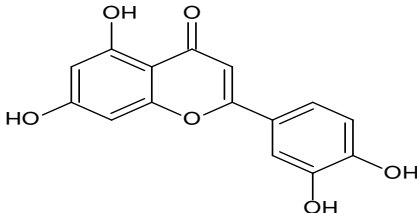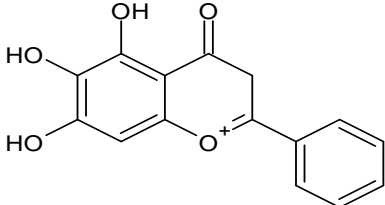
Table 1.1 Anti-neuroinflammatory potential of the selected phytochemicals*

Phytochemicals	Structure	Cellular/animal models	Anti-neuroinflammatory activity and mechanisms	Effective dosage on cells or animal	Reference
Luteolin (LU)		OxyHb/LPS stimulated BV2 microglia cells Sprague-Dawley (SD) rats with intracerebral hemorrhage (ICH)	↓TNF-α, IL-1β, IL-6, NO, iNOS, COX-2; ↑motor and sensory impairments and inhibited neuronal cell degeneration; ↓TLR4/TRAF6/NF-κB pathway; ↑Nrf2 pathway	*In vitro*: 10, 20 μM *In vivo*: 10, 20, 40, 120 mg/kg	(Kou et al., 2022; Li Z, et al., 2022; Yang Y, et al., 2020; Yao, et al., 2018; Zhou W, et al., 2021; Zhu, et al., 2011)
Baicalein (BA)		LPS-activated BV-2 microglial cells Collagenase-induced ICH rat model	↓IL-6, IL-18, TNF-α; ↓NF-κb/NLRP3/caspase-1/TLR4 pathway	*In vitro:* 100 μM *In vivo*: 50, 140, 200, 280, 560 mg/kg	(Rui, et al., 2020; Xin, et al., 2021; Yan, et al., 2020; Zhang, et al., 2017; Zhao et al., 2021)

Phytochemicals	Structure	Cellular/animal models	Anti-neuroinflammatory activity and mechanisms	Effective dosage on cells or animal	Reference
Andrographolide (AN)		Aβ (1–42) induced BV2 microglia cells Amyloid precursor protein / presenilin 1 (APP/PS1) double-transgenic mouse model	↓Amyloid-β deposition, IL-6, NO, iNOS, and COX-2; alleviated cognitive impairments; ↓NF-κB, NLRP3, JNK MAPK pathway	*In vitro*: 0.5-10 μM *In vivo*: 2.0 mg/kg	(Li X, et al., 2018; Souza et al., 2022; Tao et al., 2018; Yang R, et al., 2017)
6-shogaol (6-SG)		LPS induced BV2 mouse microglial cells Amyloid-β (1–42) induced AD mice model	↓TNF, NO, iNOS; meliorated memory impairment; ↓p38 MAPK, NF-κB pathway	*In vitro*: 0.001, 0.01 μmol/L *In vivo*: 10 mg/kg	(Ha et al., 2012; Moon et al., 2014; Park, et al 2013; Pan, et al., 2008)
Curcumin (CU)		LPS induced BV2 mouse microglial cells APP/PS1 transgenic mouse model	↓NO, TNF-α, IL-1β, COX-2, NLRP3 ↓TREM2, TLR4, NF-κB pathway	*In vitro*: 5, 10 mM *In vivo*: 15-200 mg/kg	(Chen et al., 2015; Khan, et al., 2019; Liu Z.-J, et al., 2016; Sorrenti et al., 2018; Tegenge et al., 2014; Tiwari & Chopra, 2012; Tiwari & Chopra, 2013; Xiao et al., 2017; Zhang J, et al., 2019)

Phytochemicals	Structure	Cellular/animal models	Anti-neuroinflammatory activity and mechanisms	Effective dosage on cells or animal	Reference
Hesperidin (HES)		LPS induced BV2 mouse microglial cells Middle cerebral artery occluded rats model	↓NO, IL-1β, IL-6, iNOS; protect memory loss in the mice; ↓Phosphorylation of ERK1/2, p38 MAPK, NF-κB pathway	*In vitro*: 200 mM *In vivo*: 50-200 mg/kg	(Javed et al., 2015; Justin-Thenmozhi et al., 2018; Li M, et al., 2016; Raza et al., 2011; Yıldız et al., 2022)
Tetrandrine (TE)		Amyloid-β (1–42)/LPS-induced BV2 mouse microglia cells harbouring five mutations associated with familial Alzheimer's disease mouse model	↓IL-1β, TNF-α, IL-6, COX-2, iNOS; ↓NF-κB pathway	*In vitro*: 1, 5 mM *In vivo*: 10, 20, 40 mg/kg	(Dang et al., 2014; He et al., 2011; Ren et al., 2021)
Glycyrrhizin (GLY)		LPS-induced BV2 mouse microglia cells AD mice model	↓IL-1β, TNF-α, COX-2, iNOS; ↓MAPK, NF-κB, HMGB1/GPX4 pathway, TLR4 signaling pathway	50 μmol/L 10, 30, 50 mg/kg	(Kong, et al., 2017; Liu W, et al., 2019; Ojha, et al., 2016; Song et al., 2013; Sun X., et al., 2018; Zhao et al., 2013; Zhu et al., 2022)

*The information in the table is not exhausted

1.3 Synergy in natural products

1.3.1 Definition of synergy

The efficacy of natural product combinations is believed to be based on synergy when utilising two or more ingredients together. Synergy is characterised as two or more agents in the mixture exhibiting higher efficacy than the sum of the effects from the single agents (Zhou X, et al., 2016). Synergy is also related to multi-targeted behaviour and reduced toxicity (Blumenfeld, et al., 2012). As neuroinflammation diseases involve multiple mediators and their crosstalk within the microvascular unit, synergy in natural therapies may target multiple mediators (i.e. NO, TNF, and IL-6).

Combination therapy has become an emerging therapeutic strategy for complex diseases, such as neurodegenerative diseases, that is believed to offer improved clinical outcomes through a synergistic approach (Liu J, et al., 2017; Blumenfeld, et al., 2012). For instance, caduet (amlodipine/atorvastatin) is a combination medication containing amlodipine and atorvastatin. It is a prescription medicine used to relieve symptoms of cardiovascular diseases, hypertension, and angina (chest pain) (Glass, 2004). However, the combination therapy with multiple pharmaceutical drugs also faced the challenge of magnified side effects from each component (Ascierto & Marincola, 2011). Amlodipine can exacerbate angina and the atorvastatin can lead to liver dysfunction or rhabdomyolysis. The side effects of the caduet include headache, edema, constipation, flatulence, dyspepsia, and abdominal pain (Wimett & Laustsen, 2004).

Herbal formulation has long been used in traditional medicine, in which multiple herbal ingredients are used. The fundamental treatment principle of combination therapy is synergy, where the overall effectiveness replies on the positive interaction of the herbal ingredients and achieves enhanced efficacy, reduced toxicity and a multi-target approach (Zhou X, et al., 2016). Numerous preclinical and clinical studies have demonstrated synergistic or positive relationships among the herbal ingredients used in well-designed formulations (Dey, et al., 2017; He et al., 2019; Yang et al., 2021; Yu et al., 2016). For instance,

Danshen (Salvia Miltiorrhizae Radix et Rhizoma) - Sanqi (Notoginseng Radix et Rhizoma) (DS-SQ) herb-pair is a Fufang Danshen tablet, which has been widely utilised in Chinese herbal medicines in Asian countries for the prevention and treatment of vascular disorders such as angina pectoris, stroke, and diabetic retinopathy (Lian et al., 2015; Yang R, et al., 2014). Dantonic (T89) is a botanical drug consists of extracts of Danshen (Radix Salviae Miltiorrhizae) and Sanqi (Radix Notoginseng) with borneol in a capsule form. Sun *et al.* study demonstrated that T89 exhibited multi-target behaviours, that prevented cholesterol plaque, inhibiting platelet aggregation and adhesion and suppressed thrombus development in a randomised, placebo controlled clinical trial (Sun H, et al., 2018). The preclinical study suggested that their combination with the ratio of 6:4 (50–300 μg/mL) produced synergistic effects in protecting endothelial cells against oxidative stress by restoring cell viability, reducing lactate dehydrogenase leakage and caspase-3 expressions in human cardiovascular endothelial cells (Zhou X, et al., 2019). Cai *et al.* (2016) demonstrated that esculetin (11.6 μM), curcumin (8.5 μM) and hesperetin (12.5 μM) demonstrated synergistic effects in decreasing prostaglandin E2 production in LPS-induced RAW 264.7 cells (Cai et al., 2016).

Thus, a well-developed herbal formula with a multi-compound and multi-target approach may offer a more beneficial approach to addressing neuroinflammation related complex pathological mechanisms. However, there is a general lack of robust methodologies to identify and determine synergistic interactions among bioactive phytochemicals in combination therapy. Furthermore, the mechanisms of action that are associated with synergy are largely unknown.

1.3.2 Development of synergistic combination

Synergy is related to enhanced therapeutic effect, multi-target behaviour and reduced toxicity (Blumenfeld et al., 2012). It is evident that synergy can not be concluded by comparing the activity of a combination to that of its individual ingredients (i.e. by *p*-value determined by one-way ANOVA analysis). Because it can not differentiate synergy and additive interaction, as both would show combined effects great than individual (Zhou X, et al., 2016).

Nowadays, researchers have developed various mathematical models and computer programs to determine true synergy effect, including the isobole method (Zhou X, et al., 2016), Systems biology (Dainiak, et al., 2018), dose model (Katzir, et al., 2019) and DiaMOND model (Cokol, et al., 2017). In this study, we used integrated network pharmacology, molecular docking and combination index (CI) model to understand the potential synergy mechanism and determine synergistic activity.

1.3.3 Network pharmacology

To date, various methodologies have been developed to identify and quantify the degree of drug interaction in combination therapies. Network pharmacology is a computational and mathematical model integrating literature, experimental data, and computational sciences to evaluate synergistic interaction (Sun R, et al., 2021). Recently, it has been developed to illustrate the multi-target actions of components in combination therapy (Zhou X, et al., 2016). This method can identify the key bioactive phytochemicals from a complex formulation, elucidate the gene targets associated with the disease, and build the network of the bioactive phytochemicals, gene targets and associated signaling pathways. The targeted genes and proteins from the generated network may be verified in the literature or validated by experimental data. Its increasing popularity is attributed to low research cost, a short research cycle, and comprehensive information. In drug discovery investigations, there is an emerging trend of integrating analysed information from network pharmacology with experimental results to form novel combination therapy with a known mechanism of action (He D, et al., 2019).

1.3.4 Molecular docking

Molecular docking is the computational technique that gives a prediction of the ligand-receptor complex structure and then determines the potency of any phytochemical that is used as a drug for prospects (McNutt et al., 2021). Molecular docking is usually followed by network pharmacology, which can determine the binding affinity between the key bioactive and associated protein target (An W, et al., 2021), and verifies the results of the network pharmacology (He D, et al., 2019). There are numerous computer programs to

conduct the molecular docking process, such as DOCK, AutoDock, AutoDock Vina, MOE-Dock and CB-DOCK. The parameter to predict the binding affinity of both ligand and target is the binding energy, which of best docked compounds is binding energy below −5.0 kcal/mol (Shi Y, et al., 2021).

1.3.5 Methods of quantifying synergy

1.3.5.1 Combination index model

Combination index (CI) model is a practical method for evaluating the interactions of multiple agents on the same biological target. CompuSyn is a computational software developed by Biosoft, US. It is used to analyse the interaction between two or more than two different compounds on a specific biological target based on the experimental results (Zhou X, et al., 2016; Chou T.-C., 2018). The principle of the algorithm developed in the CI model is based on the mass-action law that allows computerised simulation of dose-effect dynamics based on small size experiments and a set of data *in vitro*, in animals, and in humans (El Hassouni B, et al., 2019). The equation of the CI model to determine the synergistic/antagonistic interaction in two agents in combination is shown below (Chou T.-C., 2018). Herein, (Dx)1 and (Dx)2 are the doses of every single compound required to produce x effect level (i.e. NO inhibition), and D1 and D2 are the doses of the two compounds in combination that produce the same effect. CI was used to assess whether the combination at the certain effect level x yield a synergistic, antagonistic or additive effect. It is defined that the CI value above 1 is antagonistic, equal to 1 is additive, and below 1 is synergistic (Chou T.-C., 2018).

$$CI = \frac{D1}{(Dx)1} + \frac{D2}{(Dx)2}$$

1.3.5.2 Isobologram

The isobologram is applied to demonstrate the interaction between two agents using a graphical method at specified effect levels (Shyr, et al., 2022). The isobologram can be generated by CompuSyn software. For

iso-effective dose graphics, the isobologram is based on the CI equation. The CI model explains the synergy effect from the therapeutic effect, but the isobologram explain the synergy effect from dose level. The isobologram graphics can show synergy at three set concentrations (i.e. Fa = 0.5, Fa = 0.75 and Fa = 0.9). Combination data points that fall on the hypotenuse suggest an additive effect, those that fall on the low-left indicate a synergistic relationship, and those that fall on the upper-right indicate an antagonistic relationship.

1.4 Knowledge gap

Chronic neuroinflammation is a critical therapeutic target for neuronal degeneration and neuronal death, which can trigger and develop neurodegenerative disorders (Chen, Zhang, & Huang, 2016). However, it is a complex condition involving microvascular interplay and there is currently no viable treatment (Takata, et al., 2021). Furthermore, only single-target treatments are accessible and existing treatments almost always have side effects (Zhou Y, et al., 2021; Liu J, et al., 2017).

Many natural products are centred on a single phytochemical. Currently, these phytochemicals are thought to have modest therapeutic effectiveness or limited bioavailability (Liu J, et al., 2017). There is a lack of studies that attempt to combine single phytochemicals to form a well-designed formula to target the complex pathological mechanisms of neuroinflammation and achieve an enhanced therapeutic outcome. Moreover, a single phytochemical that is developed in a single cellular model (i.e. microglia only) often results in an unsatisfactory clinical outcome, due to various factors such as neglected drug action on microglia-neuron crosstalk and poor permeability through the BBB (Pohl F, et al., 2018). Thus, drug screening and development through a practical co- or tri-culture cellular model that can mimic the neuronal-vascular unit is needed to enhance the success rate for the novel therapeutic agent screening.

1.5 Hypothesis and aims

We hypothesise that a well-developed herbal compound-combination(s) that synergistically inhibit microglia mediated-neuroinflammation can protect neuronal viability and endothelial integrity *in vitro.* Our study aims to investigate a novel compound combination from natural products with a synergistic approach to help treat neurodegenerative diseases by targeting neuroinflammation.

The specific aims of the study are:

1) Identify synergistic anti-neuroinflammatory compound combinations in LPS-induced mono-cultured microglia.

2) Investigate the underlying mechanisms associated with the synergistic anti-neuroinflammatory activity of phytochemicals in combination with LPS-induced microglia.

3) Investigate the effect of the synergistic compound combination in inhibiting neuroinflammation, restoring the BBB, and enhancing neuronal survival in a neuroinflammation tri-culture model.

Chapter 2: Methodology

2.1 Network pharmacology

2.1.1 Gene targets associated with neuroinflammation

The two-dimensional structures of the eight phytochemicals were retrieved from the PubChem database (https://pubchem.ncbi.nlm.nih.gov/). Spatial data file of two-dimensional structures was uploaded to the PharmMapper database to generate potential gene targets. Human normalisation of Universal Protein Resource (UniProt) (https://www.uniprot.org/) was searched to filter the obtained gene targets to normalise their names and organisms subsequently. The characters of the eight phytochemicals were obtained from the Traditional Chinese Medicine Systems Pharmacology Database and Analysis Platform (TCMSP, https://tcmspw.com/tcmsp.php). According to literature reports and pharmacokinetic parameters, the phytochemicals with oral bioavailability (OB)≥30% reflect good absorption and slow metabolism after oral administration. The phytochemicals with a drug-likeness (DL)≥0.18 were chemically suitable for drug development. The phytochemicals with the BBB≥−0.3 reflect good permeability through the BBB (An et al., 2021). Neuroinflammation-related gene targets were obtained from the Online Mendelian Inheritance in Man (OMIM) Database (http://www.omim.org/), GeneCards Database (https://www.GeneCards.org/), and DisGeNET Database (http://www.disgenet.org/home/). Duplicate targets were removed after collecting all the gene targets of neuroinflammation in the three databases. The Venn diagram was drawn to show the number of overlapping gene targets related to the disease and each phytochemical.

2.1.2 Protein-protein interaction network construction

The PPI network describes physical interactions among protein targets that are associated with the phytochemical candidates and neuroinflammation taking place to mediate the assembly of proteins into protein complexes (Pippi B, et al., 2015; Doncheva N.T, et al., 2019). The STRING (Search Tool for the Retrieval of Interacting Genes/Proteins) database (https://string-db.org/) provides the relevant protein−protein associations which analyses confidence scores for each of the protein connections with quantified reliability. Overlapping gene targets of each phytochemical were input to STRING to generate

the PPI network (Doncheva N.T, et al., 2019). The disconnected edges were hidden in the default setting in the network, and the required interaction score was set at 0.9 as a minimum to obtain the network of PPI.

2.1.3 Gene Ontology and Kyoto Encyclopedia of Genes and Genomes pathway analysis

Based on the constructed PPI network of each phytochemical, the associated Gene Ontology (GO) and Kyoto Encyclopedia of Genes and Genomes (KEGG) pathways that represent gene product properties and signaling pathways were investigated. The Database for Annotation, Visualization and Integrated Discovery (DAVID) is the online enrichment analysis database (https://david.ncifcrf.gov/home.jsp) applied to explore the relevant gene function annotation and pathway enrichment. The GO targets were searched through the DAVID database to elucidate the interaction between related gene targets of each phytochemical and their associated GO when targeting neuroinflammation (Sun Y, et al., 2021). Following that, the cross-GO targets were uploaded to DAVID to obtain associated biological pathways (BP), cellular content (CC), molecular function (MF) and KEGG pathways. In the present study, the top 20 targets in each function were selected and input to Bioinformatics (http://www.bioinformatics.com.cn/) to conduct the enrichment analysis of KEGG pathways and GO enrichment used across genes, and the terms with a *p*-value less than 0.05 were filtered for the subsequent network construction (Li X, et al., 2014).

2.1.4 The construction of compound-gene targets-signaling pathway network

The compound-gene targets-signaling pathway network was constructed using Cytoscape (v.3.8.2, Institute for Systems Biology, US) (Liang, B., et al., 2021). The network was built to examine the relationships among the phytochemicals, their gene targets and associated pathways in neuroinflammation. The image of the network and associated statistics were exported from Cytoscape. The relevant parameters were obtained by the "analysis network" tool in Cytoscape, including "Degree", "Betweenness-Centrality", "Closeness Centrality", and "Stress". The most relevant gene targets and KEGG pathways were further filtered by selecting those "Degree" larger than 2 x median values (He D, et al., 2019). The importance of

the gene/protein target will be ranked by the degree, which will be used for the following experimental verification.

2.2 Molecular Docking Simulation

In order to evaluate the credibility of the connection between the core protein targets with each phytochemical against neuroinflammation, CB-Dock (v.1.0, Yang Cao Lab, China) was used to perform molecular docking (http://clab.labshare.cn/cb-dock/php/blinddock.php). CB-Dock is a protein-ligand docking model designed to identify binding sites, analyse center and size, and conduct molecular docking (Liu Y, et al., 2020). It facilitates docking procedures and increases the accuracy of molecular docking. Cavity-focused docking increases the accuracy and hit ratio with blind docking (Liu Y, et al., 2020).

The protein structures of the selected targets obtained from the network pharmacology analysis were obtained from Protein Data Bank (PDB). The crystal structures of each phytochemical candidate were sourced from the PubChem database, as shown in Section 2.1. The "spacefill" and "cartoon" parameters were set for the ligand and receptor, respectively. "Element" and "chain" were used for ligands and coloured receptors.

2.3 Establishment of mono- and tri-culture models

2.3.1 Cell culture and cell lines

The mouse brain microvascular endothelial cell line MVEC(B3) (MVEC) was obtained from Dr Jia Li, Macquarie Medical School. Mouse microglia N-11 (N11) and mouse neuroblastoma Neuro2A cell lines (N2A) were kindly donated from Professor Gerald Muench, School of Medicine, Western Sydney University. They were cultured in complete Dulbecco's modified Eagle medium (DMEM, Lonza, Australia) supplemented with 10% foetal bovine serum (FBS, Thermo Fisher Scientific, Australia) and 1% penicillin (Sigma-Aldrich Australia).

2.3.2 Cell culture for the single cell line

N11 cells, MVEC cells and N2A cells were incubated at 37˚C, 5% CO_2 in 95% air in a vented flask T75 cm² (Sigma-Aldrich, Sydney, Australia), respectively. Cultured cells up to passage 35 with approximately 90% confluency were digested with 0.25% trypsin (Thermo Fisher Scientific, Australia) to perform experiments. Cells were passaged every two-three day until passage 35.

2.3.3 LPS-stimulated neuroinflammation in mono-cultured N11 cells

N11 cells were incubated at 37˚C, 5% CO_2 in 95% air in a vented flask T75 cm² (Sigma-Aldrich, Sydney, Australia). The cells were sub-cultured every 3 days to sustain a controllable number. N11 cells (1.0×10^6 cells/mL) were seeded in 96-well plates with DMEM containing 10% FBS. LPS purified by trichloroacetic acid extraction (LPS, Sigma, Australia, batch number 070M4018), was used to stimulate inflammatory mediators, including NO, TNF-α and IL-6. After the cells were incubated with extracts for 1 h, 1 µg/mL of LPS was added to the cells and then incubated for another 24 hr.

2.3.4 LPS-stimulated neuroinflammation in tri-culture cells

A tri-cultured neuroinflammation model was established using a transwell polycarbonate membrane cell culture inserts with a 24-well plate (Corning®Costar®Transwell® Cell culture inserts, Sigma) with slight modification (Zheng Y.-F., et al., 2021). The transwell with insert membrane was placed upside down and coated with 1% polylysine (Sigma, USA) for 1 hr. Then 200 µL of N11 cells (2.0×10^6 cells/mL) were seeded on the top of the transwell with DMEM containing 10% FBS and kept upside down in the incubator to ensure N11 cells adhered to the top of the transwell by the surface tension. In parallel, 500 µL of N2A cells (1.0×10^6 cells/ mL) were seeded in a fresh 24-well plate with DMEM containing 10% FBS. After 4 hr, the transwell with N11 cells was inverted and placed within a 24-well plate immersed with 375 µL DMEM containing 10% FBS in each well, and the MVEC cells (1.0×10^6 cells/mL) were seeded with 250

µL DMEM containing 10% FBS in the same insert of N11 cells. Please see **Figure 2.1** for the constructed tri-culture cells in the transwell system.

After 24 hr, the medium in the lower compartment was replaced with serum-free DMEM for the tri-culture, and the upper compartment and the mono-culture medium were replaced with either serum-free DMEM (normal control), 1 µg/ml LPS or samples for another 24 hr before bioassays. The cell supernatants from the mono-culture system and both the upper and lower compartments in the tri-culture were stored in −20°C for the following bioassays.
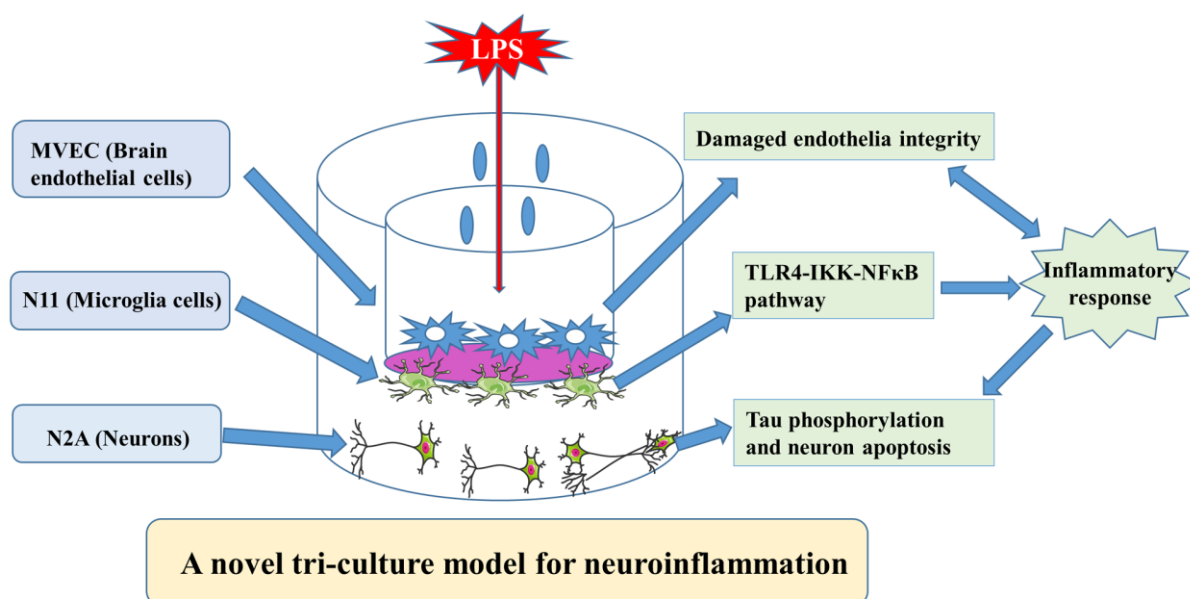
Figure 2.1 LPS-induced *in vitro* tri-culture neuroinflammation model (Zheng Y. F, et al., 2021).

2.4 Preparation of phytochemicals

The pure isolated phytochemicals, LU, BA, AN, 6-SG, CU, HES, TE and GLY (purity > 98%), were purchased from Chengdu Biopurify (China). The identity and purity were confirmed by the high-performance liquid chromatography (**Appendix 1**). Each phytochemical was dissolved in dimethyl sulfoxide (DMSO) at a concentration of 100 mM. They were diluted with DMEM serum-free media before adding to the cells with a DMSO concentration of 0.1%.

In LPS-stimulated mono-cultured N11 cell, each phytochemical at 100 mM was serially diluted by a factor of two, and dissolved in serum free DMEM by 1:1000 dilution when adding the cells. The pair-wised combinations were prepared by mixing each two of the phytochemicals in 1:1 ratio (*v/v*) in DMSO at 100 mM, and subjected to serial dilution before adding to N11 cells in the 96-well plate. Note that the unit of uM and its equivalent ug/mL are used for all the tested combinations throughout the text for convenience and simplicity. In the LPS-stimulated tri-culture system, individual AN, 6-SG, and BA were prepared at 25 mM in DMSO, and diluted with serum free DMEM for 1:1000 before adding to the transwell. The combinations were prepared as AN-SG 25 mM [AN (12.50 mM) + 6-SG (12.50 mM), total concentration of 7.83 mg/mL] and BA-SG 25 mM [BA (12.50 mM) + 6-SG (12.50 mM), total concentration of 6.83 mg/mL] in DMSO. Then they were diluted in serum free DMEM in 1:1000 dilution before adding to the transwell. The cells were also treated with serum free DMEM with vehicle (0.1% DMSO) as the vehicle control (blank) 1 h prior to the stimulation of LPS (1 µg /mL). The cells and cell supernatant were then subjected to the bioassays after 24hr. In the tri-culture, we only selected one concentration (25 µM) for the testing of individual and paired combinations as the working concentration, due to the tight timeframe.

2.5 Neuroinflammatory bioassays

2.5.1 Anti-inflammatory bioassays

2.5.1.1 Griess reaction NO measurement

After 24 hr of LPS stimulation, the supernatants in the 96-well plate or upper and lower compartment (90 µL) of the tri-culture system were collected for the measurement of nitrite level by mixing with an equal amount of the Griess reaction (1% sulfanilamide in 5% phosphoric acid and N-(1-naphthyl)-ethylene diamine dihydrochloride) (Tsikas, 2007; Yoon, et al., 2010)). Nitrite production was determined by measuring the optical density at 540 nm using a microplate reader (BMG Labtech Fluostar Optima, Mount Eliza, Victoria, Australia). Used nitrite production as an indirect indicator of NO levels (Tsikas, 2007). The

rest of the supernatant was subjected to TNF-α and IL-6 enzyme-linked immunosorbent assay (ELISA) assay.

2.5.1.2 TNF-α and IL-6 ELISA assay

The levels of IL-6 and TNF-α in the supernatant from the mono-cultured N11 cells, the upper and lower compartment of the tri-culture system were measured using commercial IL-6 and TNF-α immunosorbent assay (ELISA) kits (cat. no. 431304 and 900-K45, Biogems) according to manufacturers' instructions. The absorbance was measured at 410 nm with a microplate reader (BMG Labtech Fluostar Optima, Mount Eliza, Victoria, Australia). The concentrations of IL-6 and TNF-α were calculated using standard curves.

2.5.2 Cell viability bioassays

2.5.2.1 Alamar blue assay

Cell viability of N11 in the 96-well plate and N2A cells in the tri-culture system was evaluated 24 hr after the LPS stimulation. After removing supernatants, the cells were incubated with 100 μL in the 96-well plate or 500 μL of Alamar Blue (0.01 mg/mL resazurin) in the 24-well plate (Schober et al., 2021). The cells were then incubated for 2 h in a humidified incubator at 37 °C. The optical density of each well was measured from excitation of 545 nm and emission of 595 nm using a microplate reader (BMG Labtech Fluostar Optima, Mount Eliza, Victoria, Australia).

2.5.2.2 3-(4,5-Dimethylthiazol-2-yl)-2,5-Diphenyltetrazolium Bromide (MTT) assay

The N2A cells were co-incubated with MTT solution [final concentration 0.5 mg/mL in phosphate-buffered saline (PBS)] was added to the cells and incubated for 2 h at 37 °C with 5% CO_2. DMSO was then added to dissolve the insoluble formazan crystal. The absorbance was measured at 510 nm using a microplate reader. The density of formazan formed in control (medium with vehicle) cells was taken as 100% of cell viability. The cell viability of the measured sample is determined using the equation: Cell

viability % = absorbance of treated cells/absorbance of blank control (cells with 0.1% DMSO in serum free

DMEM) * 100%.

2.5.3 Endothelial barrier permeability

2.5.3.1 Transendothelial electrical resistance values

The transendothelial electrical resistance (TEER) values of MVEC cells in the tri-culture 24-well systems

were measured by an epithelial-volt-ohm resistance meter (ERS-2, cat.no. MERS00001; Merck) according

to the manufacturer's instructions. The background TEER value was measured in the well that has serum

DMEM only. The final results were calculated by TEER in each group subtracted from the background

TEER values. The values are shown as $\Omega \times cm^2$.

2.5.3.2 Evans blue permeability test

For Evans blue permeability test, the lower compartment in the tri-culture system was replaced with 0.5

mL PBS and the upper compartment was filled with 0.2 mL of Evans blue [0.25% Evans blue, (cat.no.

E2129; Sigma)] 24 hr's after the LPS stimulation. After 0.5 hr's incubation, the solution in the lower

compartment was tested for absorbance at 450 nm using a microplate reader (BMG Labtech Fluostar

Optima, Mount Eliza, Victoria, Australia).

2.6 Mechanistic study on neuroinflammatory associated-protein targets

2.6.1 Immunoblotting

N11 cells were grown in T75 cell flasks (SARSTEDT, Australia) until confluence. After the LPS

stimulation for 40 min or 24 hr, cell pellets were harvested by centrifugation at 500 g for 5 min at 4°C. The

cell pellets were mixed with radioimmunoprecipitation assay buffer (Santa Cruz Biotechnology, Australia)

with 1% proteinase inhibitors (Cell Signaling Technologies, United States) and their concentrations were

elucidated using Pierce™ BCA Protein Assay Kit (Thermo Fisher Scientific, Australia). The total proteins

from each sample at 10 mg/mL were loaded to the 10-well gel (BioRad, Australia) and separated by the SDS-PAGE electrophoresis (PowerPac HC, BIORAD, Australia), then the proteins were transferred to the PVDF membrane by the iBlot 2 device (Thermo Fisher Scientific, Australia). The membranes were incubated with 3% Bovine Serum Albumin (BSA, Scientifix, Australia) dissolved in PBST [PBS buffer plus 1% tween 20 (Thermo Fisher Scientific, Australia)] for 1 h at room temperature (Zhou X, et al., 2022). The membranes were incubated with primary antibodies against phospho-p38 MAPK (1:1000, cat.no. 4511), p38 MAPK (1:1000, cat.no. 8690), and iNOS (1:1000, cat.no. 13120) overnight at 4° C. GAPDH (1:1000, cat.no. 5174) was used as a loading control. The primary antibodies were probed with anti-rabbit HRP conjugated secondary antibodies (1:5000, cat.no. 7074) at room temperature for 2 h. All these antibodies were purchased from Cell Signaling Technology (United States). The immunoreactive bands on the membranes were incubated by the SuperSignal West Pico Plus ECL kit (Thermo Fisher Scientific, Australia) and visualised by the iBright 750 (Thermo Fisher Scientific, Australia). Specific bands were analysed and the intensity was quantified using ImageJ software.

2.6.2 Immunofluorescent staining

The N2A cells were seeded on a 1 cm cover slide in the 24-well. The tri-culture system was established and treated overnight using the same protocol as described above. Each cell line was washed with cold PBS and fixed with 4% paraformaldehyde for 20 min at room temperature. Triton-X 100 (0.1%) was added to cells for 20 min and followed by blocking with 3% Bovine Serum Albumin (BSA, Scientifix, Australia) for 1 h (Zhou X, et al., 2022). Primary antibodies were then added to the system, including zonula occludens-1 (ZO-1; 1:100, cat no. 13663S), phosphorylated tau (p-tau; 1:200, cat no. 49561) or NF-κB p65 (p65; 1:100, cat no.8242), all purchased from Cell Signaling Technologies, USA. The cells were then washed with PBS three times and each cell line was then stained with mixed secondary antibodies, including donkey anti-mouse IgG Alexa Fluor 488 (green; 1: 1,000, cat no. A32766), donkey anti-goat IgG Alexa Fluor 680 (yellow; 1: 250, cat no. A32680) and donkey anti-rabbit IgG Alexa Fluor 594 (red; 1: 1,000, cat no. A32754), all purchased from Thermo Fisher Scientific, Australia. The insert membrane was cut for the collection of

either the N11 or the MVEC cells. Cotton was used to swap the other side of the membrane of the cell line and then put on the new slide. Finally, the anti-fade mounting medium with DAPI (Sigma, Australia) was added to the cells and subjected to immunofluorescent imaging using an Inverted Leica TCS SP5 laser scanning confocal microscope (School of Medicine, Western Sydney University, Australia).

2.7 Synergy determination

2.7.1 CI method

The CI model was applied to analyse the synergistic/antagonistic interaction. The data of the concentration-response curves of single phytochemicals and their combinations derived from NO and ELISA bioassays was input to the CompuSyn software 2.0 (ComboSyn, Inc., USA) (El Hassouni et al., 2019). The computer program produced the isobologram figure, CI values, and CI-fraction affected (Fa, refers to the effect level of NO/IL-6/TNF-α inhibition ranged from 0-1) curves to show the interaction (El Hassouni, 2019).

2.8 Statistical analysis

Statistical analysis was conducted using GraphPad Prism 9.0 software (GraphPad Software Inc., USA). The data was shown as mean ± standard error of the mean (SEM) from at least three individual experiments. The IC_{50} and LC_{50} values were determined from the constructed dose-response curves. The statistical comparison between groups was conducted by one-way analysis of variance (ANOVA), with Tukey test and $p<0.05$ was considered statistically significant. An overarching work flowchart for the development of synergistic herbal compound combinations targeting neuroinflammation show in the **Figure 2.2**.
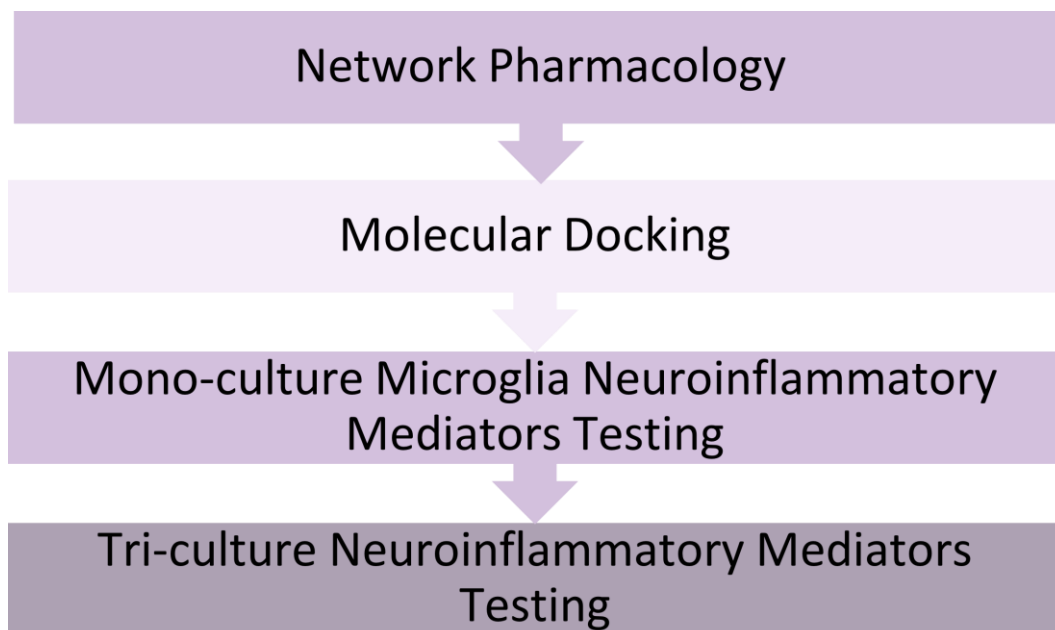
Figure 2.2 An overarching work flowchart for the development of synergistic herbal compound combinations targeting neuroinflammation.

Chapter 3: Network Pharmacology Analysis and Molecular Docking

3.1 Introduction

Network pharmacology is effective for constructing a "compound-gene target-pathway-disease" network for a combination therapy and disclosing the mechanisms of pharmacological effects and interactions among the constitutes with many gene and protein targets (Zhang R, et al., 2019). Molecular docking is usually followed after network pharmacology that is used to anticipate how the predicted target protein would interact with the constituent (Stanzione et al., 2021). Network pharmacology and molecular docking have established themselves as a crucial component of the drug discovery toolkit, partly due to it is ease of usage and relatively minimal cost implications. In addition, it has been frequently used to predict or illustrate the complex pharmacological actions and associated mechanisms of constituents used in combination therapy such as traditional herbal formulations.

This chapter reports the key gene targets and KEGG pathways of single phytochemical and their combination involved in the neuroinflammation pathological condition. The main findings in this chapter suggested that MAPK14, MAPK8, NOS3, EGFR and SRC were the top five hub genes for the eight phytochemicals against neuroinflammation. The top common KEGG pathway was the MAPK signaling pathway. Molecular docking analysis confirmed that each phytochemical had a high affinity to bind with MAPK and NOS as the top molecular targets.

3.2 The molecular actions and common targets of each phytochemical against neuroinflammation

3.2.1 Characteristic molecular actions of eight phytochemicals in neuroinflammation

The compound-gene targets-signaling pathway network was constructed to reveal the pharmacological action of each phytochemical in relation to neuroinflammation (**Figure 3.1**).
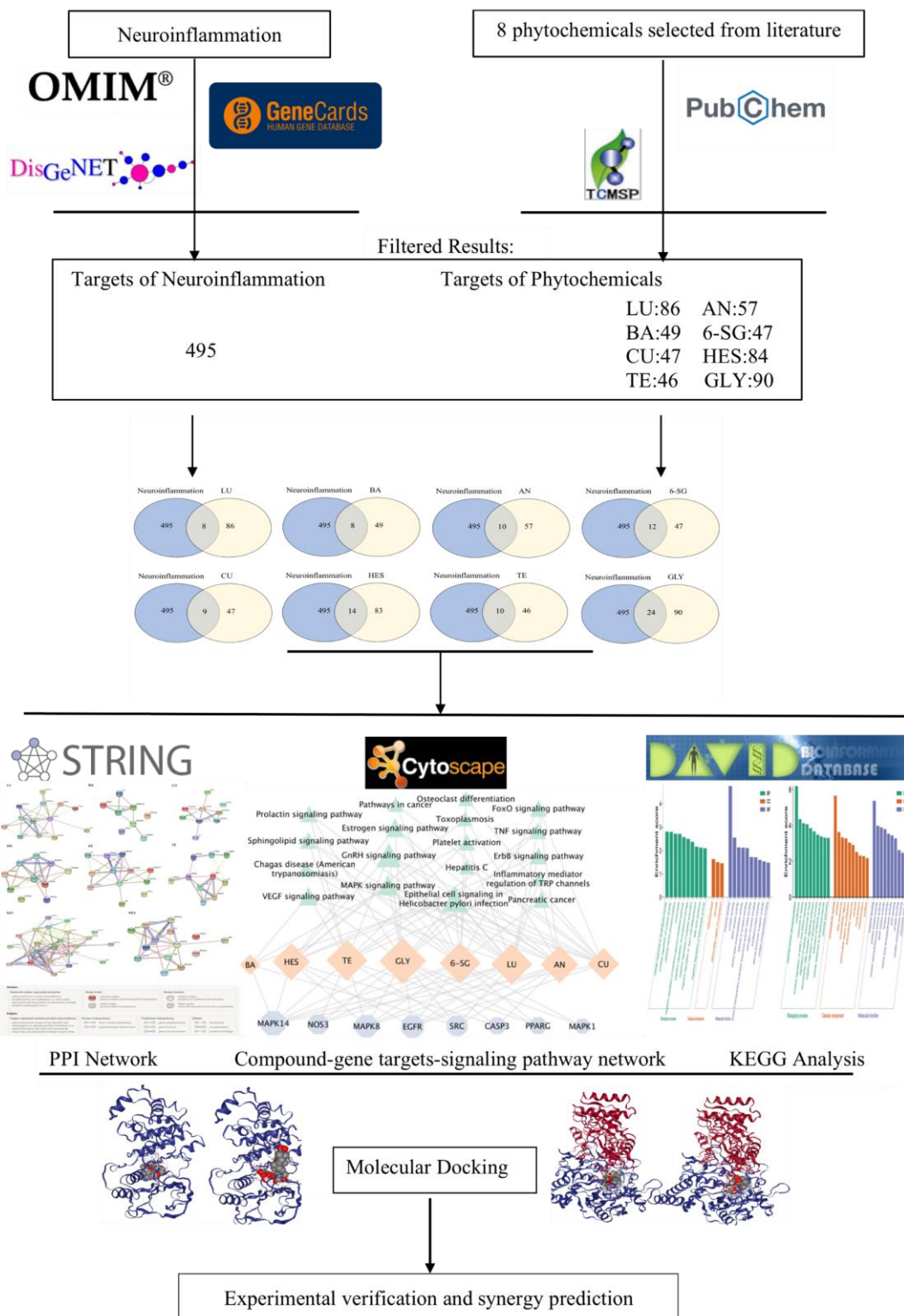
Figure 3.1 Workflow of the study from network pharmacology analysis, molecular docking to experimental investigations.

Our results showed that 495 gene targets were associated with neuroinflammation, and the top 100 gene targets were selected to check the intersection genes with each phytochemical. The characteristics of each phytochemical, the number of total gene targets, and the intersections of genes with neuroinflammation are shown in **Table 3.1**. The Venn diagrams for the number of gene targets and intersections of gene targets for each phytochemical are shown in **Figure 3.2**. The drug-like criteria of the eight phytochemicals were set as follows: BBB ≥ −0.3, DL ≥ 0.18, OB ≥ 30% (Gu et al., 2020). As shown in **Table 3.1**, BA was suggested to have the highest drug-like property with OB ≥ 30%, DL ≥ 0.18, and BBB ≥ −0.3. The rest of the herbal compounds did not meet all three criteria, with CU and HES met DL ≥ 0.18, TE showed BBB ≥ −0.3. Interestingly, all the parameters of GLY were below standard, it connects with the highest amount of total gene targets and intersections gene targets associated with neuroinflammation, suggesting its multi-target (non-specific) pharmacological action.
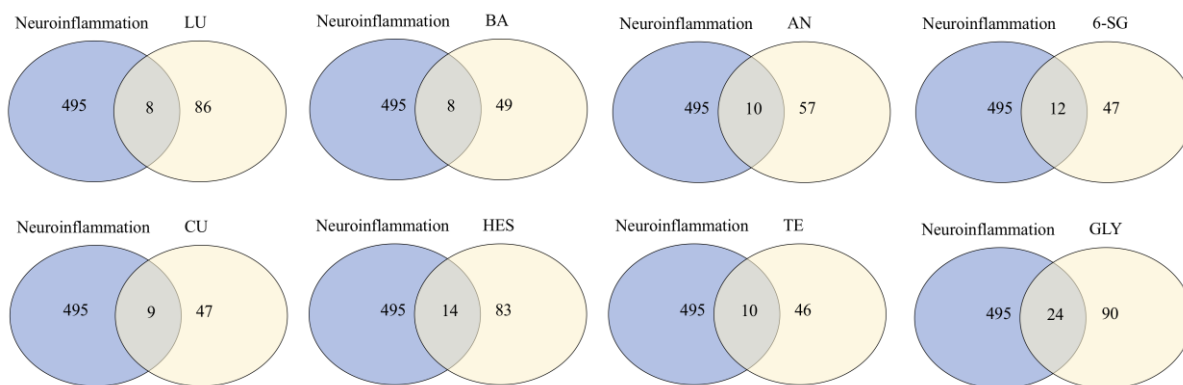
Figure 3.2 Venn diagram of the number of relevant gene targets of eight phytochemicals and neuroinflammation.

Table 3.1 Characteristic pharmacological actions of eight phytochemicals with potential anti-neuroinflammatory activity.

Phytochemicals	Molecular formula	Molecular weight (g/mol)	OB	DL	BBB	Number of the total gene targets	Intersections gene targets with neuroinflammation
LU	$C_{15}H_{10}O_6$	286.24	36.16	0.25	-0.84	86	8
BA	$C_{15}H_{10}O_5$	270.24	33.52	0.21	-0.05	49	8

AN	$C_{20}H_{30}O_5$	350.45	53.44	0.35	-0.94	57	10
6-SG	$C_{17}H_{24}O_3$	276.37	31.00	0.14	0.49	47	12
CU	$C_{21}H_{20}O_6$	368.38	5.15	0.41	-0.76	47	9
HES	$C_{28}H_{34}O_{15}$	610.18	13.33	0.67	-2.70	83	14
TE	$C_{38}H_{42}N_2O_6$	622.70	26.64	0.10	0.44	46	10
GLY	$C_{42}H_{62}O_{16}$	822.90	19.62	0.11	-2.86	90	24

3.2.2 PPI network construction and analysis

The phytochemicals-disease PPI interaction network for each of the eight phytochemicals were created using the STRING database (**Figure 3.3**). In the PPI network, GLY displayed the most interactive PPI network constructed by 24 nodes and 89 edges, with the averaged node degree at 7.42. It was followed by HES (nodes: 14, edges: 32), LU (nodes: 13, edges: 30), 6-SG (nodes: 12, edges: 26) and AN (nodes: 10, edges: 23). BA, CU and TE all showed 8, 9 and 10 nodes and the average node degrees were under 4, respectively.

LU BA CU

AN 6-SG TE

GLY HES
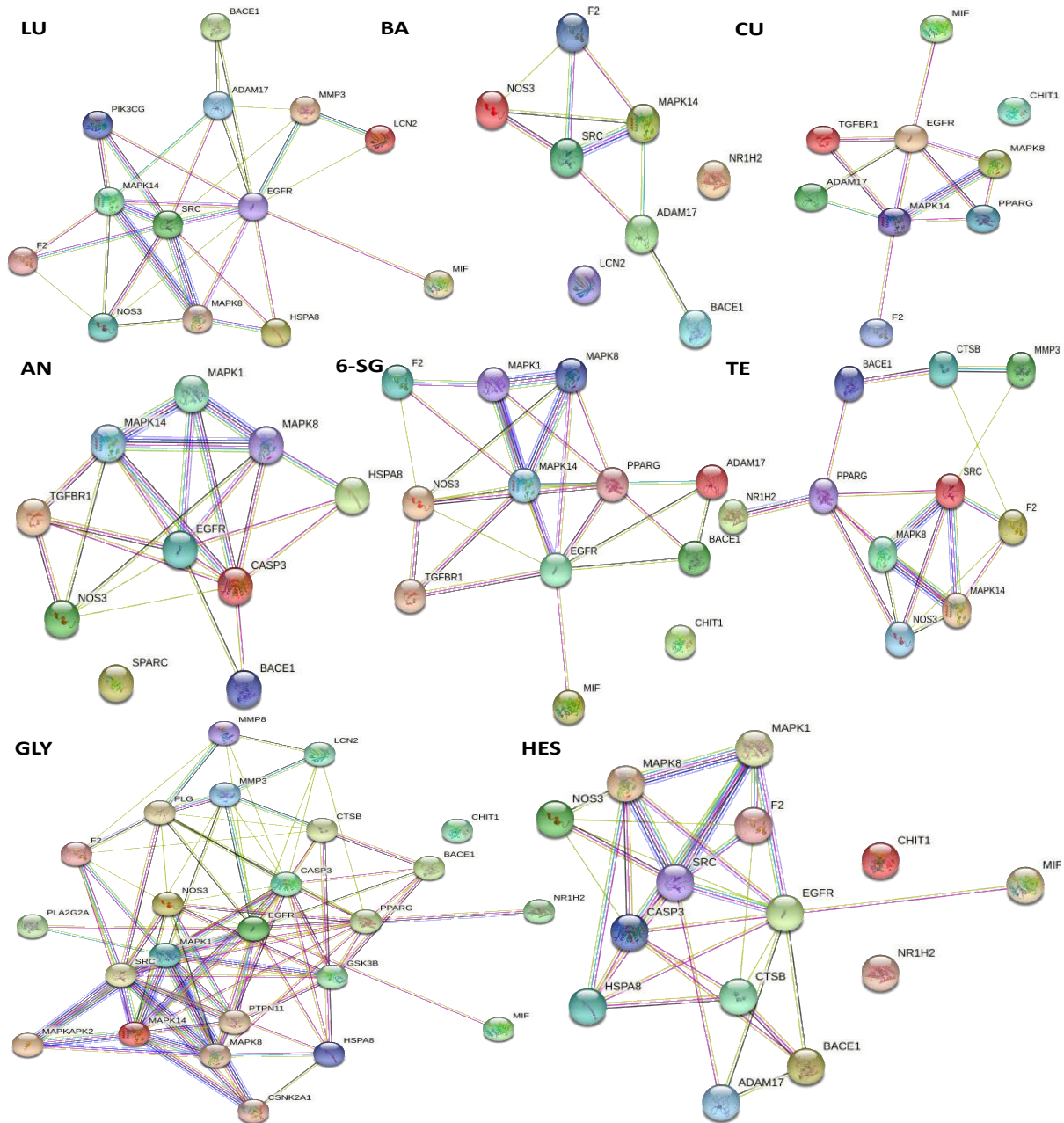
Nodes:

Network nodes represent proteins

splice isoforms or post-translational modifications are collapsed, i.e. each node represents all the proteins produced by a single, protein-coding gene locus.

Node Color

colored nodes:
query proteins and first shell of interactors

white nodes:
second shell of interactors

Node Content

empty nodes:
proteins of unknown 3D structure

filled nodes:
some 3D structure is known or predicted

Edges:

Edges represent protein-protein associations

associations are meant to be specific and meaningful, i.e. proteins jointly contribute to a shared function; this does not necessarily mean they are physically binding to each other.

Known Interactions

from curated databases

experimentally determined

Predicted Interactions

gene neighborhood

gene fusions

gene co-occurrence

Others

textmining

co-expression

protein homology

Figure 3.3 The PPI interaction network for eight phytochemicals related to neuroinflammation. The nodes in the figure represent proteins, and the edges represent the interrelationships among proteins.

3.2.3 Analysis of GO enrichment and KEGG pathways

The GO and KEGG pathway analysis were conducted to investigate the associated protein targets and signaling pathways (**Appendix 2** and **Appendix 3**). A total of 202 GO entries were identified for all the phytochemicals. The top 10 significantly enriched terms of each phytochemical in the BP, MF, and CC categories are listed in **Appendix 2**.

The top 20 KEGG pathways of each phytochemical are shown in **Appendix 3**. The KEGG pathways of LU, AN, 6-SG, HES and GLY showed various patterns of distribution. TE only showed 11 KEGG pathways, and the pathways were at comparable degrees with no apparent distinction. CU and BA showed 9 and 3 pathways, respectively. The top common pathway among all eight phytochemicals was identified as the MAPK signaling pathway.

3.2.4 Construction of compound-gene targets-signaling pathway network

The network of the eight phytochemicals was constructed with 34 nodes and 99 edges (**Figure 3.4**). The statistical analysis from the network showed that GLY was connected with the highest number of genes and signaling pathways (17 nodes and 16 edges). The top five gene targets assessed by the number of connections and degrees for the eight phytochemicals network included MAPK14, MAPK8, NOS3, EGFR and SRC. The top common KEGG pathway was the MAPK signaling pathway. It was noticed that the network clearly displayed a multi-targeted pattern of each phytochemical that has been associated with multiple genes and signaling pathways, and they also have crosstalk as reflected by the overlapping gene targets and signaling pathways.
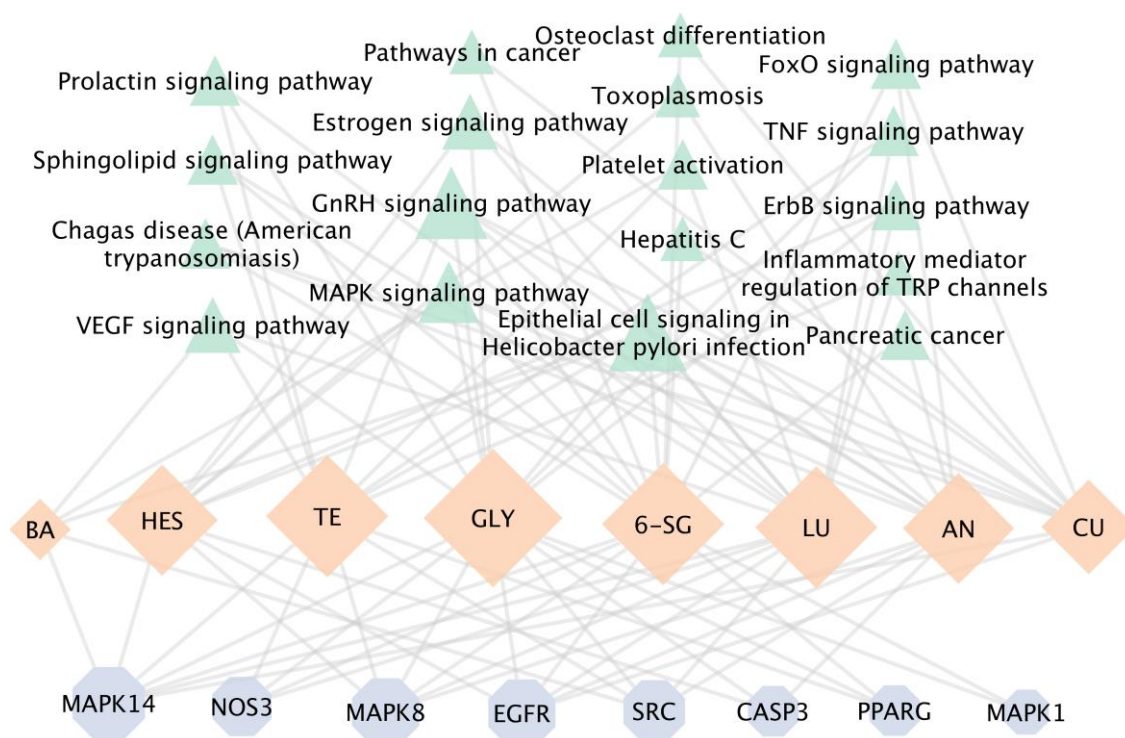
Figure 3.4 The compound-gene targets-signaling pathway network of the eight phytochemicals related to neuroinflammation. Orange nodes represent each phytochemical, blue nodes refer to gene targets, and the green nodes display the KEGG pathway. The size of each node represents its degree in the network. The gray connecting lines reflect that each node is interconnected.

3.3 Molecular docking analysis

Based on the network pharmacology analysis, MAPK14 and NOS3 were the top two hub gene targets for all the eight phytochemicals. In order to verify this analysis, molecular docking was performed to evaluate the binding affinity of each phytochemical on the proteins of MAPK14 and NOS3 using CB-dock method. The protein-ligand binding of each phytochemical on MAPK and NOS3 are shown in **Figure 3.5A** and **3.5B**, respectively. The Cavity size and Affinity were evaluated using CB-Dock. The Centre represents the docking pocket centre coordinates. The size parameters x, y, and z represent the directions of the docking pocket.
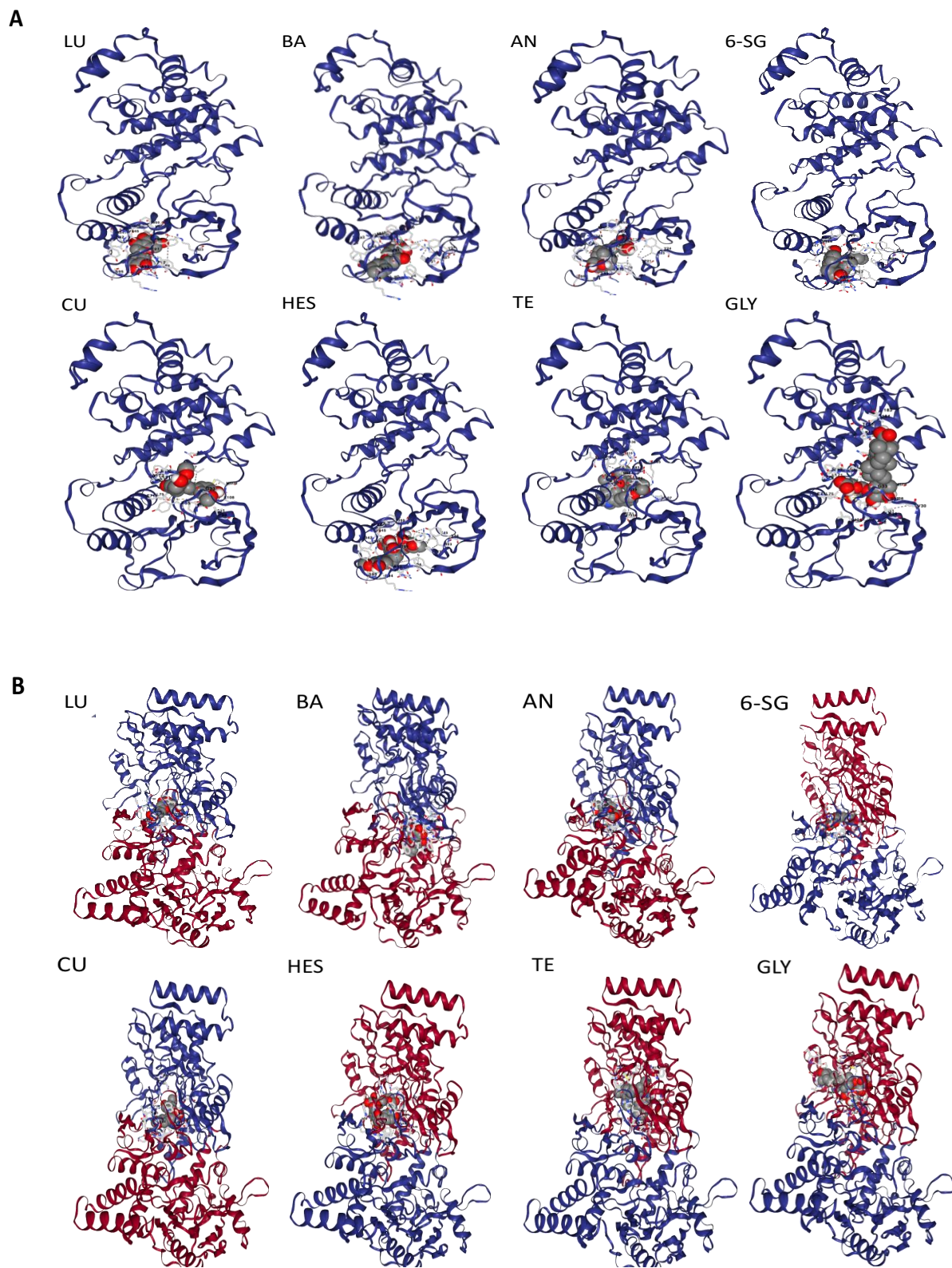
Figure 3.5 Molecular docking analysis of the eight phytochemical candidates with MAPK14 (A) and NOS3 (B) analysed by CB dock.

The relevant indices including affinity, cavity size, and binding location (center and size) for MAPK14 and NOS3 are shown in **Table 3.2** and **3.3**, respectively. The binding energy <-5 kcal/mol was considered as the high affinity between the disease and the target (Shi Y, et al., 2021). Herein, the binding affinity of the eight phytochemical candidates with MAPK14 and NOS3 are all less than -5, suggesting high affinity (Shi et al., 2021). Particularly, GLY and HES had better binding activities with MAPK14 (affinity<-10) than other phytochemicals, and TE showed the most effective binding with iNOS (affinity<-10).

Table 3.2 Binding indices of the eight phytochemicals with MAPK14 analysed by molecular docking.

Chemicals	Affinity (kcal/mol)	Cavity size	Center (x,y,z)	Size (x,y,z)
LU	-9.80	12601	18,9,37	34,34,35
BA	-9.20	12601	18,9,37	34,34,35
AN	-8.60	12601	18,9,37	34,34,35
6-SG	-7.40	12601	18,9,37	34,34,34
CU	-8.80	12601	18,9,37	34,34,35
HES	-10.10	12601	18,9,37	34,34,35
TE	-9.60	574	34,9,22	23,23,23
GLY	-10.10	574	34,9,22	30,30,30

Table 3.3 Binding indices of the eight phytochemicals with NOS3 analysed by molecular docking.

Chemicals	Affinity (kcal/mol)	Cavity size	Center (x,y,z)	Size (x,y,z)
LU	-9.40	12459	17,9,40	35,35,35
BA	-9.50	12459	17,9,40	35,35,35
AN	-8.10	12459	17,9,40	35,35,35
6-SG	-7.70	12459	17,9,40	35,35,35
CU	-9.00	12459	17,9,40	35,35,35
HES	-10.20	12459	17,9,40	35,35,35
TE	-10.30	12459	17,9,40	35,35,35
GLY	-10.20	12459	17,9,40	35,35,35

3.4 Conclusion

The network pharmacology results showed eight phytochemicals LU, BA, AN, 6-SG, CU, HES, TE and GLY have the top five hub genes against neuroinflammation, including MAPK14, MAPK8, NOS3, EGFR and SRC. The top common KEGG pathway was the MAPK signaling pathway. The molecular docking analysis demonstrated each phytochemical have a strong binding affinity to bind with MAPK and iNOS.

Chapter 4: Identification of Synergistic Combinations in LPS-induced N11 cells

4.1 Introduction

Neuroinflammation refers to an inflammatory reaction with excessively expressed pro-inflammatory cytokines including IL-6, TNF, and small-molecule messengers such as NO produced by innate immune cells in the CNS (Milatovic, et al., 2017). Combination therapy is an emerging intervention for treating complicated disorders such as neuroinflammation through a synergistic approach (Zhou X, et al., 2016). Synergy in pharmacodynamics investigations refers to a beneficial interaction between two or more compounds on the same therapeutic target or receptor that results in an overall therapeutic benefit that is higher than the sum of the individual effects (Zhou X, et al., 2016). A combination treatment synergy effect has more excellent bioactivity, multi-target behaviour, and reducing side effects or toxicity with a lower dosage from each component (Liebner et al., 2018). The interaction (synergism, addition, or antagonism) of combinations is examined in this work using the CI model (Chou T.-C., 2018).

This chapter reports the results of identifying synergistic phytochemicals in combination in inhibiting pro-inflammatory mediators including NO, IL-6 and TNF-α on LPS-induced N11 cells. The observed synergy in the combinations AN-SG and BA-SG was demonstrated by the CI values and isobologram graph. We have also demonstrated the associated mechanisms of synergy which was partly associated with downregulated p38MAPK and iNOS protein expressions based on the network pharmacology analysis shown previously in Chapter 3.

4.2 Identification of potential synergy among eight phytochemicals against neuroinflammation

4.2.1 Cytotoxicity of single phytochemical detected by Alamar Blue assay

Alamar blue assay was conducted to examine the cytotoxicity of the eight phytochemicals on N11 cells. Among them, TE exhibited cytotoxicity from 10 µM (7.78 µg/mL), and HES, LU and CU showed cytotoxicity when the concentration was above 50 µM (30.50, 14.31 and 18.41 µg/mL, respectively). In

contrast, AN, BA, 6-SG and GLY did not induce any cytotoxicity with concentration up to 100 µM (35.04, 27.02, 27.64 and 82.29 µg/mL, respectively) (**Figure 4.1**).

4.2.2 NO inhibitory activity of single phytochemical on LPS-induced N11 cells

The stimulation of LPS led to an excessive amount of NO at 24.48 ± 0.21 ng/mL ($p<0.0001$ *vs.* blank control: 0.41 ± 0.12 ng/mL). All phytochemicals lowered LPS-induced NO expression levels in a dose-dependent manner in N11 cells (**Figure 4.1**). Based on the dose-response curves, the IC_{50} values for each active phytochemical were analysed by GraphPad prism 9. Among all the phytochemicals, AN showed the highest potency (IC_{50}=14.88 µM, 5.22 µg/ mL), followed by 6-SG (IC_{50}=15.02 µM, 4.15 µg/mL), LU (IC_{50}=17.24 µM, 4.94 µg/ mL), BA (IC_{50}=20.30 µM, 5.49 µg/ mL), TE (IC_{50}=27.70 µM,17.25 µg/ mL), CU (IC_{50}=55.80 µM, 20.54 µg/ mL), HES (IC_{50}=60.06 µM, 36.61 µg/ mL). It was noticed that GLY did not exhibit any obvious NO inhibition within the tested concentrations, and the IC_{50} value was estimated to be 269 µM, 221.54 µg/ mL. In **Table 4.1**, among the eight phytochemicals, BA therapeutic index have the highest value as 6.72, followed by 6-SG, LU and AN therapeutic index as 6.66, 5.80 and 4.93, then the HES has the lowest therapeutic index value as 0.37.
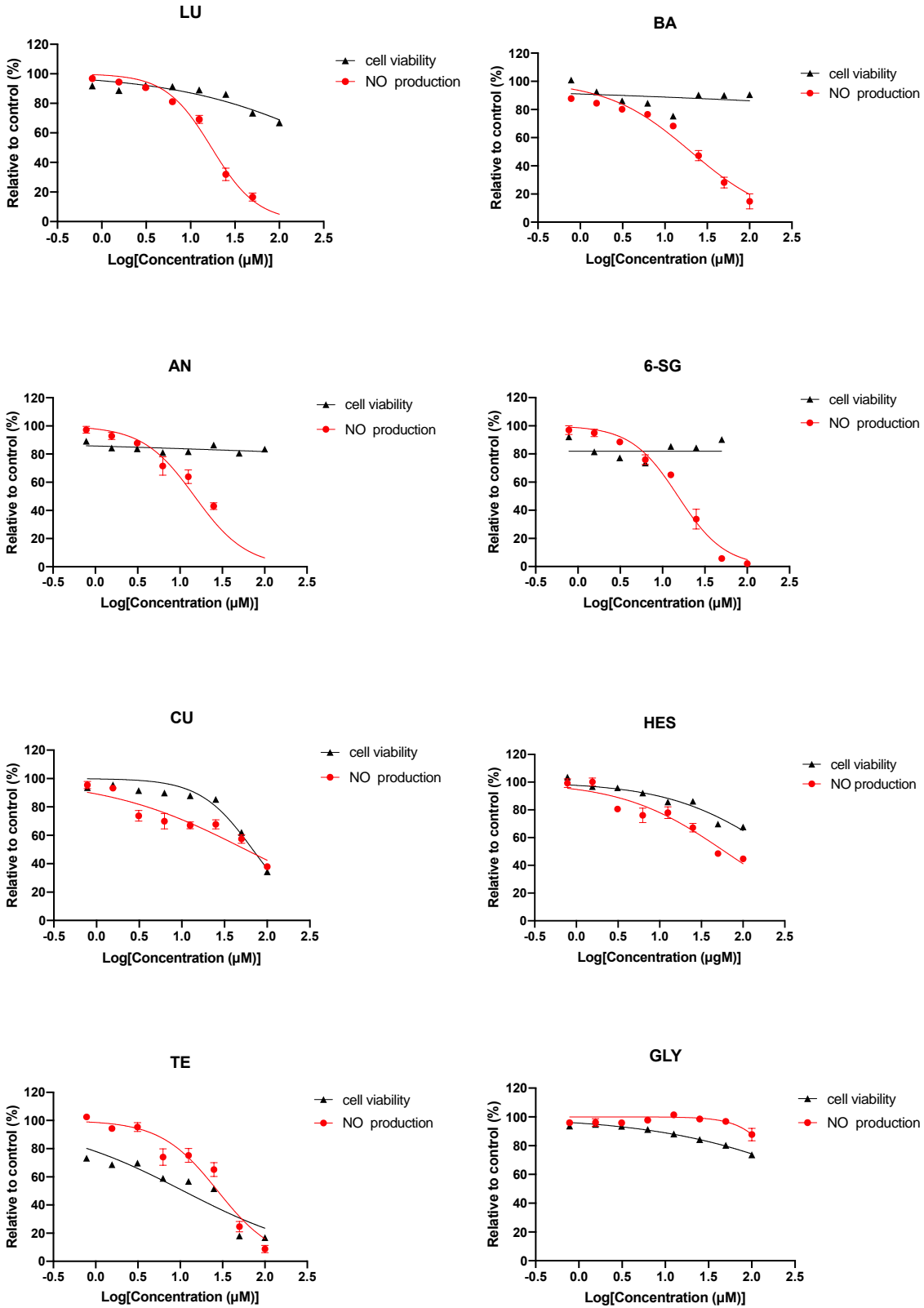
Figure 4.1 NO production of LU, BA, AN, 6-SG, CU, HES, TE and GLY in LPS-activated N11 microglial cells. Data are shown as mean ± SEM (n > 3). Figures generated by Graph pad prism 9.0.

Table 4.1 IC$_{50}$ values of single phytochemicals in inhibiting LPS-induced NO in N11 cells (µM), n≥3.

Phytochemicals	LU	BA	AN	6-SG	TE	CU	HES	GLY
Averaged IC$_{50}$ (µM)	17.24 ± 1.51	20.30 ± 3.10	14.88 ± 3.38	15.02 ± 1.67	27.70 ± 5.11	55.80 ± 24.32	60.06 ± 22.60	>269.00
Averaged LC$_{50}$ (µM)	100*	100*	100*	100*	10.87 ± 5.33	67.71 ± 7.41	100.00*	100.00*
Therapeutic index	>5.80	>6.72	>4.93	>6.66	0.39	1.67	>0.37	>1.21

*No obvious cytotoxicity was observed within tested concentrations (0-100 µM), and thus the LC$_{50}$ values were set as their highest testing concentration 100 µM.

4.3 Determination of anti-neuroinflammatory activity of pair-wised combinations

4.3.1 Measurement of NO formation using the Griess assay

The paired combinations of the eight phytochemicals were tested in LPS-induced N11 cells. Our results showed that two paired combinations, AN-SG and BA-SG (0.39-100 µM), appeared to be more potent than their individuals, and the enhanced NO inhibitory activities were not associated with cytotoxicity (**Figure 4.2**).
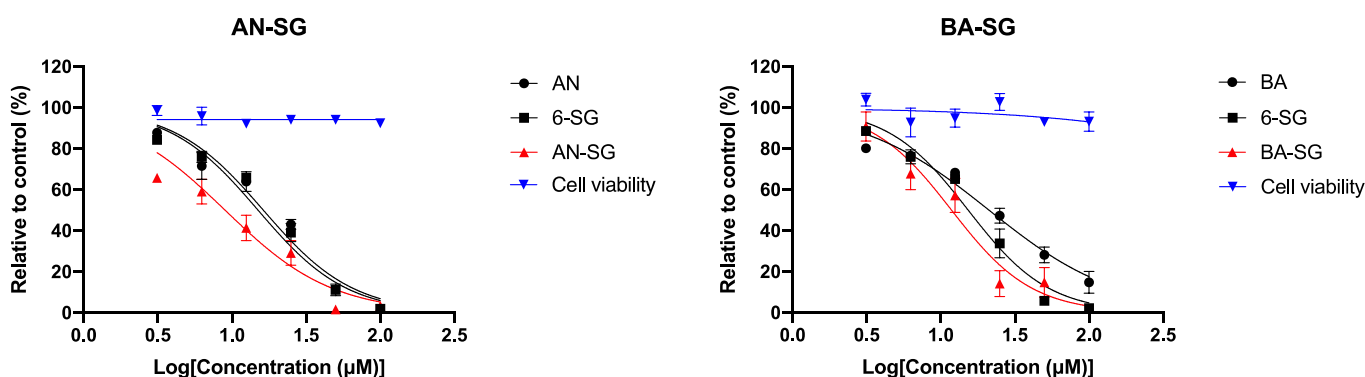
Figure 4.2 AN-SG and BA-SG combinations inhibitory effects on LPS-induced NO production and cell viability in N11 cells. (A) AN, 6-SG, and AN-SG dose-dependently inhibited LPS-induced NO production and cell viability in N11 cells (n≥3). (B) BA, 6-SG, and BA-SG dose-dependently inhibited LPS-induced NO production and cell viability in N11 cells (n≥3).

The rest of pair-wised combinations did not show higher potencies than their individual components (**Figure 4.3**). Alamar blue assay was conducted to test the cytotoxicity of the combinations on N11 cells. LU-HES exhibited the highest cytotoxicity (LC_{50}=0.39 µM) followed by LU-TE (LC_{50} = 19.26 µM), LU-SG (LC_{50} = 27.05 µM), CU-TE (LC_{50} = 33.21 µM), LU-CU (LC_{50} = 50.45 µM), AN-CU (LC_{50} = 60.91 µM) and BA-CU (LC_{50} = 95.99 µM). Combinations LU-AN, LU-BA, BA-HES, BA-TE, AN-BA, AN-HES, AN-TE and TE-SG did not display any obvious cytotoxicity from 0.78-100 µM.

All combinations lowered LPS-induced NO expression levels in a dose-dependent manner in N11 cells (**Figure 4.2** and **4.3**). Among all the combinations, AN-SG exhibited the highest potency (IC_{50} = 9.12 ±

64

2.95 µM), followed by BA-SG (IC_{50} = 12.02 ± 2.99 µM). The IC_{50} values of most combinations fell in the range of 12.50-57.16 µM. Three combinations did not show any significant NO inhibitory activities, including CU-SG ($IC_{50} \geq 146$ µM), BA-CU ($IC_{50} \geq 163.3$ µM), and SG-TE ($IC_{50} \geq 1106$ µM).
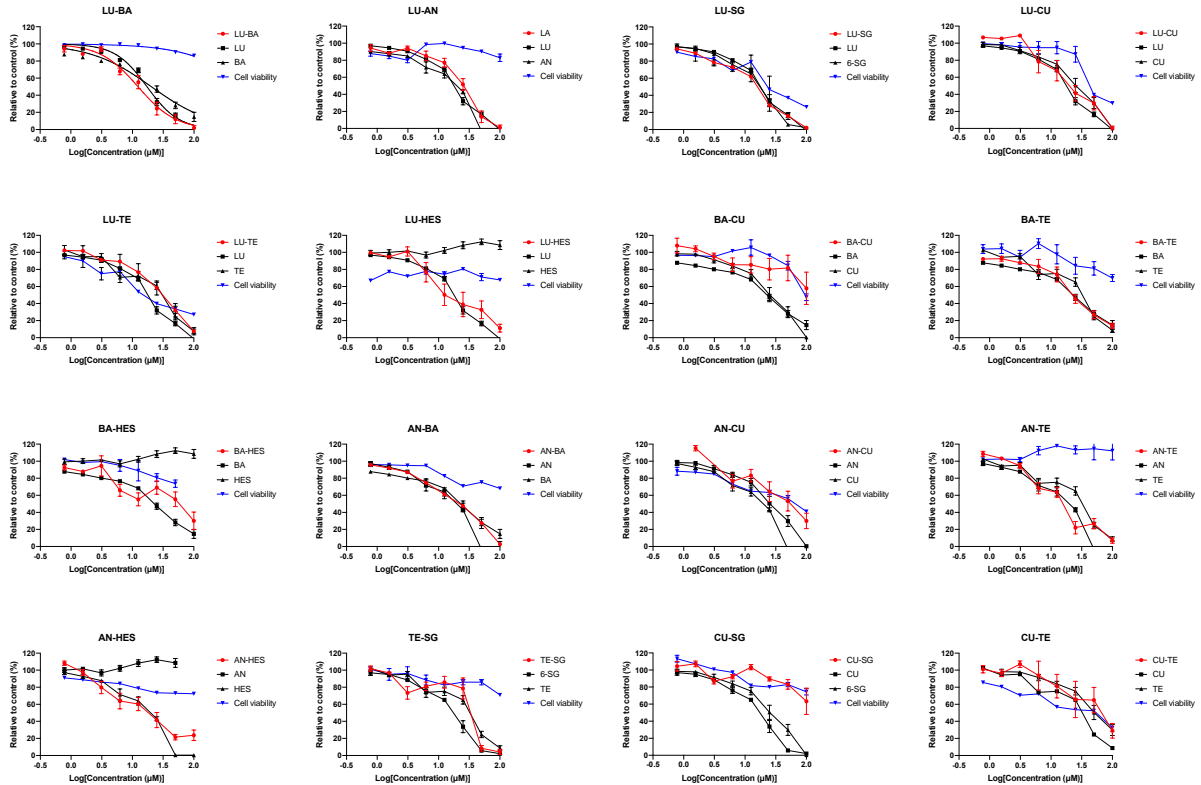
Figure 4.3 The dose-response curves of paired combinations and their corresponding component of eight phytochemicals that dose-dependently inhibited NO and cell viability of in LPS-induced N11 cells (n≥3).

As shown in the **Table 4.2**, AN-SG showed the highest therapeutic index, which was 10.96, followed by BA-SG (therapeutic index=8.32). LU-HES and CU-TE displayed the lowest therapeutic index, which were 0.02 and 0.58, respectively. In **Figure 4.4**, all combinations exhibited no or weak synergistic effect on inhibiting NO production in LPS-induced microglia cells.

Table 4.2 IC_{50} and LC_{50} values of pair-wised combinations in inhibiting LPS-induced NO in N11 cells (μM), n≥3.

Phytochemicals	IC_{50} (μM)	LC_{50} (μM)	Therapeutic index
LU-AN	23.00 ± 4.26	100*	>4.35
LU-AB	12.50 ± 2.69	100*	>8.00
LU-SG	15.73 ± 3.23	27.05	1.72
LU-TE	29.00 ± 8.63	19.26	0.66
LU-CU	21.00 ± 7.06	50.45	2.40
LU-HES	17.77 ± 9.14	0.39	0.02
AN-BA	18.98 ± 4.36	100*	>5.27
AN-SG	9.12 ± 2.95	100*	>10.96
AN-TE	14.62 ± 3.94	100*	>6.84
AN-CU	48.19 ± 33.72	60.91	1.26
AN-HES	17.55 ± 6.94	100*	>5.63
BA-HES	42.01 ± 93.19	100.00*	>2.38
BA-CU	>100.00	95.99	0.95
BA-SG	12.02 ± 2.99	100*	>8.32
BA-TE	24.06 ± 7.02	100*	>4.16
TE-SG	>100.00	100*	>1.00
CU-TE	57.16 ± 77.64	33.21	0.58
CU-SG	>100.00	100*	>1

*No obvious cytotoxicity was observed within tested concentrations (0-100 μM), and thus the LC_{50} values were set as their highest testing concentration 100 μM.
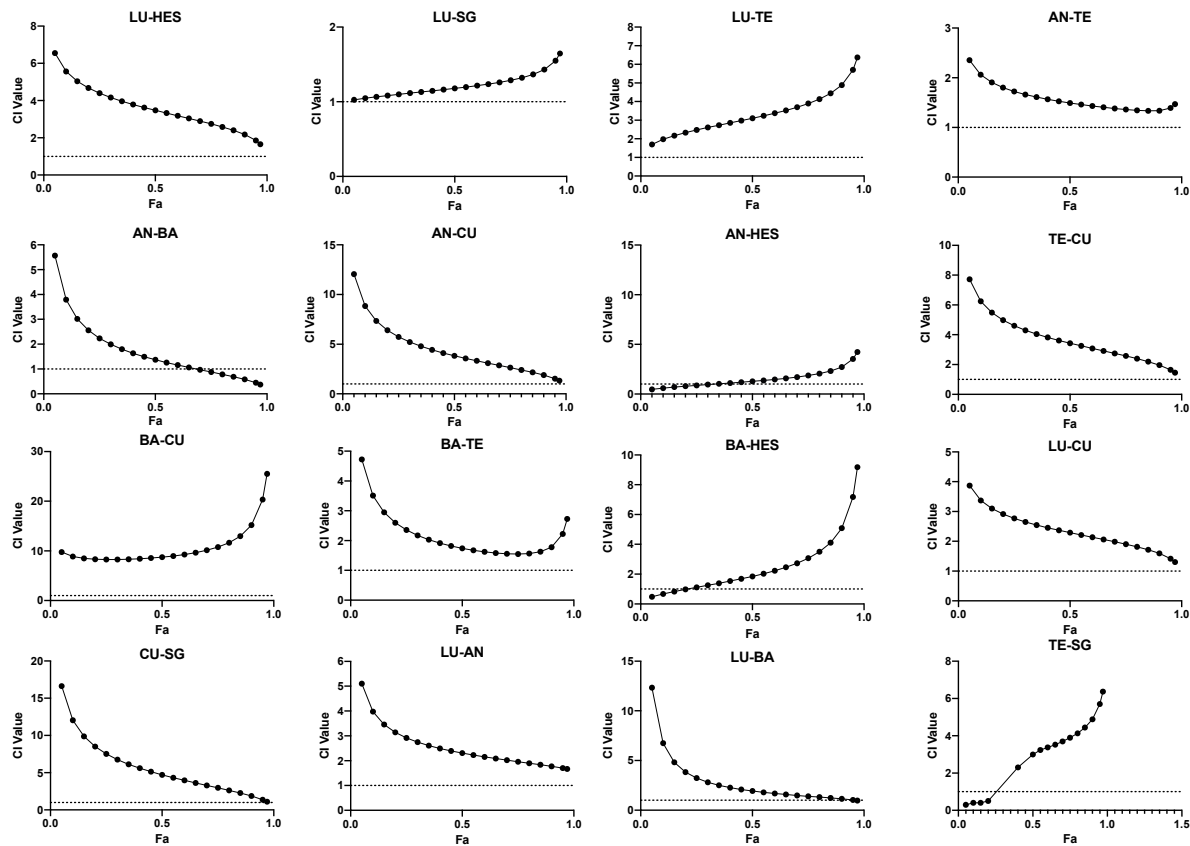
Figure 4.4 The synergistic NO inhibitory effect of combinations was determined by the CI-Fa curves. CI values represent the interaction in the combinations, with CI < 1, CI = 1 and CI > 1 referring to synergy, addition and antagonism, respectively. Fa on the X-axis is defined as the fraction effect level, and herein it refers to the NO inhibitory effect, respectively.

4.3.2 Synergistic determination of AN-SG and BA-SG

The CI model was then performed to evaluate whether the enhanced activity in the combination is synergy. The CI-Fa curve (**Figure 4.5A**) displayed a strong synergy of the AN-SG combination in inhibiting NO, with CI values ranging from 0.39 to 0.99 when the Fa was above 0.20 (20%–97% NO inhibitory effect). The isobologram (**Figure 4.5B**) also supported the observed synergy of AN-SG in reducing LPS-stimulated NO when Fa values were at 0.50 (representing 50% of the NO inhibition).

The CI model also revealed a synergistic interaction of BA and 6-SG when used together to suppress NO (**Figure 4.5C**). At the concentration range of 3.89 - 8.56 µg/mL, a synergistic effect (CI<1) was observed

with CI values ranging from 0.09 to 0.99 when the Fa was over 0.45 (45%-97% NO inhibitory effect). When Fa values were at 0.5 (representing 50% of the NO inhibition), the isobologram in **Figure 4.5D** further corroborated the reported synergy of BA-SG in decreasing LPS-stimulated NO.
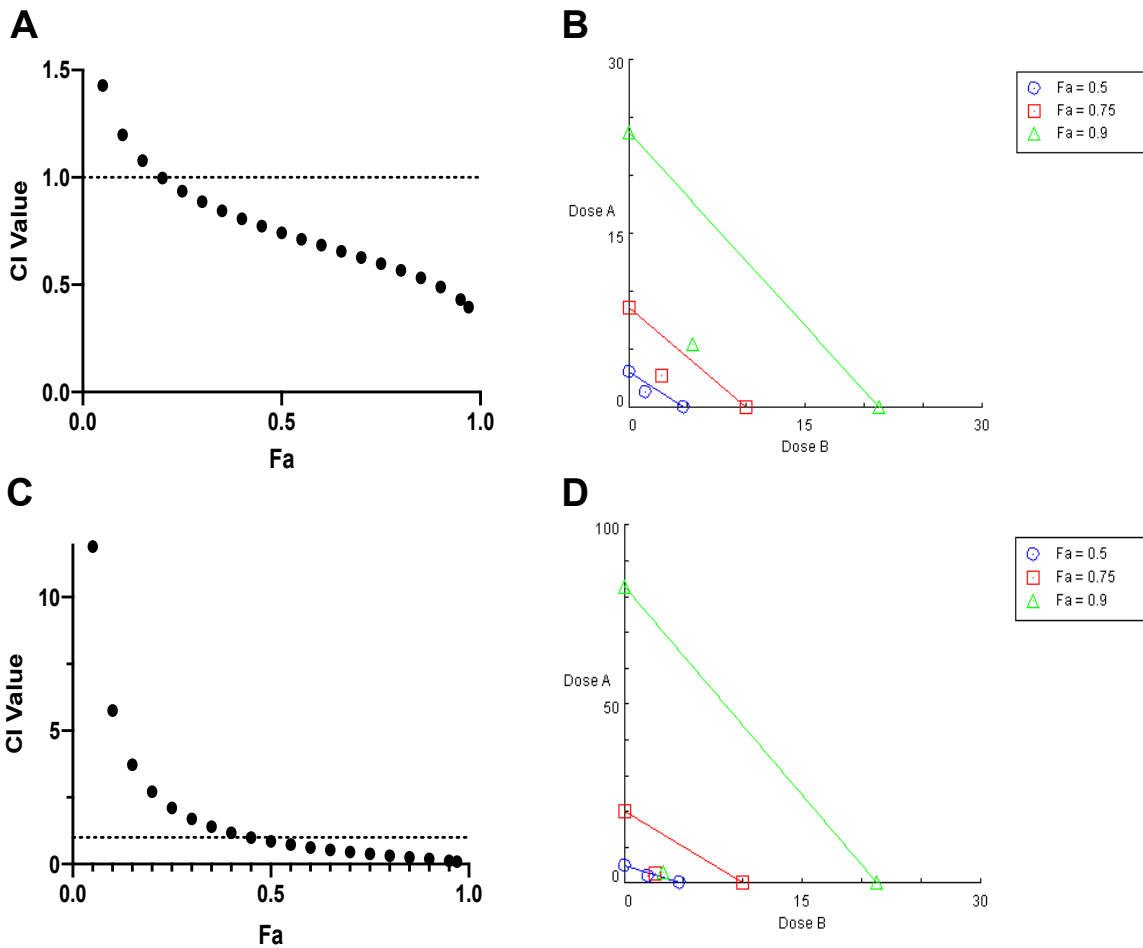
Figure 4.5 AN-SG and BA-SG combinations exhibited synergistic inhibitory effects on LPS-induced NO production in N11 cells. (A) The synergistic NO inhibitory effect of AN-SG was determined by the CI-Fa curves. CI values represent the interaction in AN-SG, with CI < 1, CI = 1 and CI > 1 referring to synergy, addition and antagonism, respectively. Fa on the X-axis is defined as the fraction effect level, and herein it refers to the NO inhibitory effect, respectively. (B) Isobologram analysis of AN-SG in NO inhibition when the default set of Fa values at 0.50, 0.75 and 0.9. (C) The synergistic NO inhibitory effect of BA-SG was determined by the CI-Fa curves. CI values represent the interaction in BA-SG, with CI < 1, CI = 1 and CI > 1 referring to synergy, addition and antagonism, respectively. Fa on the X-axis is defined as the fraction effect level, and herein it refers to the NO inhibitory effect, respectively. (D) Isobologram analysis of BA-SG in NO inhibition when the default set of Fa values at 0.50, 0.75 and 0.9.

4.3.3 Synergistic inhibitions of IL-6 and TNF-α productions by AN-SG and BA-SG on mono-cultured N11 cells

The IL-6 and TNF-α inhibitory effects of AN-SG were tested in LPS-induced mono-cultured N11 cells against their individual components. In **Figure 4.6A** and **4.5D**, LPS-stimulated cells demonstrated significantly increased amounts of IL-6 (12.29 ± 1.13 ng/mL $vs.$ 2.06 ± 0.08 ng/mL, $p<0.0001$) and TNF-α (78.52 ± 0.35 ng/mL $vs.$ 14.25 ± 0.14 ng/mL, $p<0.0001$) compared to that of the blank control. All the individual and combined treatments suggested dose-dependent reductions of IL-6 and TNF-α compared to that of LPS (all $p<0.0001$) on mono-cultured N11 cells. AN-SG (0.39-100 µM) appeared to be more potent than their individuals used alone at all tested concentrations. The IC_{50} value of AN-SG in inhibiting IL-6 was determined to be 1.18 ± 0.38 µM, which was significantly lower than that of AN (3.54 ± 1.19 µM, $p<0.01$) or 6-SG (5.46 ± 1.41 µM, $p<0.01$). Similarly, the IC_{50} value of AN-SG in inhibiting TNF-α was also the lowest (3.47 ± 0.64 µM) compared to that of AN (7.24 ± 1.90 µM, $p<0.05$) or 6-SG (13.93 ± 6.37 µM, $p<0.001$).

At 25 µM, the IL-6 production of AN-SG (2.51 ± 0.81 ng/mL, $p<0.0001$ $vs.$ LPS) was significantly lower than that of AN (4.14 ± 0.71 ng/mL, $p<0.01$) or 6-SG (4.28 ± 0.77 ng/mL, $p<0.01$). The TNF-α release of AN-SG (24.76 ± 1.41 ng/mL, $p<0.0001$ $vs.$ LPS) was also significantly lower than that of AN (34.22 ± 3.14 ng/mL, $p<0.05$) or 6-SG (44.89 ± 2.63 ng/mL, $p<0.001$) at 25 µM. Thus, this concentration was selected for AN, 6-SG and AN-SG to be tested in the tri-culture system.

The CI model was then performed to evaluate whether the enhanced activity of the AN-SG combination was due to a synergistic interaction. In **Figure 4.6B**, the CI values ranged from 0.24 to 0.97 when the Fa was above 0.15 (15%–97% IL-6 inhibitory effect), suggesting a strong synergy of AN-SG combination in inhibiting IL-6. The isobologram (**Figure 4.6C**) also suggested a synergistic interaction between AN and 6-SG in reducing LPS-stimulated IL-6 with Fa values at 0.50, 0.75 and 0.9 (representing 50%, 75% and 90% of the IL-6 inhibition). Similarly, in the **Figure 4.6E**, AN-SG synergistically inhibited TNF-α with CI

values ranging from 0.56 to 0.97 when the Fa was above 0.4 (40%–97% TNF-α inhibitory effect). The results of the isobologram (**Figure 4.6F**) also supported this finding with Fa values at 0.50, 0.75 and 0.9.
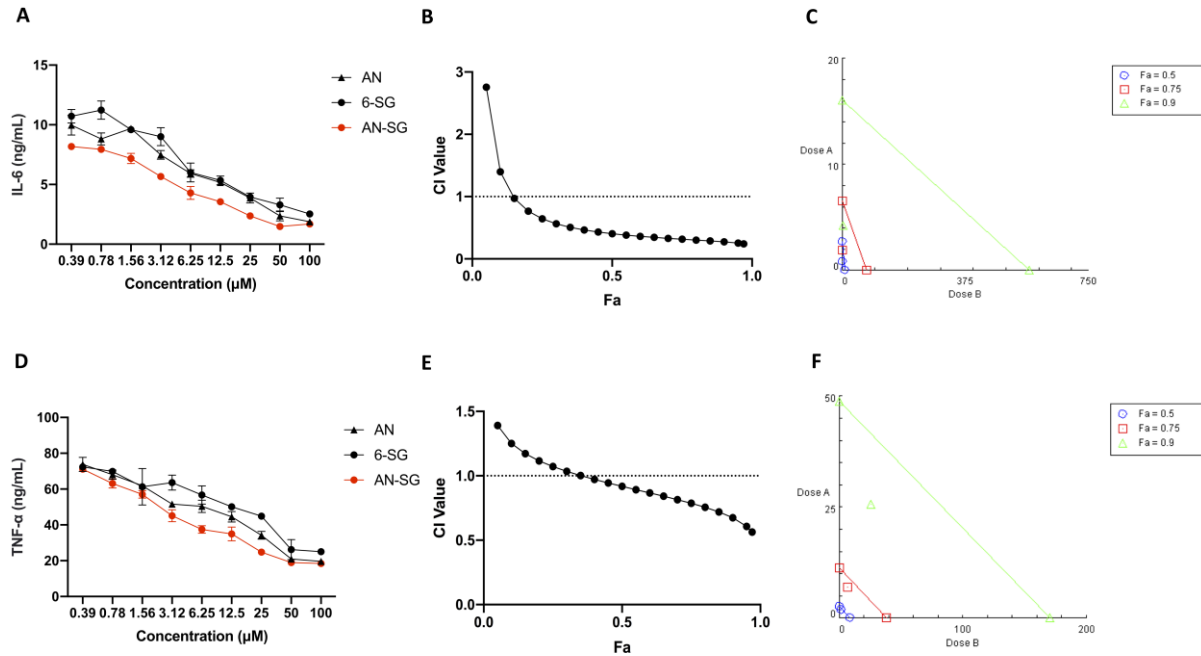
Figure 4.6 The AN-SG combination exhibited synergistic effects on inhibition of LPS-induced IL-6 and TNF-α productions on mono-cultured N11 cells. AN, 6-SG, and AN-SG dose-dependently inhibited LPS-induced IL-6 (A) and TNF-α (D) in N11 cells (n=3). The synergistic IL-6 (B) and TNF-α (E) inhibitory effects of AN-SG were determined by the CI-Fa curves. CI values represent the interaction in AN-SG, with CI < 1, CI = 1 and CI > 1 referring to synergy, addition and antagonism, respectively. Fa on the X-axis is defined as the fraction effect level, and herein it refers to the IL-6 and TNF-α inhibitory effect, respectively. Isobologram analysis of AN-SG in IL-6 (C) and TNF-α (F) inhibition when the default set of Fa values at 0.50, 0.75 and 0.9. Data are shown as mean ± SEM.

The IL-6 and TNF-α inhibitory effects of BA-SG were examined in LPS-induced mono-cultured N11 cells against their individual components. Compared with LPS-stimulation, all the BA, 6-SG and BA-SG produced dose-dependent IL-6 and TNF-α inhibitory effects (**Figure 4.7A** and **4.7D**). The IC_{50} value of BA-SG in inhibiting IL-6 was determined to be 1.44 ± 0.37 μM, which was significantly lower than that of BA (3.65 ± 0.90 μM, $p<0.05$) or 6-SG (5.46 ± 1.41 μM, $p<0.01$). Similarly, the IC_{50} value of BA-SG for the TNF-α inhibition was also the lowest (3.26 ± 1.09 μM) compared to that of BA (6.52 ± 2.93 μM, $p<0.05$) or 6-SG (13.93 ± 6.37 μM, $p<0.01$).

At 25 µM, BA-SG exhibited greater inhibitory effects on the IL-6 (2.47 ± 0.78 ng/mL, *p*<0.0001 *vs.* LPS) compared with BA (4.14 ± 0.63 ng/mL, *p*<0.05) or 6-SG (4.28 ± 0.77 ng/mL, *p*<0.05) alone. The TNF-α reduction by BA-SG was also significantly greater than that of BA (42.08 ± 3.62 ng/mL, *p*<0.05 *vs.* LPS) or 6-SG (44.89 ± 2.63 ng/mL, *p*<0.05) alone at 25 µM. Thus, this concentration was selected for BA, 6-SG and BA-SG to be tested in the tri-culture system.

CI and isobologram models (**Figure 4.7B**, **4.7E**) demonstrated a synergistic effect of BA-SG in inhibiting IL-6 and TNF-α at the concentration range of 0.78-100 µM and 0.39-100 µM (CI<1) were observed. The isobologram also supported the observed synergy of the BA-SG combination in reducing LPS-stimulated IL-6 (**Figure 4.7C**) and TNF-α (**Figure 4.7F**) when Fa values were at 0.50, 0.75 and 0.9.
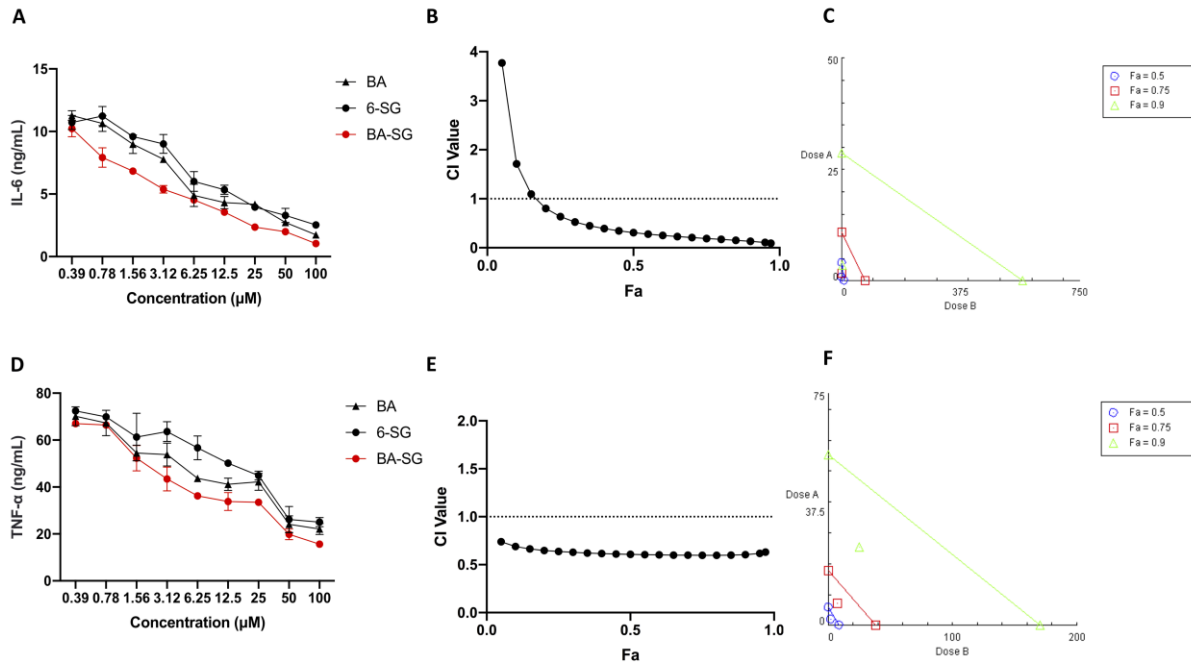
Figure 4.7 The BA-SG combination exhibited synergistic effects on inhibition of LPS-induced IL-6 and TNF-α productions on mono-cultured N11 cells. BA, 6-SG, and BA-SG dose-dependently inhibited LPS-induced IL-6 (A) and TNF-α (D) in N11 cells (n=3). The synergistic IL-6 (B) and TNF-α (E) inhibitory effects of BA-SG were determined by the CI-Fa curves. CI values represent the interaction in BA-SG, with CI < 1, CI = 1 and CI > 1 referring to synergy, addition and antagonism, respectively. Fa on the X-axis is defined as the fraction effect level, and herein it refers to the IL-6 and TNF-α inhibitory effect, respectively. Isobologram analysis of BA-SG in IL-6 (C) and TNF-α (F) inhibition when the default set of Fa values at 0.50, 0.75 and 0.9. Data are shown as mean ± SEM.

4.4 Potential hub gene targets of AN-SG and BA-SG by network pharmacology

The compound-gene targets-signaling pathway networks of the AN-SG (**Figure 4.8A**) and BA-SG (**Figure 4.8B**) combinations in inhibiting NO in relation to downregulated MAPKp38 and iNOS were built to understand the associated mechanisms of their synergistic interaction. As shown in **Figure 4.8**, MAPK14 and NOS3 appeared to be the top overlapping gene targets, and the MAPK signaling pathway is the top overlapping pathway for both paired combinations. Then, the modulatory effects of these two combinations compared with their individual component on MAPK14 and iNOS protein expressions were examined by Western blot assay.

In the Chapter 3, GO enrichment analysis and KEGG map were conducted for each tested phytochemical. Special attention was paid to the hub KEGG pathway for two synergistic combinations, AN-SG and BA-SG, where the crosstalk is likely to occur. In **Appendix 2**, the top common BPs of AN and 6-SG included peptidy-serine phosphorylation; sequence-specific DNA binding transcription factor activity; lipopolysaccharide-mediated signaling pathway; response to stress; positive regulation of cyclase activity. The overlapping BPs for BA and 6-SG included positive regulation of cell growth; lipopolysaccharide-mediated signaling pathway. The common CC was late endosome and caveola in AN and 6-SG, and BA and 6-SG, respectively. There were several common MF involved in both AN and 6-SG including MAP kinase activity; ATP binding, protein serine/threonine kinase activity; protein binding, protein kinase activity and protein phosphatase binding. However, BA and 6-SG only showed enzyme binding as the common MF. In particular, in the **Appendix 3,** showed the overlapping pathway of AN and 6-SG was MAPK signaling pathway, whereas the top common pathway for BA and 6-SG was VEGF signaling pathway. It was noticed that the MAPK signaling pathway had been shown to play a critical role in neuroinflammation (Schnöder et al., 2016).
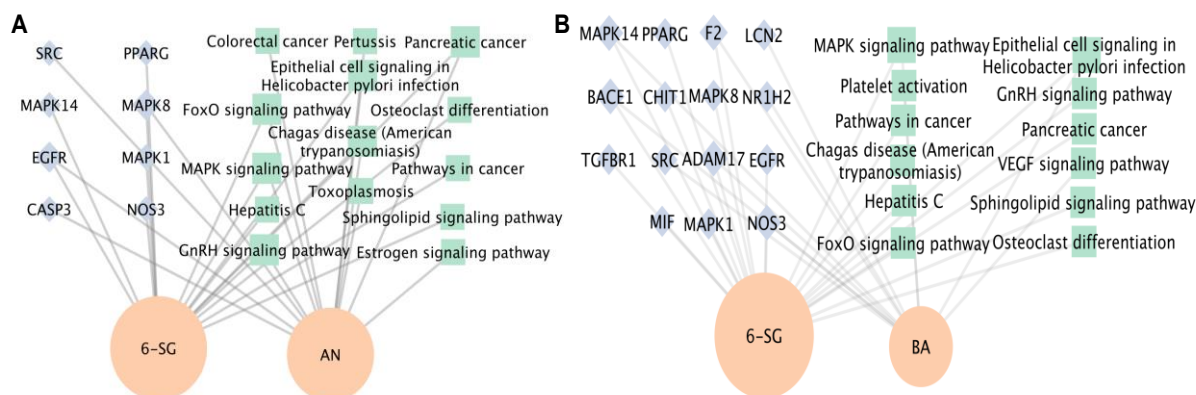
Figure 4.8 Compound-gene targets-signaling pathway networks for the AN-SG (A) and BA-SG (B). The green nodes represent the signaling pathway, the orange nodes represent the phytochemicals, and the blue nodes represent potential common phytochemical targets in neuroinflammation. The size of each label represents its degree.

4.5 The enhanced effect of AN-SG and BA-SG in inhibiting phosphor-MAPKp38/MAPKp38 and iNOS protein expression

To verify the network pharmacology analysis and investigate synergistic mechanism of AN-SG and BA-SG, the protein levels of phosphor-MAPKp38/MAPKp38 (p-p38/p38) and iNOS were investigated.

As shown in **Figure 4.9A** and **4.9B**, the stimulation of LPS (1 μg/mL) led to upregulated expressions of p-p38/p38 ($p<0.0001$) and iNOS ($p<0.001$) in comparison to that of the untreated cells, with fold increases of 2.06 ± 0.22 and 4.16 ± 0.08, respectively. AN was shown to inhibit the increased fold change of p-p38/p38 ($p<0.05$) and iNOS ($p<0.01$). 6-SG also showed potent inhibition of p-p38/p38 ($p<0.01$) and iNOS ($p<0.05$). AN-SG showed potent inhibition of p-p38/p38 ($p<0.05$) and iNOS ($p<0.01$). In addition, the inhibitory effect of the AN-SG combination was greater than that of AN or 6-SG on iNOS ($p<0.05$ *vs*. AN or 6-SG).

The LPS stimulation (1 μg/mL) caused elevated expressions of p-p38/p38 ($p<0.0001$) and iNOS ($p<0.0001$) with fold increases of 2.01 ± 0.21 and 7.07 ± 0.49, respectively, in contrast to that of the untreated cells (Figure **4.9C** and **4.9D**). BA significantly downregulated the fold change of p-p38/p38 ($p<0.05$) and iNOS ($p<0.05$). 6-SG also demonstrated strong suppressions of p-p38/p38 ($p<0.001$) and iNOS ($p<0.05$). BA-SG

had similar inhibitory effects on p-p38/p38 ($p<0.05$) and iNOS ($p<0.05$). However, the combined inhibitory effects were not as strong as that of BA alone.
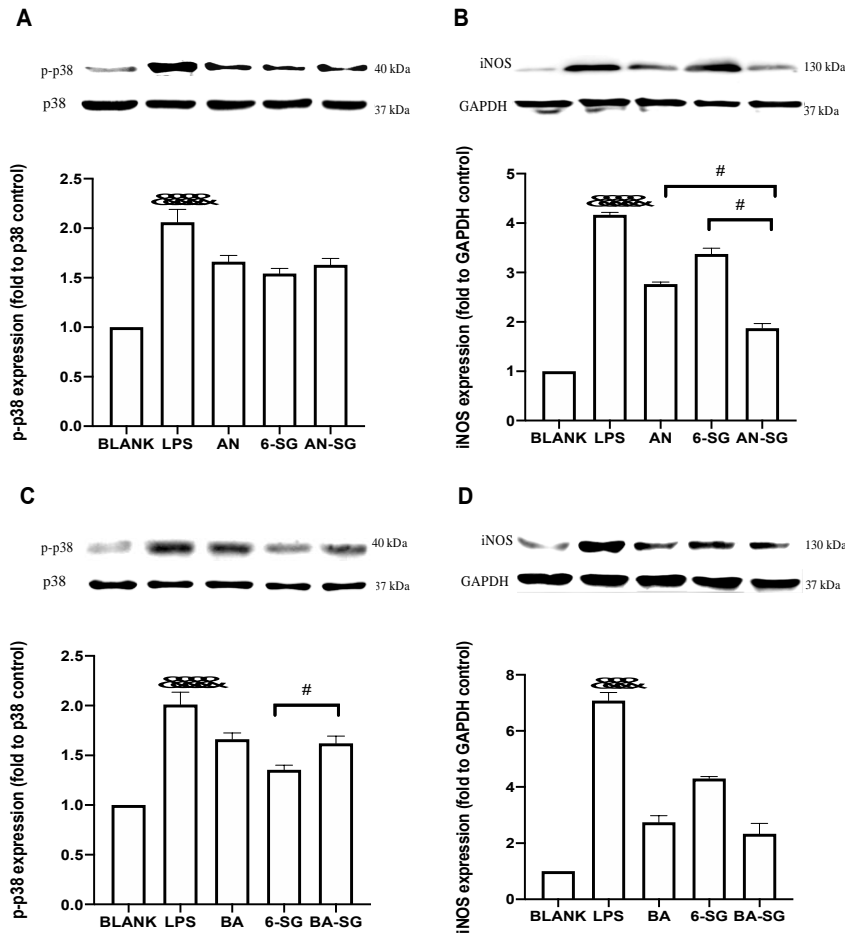
Figure 4.9 Cells were cultured in T75 cell flasks and were pre-treated with AN, BA, 6-SG, AN-SG and BA-SG 1 h prior to LPS (1 μg/mL) for 0.5 hr or 24 hr. Protein expression levels of p-p38/p38 (A, C), iNOS (B, D) were analysed by western blot. All results (n = 3) are expressed as the mean ± SEM, &&&& $p<0.0001$, &&& $p<0.001$ *vs.* BLANK, * $p<0.05$, ** $p<0.01$, *** $p<0.001$, **** $p<0.0001$ *vs.* LPS, # $p<0.05$ *vs.* combination, by one-way ANOVA analysis with Tukey test for group comparison in GraphPad Prism 9.

4.6 Conclusions

The AN-SG and BA-SG combinations showed synergistic effects in inhibiting neuroinflammation mediators, include NO, IL-6 and TNF-α, which have enhanced effects in inhibiting phosphor-MAPKp38/MAPKp38 and iNOS protein expression. Network pharmacology analysis suggested that

MAPK14, MAPK8 and NOS3 are the main gene targets of AN, 6-SG and BA, and the top pathway is the MAPK signaling pathway. The present study provides insight into the synergistic interactions of the AN-SG and BS-SG combinations against neuroinflammation and the associated molecular mechanisms.

Chapter 5: Enhanced Anti-neuroinflammatory Activity of AN-SG and BA-SG Combinations in the Tri-culture Model

5.1 Introduction

Neuroinflammation is associated with the interaction of numerous cell types in the brain (De la Fuente, 2008). Pathological conditions can cause the over expressions of proinflammatory cytokines (including IL-6, NO, TNF-α) released from neurons, astrocytes, microglial, or endothelial cells (Ha et al., 2012; Milatovic, et al., 2017; Adriani, et al., 2017). Microglia and astrocytes are the main innate immune cells active (Block and Hong, 2005). Endothelial cells also contribute to neuroinflammation when the BBB is damaged (Li Q, & Barres, 2018).

A tri-culture inflammatory model has been established to imitate the molecular processes, cellular interactions, and microenvironment of neuroinflammation (Zheng, et al., 2021). It offers a reliable *in vitro* model to investigate the processes behind neuroinflammation and search for novel treatments to address different neurodegenerative disorders.

In this chapter, we utilised the above-mentioned neuroinflammation tri-culture model to investigate the anti-neuroinflammatory and neuroprotective activities of the AN-SG and BA-SG combinations. The main findings implied that AN-SG and BA-SG exhibited improved pharmacological actions in preventing LPS-induced proinflammatory mediators, such as NO, IL-6 and TNF-α compared with their individual component, which was associated with downregulated NF-κB p65 translocation. Subsequently, these two combinations were found to exhibit enhanced activities in inhibiting p-tau expression and restoring endothelial tight junction in the tri-culture system.

5.2 Enhanced inhibitory effects of AN-SG and BA-SG on NO, IL-6 and TNF-α productions in tri-culture system

In the tri-culture model, the NO, IL-6 and TNF-α inhibitory effects of AN-SG and BA-SG against LPS stimulation were compared to that of AN, BA or 6-SG alone at 25 µM.

As shown in **Figure 5.1A**, LPS generated an excessive amount of NO in the upper compartment at 29.71 ± 0.97 ng/mL ($p<0.0001$ *vs.* blank control: 0.24 ± 0.13 ng/mL). The combination of AN-SG [AN (12.5 µM) + 6-SG (12.5 µM), total concentration of 7.83 µg/mL] significantly lowered the level of NO to 15.16 ± 1.06 ng/mL ($p<0.0001$ *vs.* LPS stimulation) and the reduction was significantly greater than that of AN (20.09 ± 0.71 ng/mL) or 6-SG (20.30 ± 2.42 ng/mL) alone at the same concentration level ($p<0.001$ *vs.* AN, $p<0.001$ *vs.* 6-SG). Similarly, BA-SG [BA (12.5 µM) + 6-SG (12.5 µM), total concentration of 6.83 µg/mL] significantly reduced NO to 7.78 ± 3.16 ng/mL, which was significantly greater than BA (16.49 ± 2.09 ng/mL) or 6-SG (19.56 ± 3.14 ng/mL) ($p<0.0001$ *vs.* LPS stimulation, $p<0.001$ *vs.* BA, $p<0.0001$ *vs.* 6-SG) (**Figure 5.1B**).

The stimulation of LPS also generated an excessive amount of NO in the lower compartment to 23.23 ± 1.40 ng/mL ($p<0.0001$ *vs.* blank control: 0.24 ± 0.17 ng/mL), **Figure 5.1A**. The combination of AN-SG significantly lowered the level of NO to 15.16 ± 1.06 ng/mL ($p<0.0001$ *vs.* LPS stimulation), and the single phytochemicals AN and 6-SG also reduced NO productions to 15.52 ± 0.71 ng/mL and 15.57 ± 0.29 ng/mL, respectively. However, the combined activities of AN-SG were not significantly higher than that of the single components. Similarly, BA-SG significantly reduced NO to 11.00 ± 3.86 ng/mL, which was significantly greater than BA (19.34 ± 1.09 ng/mL) or 6-SG (16.81 ± 2.44 ng/mL) ($p<0.0001$ *vs.* LPS stimulation, $p<0.01$ *vs.* BA, $p<0.05$ *vs.* 6-SG), **Figure 5.1B**.

As shown in **Figure 5.1C-F**, LPS-stimulated cells produced significantly higher IL-6 (12.53 ± 3.70 ng/mL *vs.* 2.04 ± 0.11 ng/mL, $p<0.0001$) and TNF-α (79.67 ± 0.10 ng/mL *vs.* 15.35 ± 0.01 ng/mL, $p<0.0001$) in the upper compartment compared to that of the blank control. AN-SG significantly lower the IL-6 production (**Figure 5.1C**, 1.66 ± 0.62 ng/mL, $p<0.0001$ *vs.* LPS) and TNF-α productions (**Figure 5.1E**, 20.40 ± 0.03 ng/mL, $p<0.0001$ *vs.* LPS) in the upper compartments. Furthermore, the IL-6 reduction by AN-SG was greater than that of AN (4.86 ± 0.51 ng/mL, $p<0.0001$) or 6-SG (3.40 ± 0.57, $p<0.01$) alone (**Figure 5.1C**). Similarly, in the **Figure 5.1E**, the TNF-α reduction by AN-SG was greater than that of AN (37.30 ± 0.38 ng/mL, $p<0.0001$) or 6-SG (38.13 ± 0.20 ng/mL, $p<0.0001$) alone.

The combination of BA-SG significantly lowers the IL-6 production (**Figure 5.1D**, 2.64 ± 0.70 ng/mL, $p<0.0001$ *vs.* LPS) and TNF-α productions (**Figure 5.1F**, 29.00 ± 6.36 ng/mL, $p<0.0001$ *vs.* LPS) in the upper compartments. However, there was no significant difference in the IL-6 reduction compared between BA-SG to BA (3.83 ± 0.52 ng/mL, $p>0.05$) or 6-SG (2.63 ± 0.94 ng/mL, $p>0.05$), **Figure 5.1D**. The TNF-α reduction by BA-SG was significantly greater compared to BA (38.57 ± 0.56 ng/mL, $p<0.01$) or 6-SG (38.13 ± 0.26 ng/mL, $p<0.01$) alone, **Figure 5.1F**. In the lower compartments, the TNF reduction showed similarly results with the upper compartments, the IL-6 reduction was found to be significant against LPS stimulation but showed comparable effects among individual and combination.
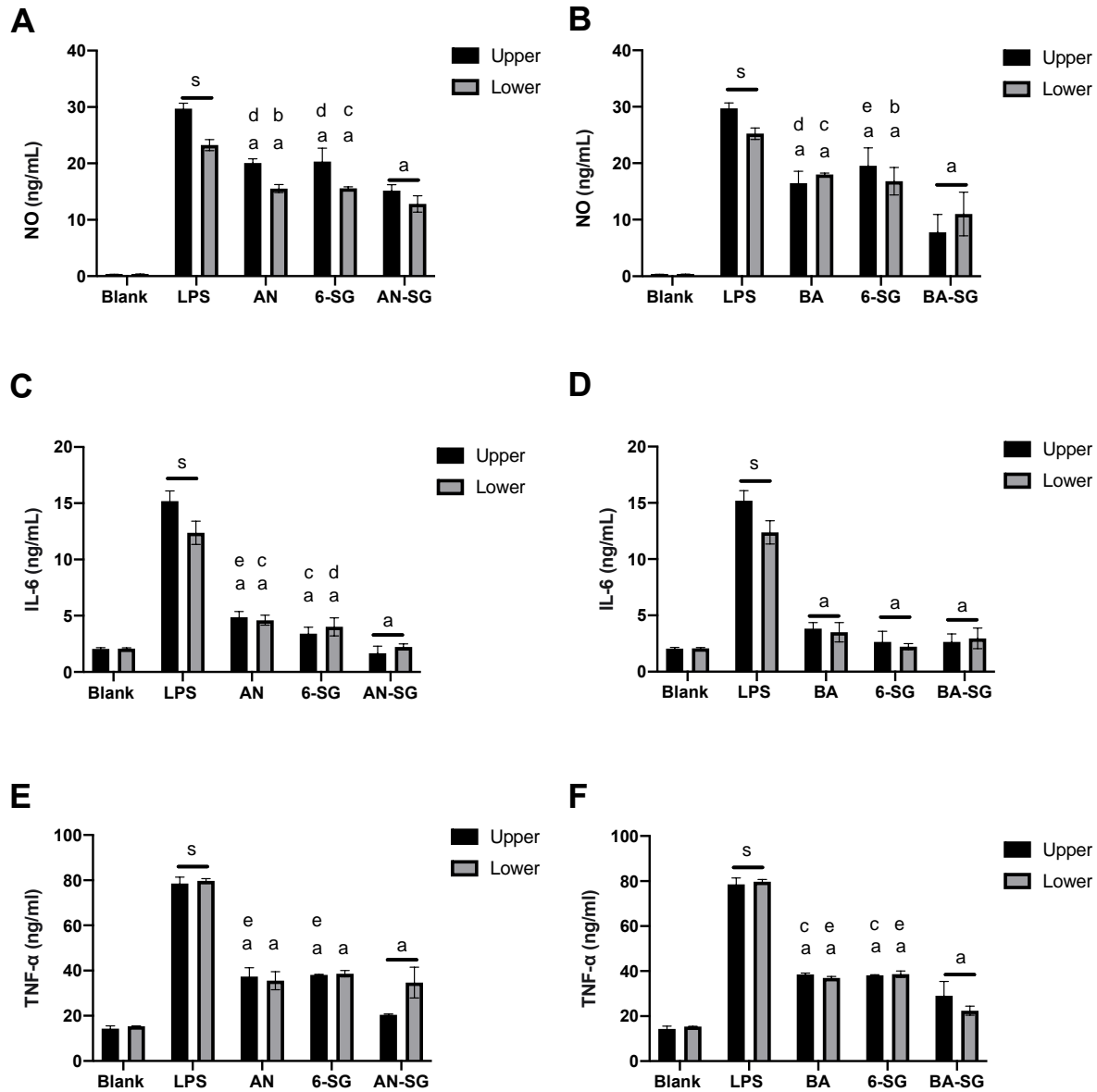
Figure 5.1 AN-SG and BA-SG generally exhibited greater effects in reducing NO, IL-6 and TNF-α productions than that of the individual component in the tri-culture system. AN-SG inhibited NO (A), IL-6 (C), and TNF-α (E) productions and BA-SG inhibited NO (B), IL-6 (D) and TNF-α (F) productions in LPS-activated tri-culture model in both upper and lower compartments. Data are shown as mean ± SEM (n = 3). The statistical comparison between groups was conducted by one-way ANOVA analysis with Tukey test for group comparison in GraphPad Prism 9. s: $p<0.0001$ *vs.* Blank, a: $p<0.0001$ *vs.* LPS, b: $p<0.05$ *vs.* combinations, c: $p<0.01$ *vs.* combinations, d: $p<0.001$ *vs.* combinations, e: $p<0.0001$ *vs.* combinations.

5.3 Enhanced effects of AN-SG and BA-SG in inhibiting the NF-κB p65 nuclear translocation of N11 cells in the tri-culture model

The results of our previous study suggested that in the tri-culture model, the LPS-induced neuroinflammation was mediated by the NF-κB p65 translocation in the microglia cells (Zheng Y. F, et al., 2021). In this study, the effect of AN-SG and BA-SG in inhibiting neuroinflammation on N11 cells in the tri-culture model was examined on the NF-κB p65 translocation by immunofluorescence staining.

As shown in **Figure 5.2**, the blank control showed that the NF-κB p65 (green fluorescence) was mostly expressed outside the nucleus (DAPI, blue fluorescence). In response to the LPS stimulation, increased expressions of NF-κB p65 were observed in the nucleus, as evidenced by the overlapping green in the blue fluorescence, suggesting that LPS triggered the increased translocation of NF-κB p65 to the cell nucleus after the 0.5 hr's incubation. All the individual and combined treatments appeared to inhibit the translocation to various degrees (**Figure 5.2A**, **B**). The statistical analysis (**Figure 5.2C**) demonstrated that AN-SG downregulated the integrated intensity of nuclear positive NF-κB p65 (77.96 ± 19.95, *vs.* LPS=210.23 ± 28.00, *p*<0.0001). The nuclear positive NF-κB p65 of AN-SG was significantly lower than that of AN (104.07 ± 24.78, *p*<0.05) or 6-SG (140.93 ± 27.60, *p*<0.001). BA-SG also significantly suppressed NF-κB p65 translocation (85.16 ± 8.91 *vs.* LPS=210.23 ± 28.00, *p*<0.0001), which the nuclear positive integrated intensity was significantly lower than that of BA (129.16 ± 19.34, *p*<0.0001) or 6-SG (140.93 ± 27.60, *p*<0.0001) alone (**Figure 5.2D**).
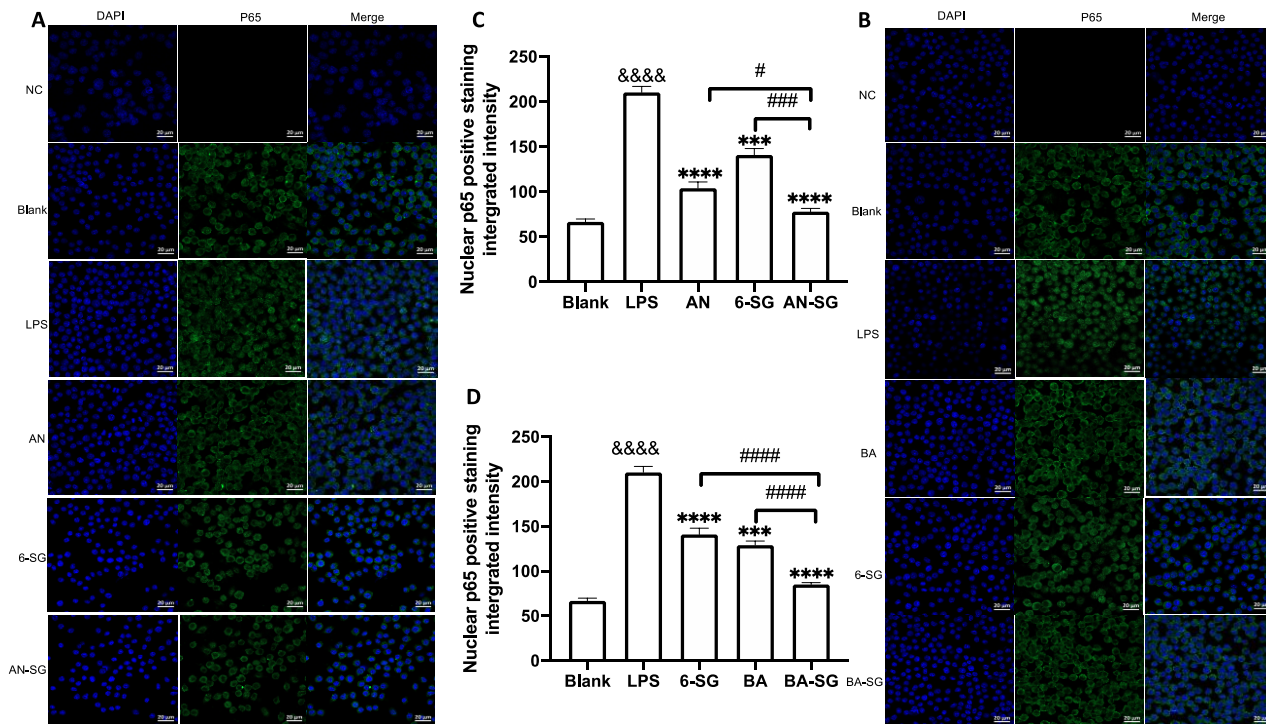
Figure 5.2 AN-SG and BA-SG exhibited greater effects in inhibiting LPS-induced NF-κB nuclear translocation than the individual component in the N11 cells of the tri-culture model. (A) AN-SG and (B) BA-SG for the immunofluorescence staining of NF-κB p65. Images were taken using a confocal microscope with 63× magnification. Blue: DAPI in the nucleus, green: NF-κB p65 in the N11 cells. Scale bar = 20 μm. NC represents the negative tri-culture control group without primary antibody added before immunofluorescence staining. (C, D) Statistical analysis of the NF-κB p65 translocation activities by AN-SG and BA-SG using ImageJ. Data are shown as mean ± SEM (n > 3). &&&& $p<0.0001$ *vs.* Blank, *** $p<0.001$, **** $p<0.0001$ *vs.* LPS, # $p<0.05$, ### $p<0.001$, #### $p<0.0001$ *vs.* combination, by one-way ANOVA analysis with Tukey test for group comparison in GraphPad Prism 9.

5.4 Enhanced effects of AN-SG and BA-SG in protecting endothelial tight junction of MVEC cells in the tri-culture system

In the MVEC cells of the tri-culture system, LPS exposure induced impaired endothelial tight junction as evidenced by a significant reduction of the TEER value in the LPS stimulated group (162 ± 12 Ω) compared with the blank control (207 ± 18 Ω, $p<0.01$). As shown in **Figure 5.3A**, AN significantly restored the TEER value to 181 ± 12 Ω ($p<0.05$ v*s.* LPS), and 6-SG also increased the TEER value to 176 ± 6 Ω ($p<0.01$ *vs.* LPS). However, AN-SG demonstrated the highest effect in restoring TEER value (205 ± 12 Ω, $p<0.01$ *vs.* LPS), which was significantly greater than that of AN and SG alone (both $p<0.01$).

The increased Evans blue absorbance also suggested the damaged endothelial tight junction upon the LPS simulation in the LPS group (0.28 ± 0.08) compared with the Blank group (Blank: 0.20 ± 0.06, $p<0.01$, **Figure 5.3C**). Both AN and 6-SG alone significantly lowered the Evans blue absorbance to 0.22 ± 0.03 and 0.20 ± 0.04, respectively, $p<0.01$ *vs.* LPS. AN-SG also lowered Evans blue absorbance (AN-SG: 0.21 ± 0.07 *vs.* LPS, $p<0.01$). However, the combined treatment was not significantly stronger than the individual treatment.

In **Figure 5.3B**, both BA and 6-SG significantly increased the TEER value to 177 ± 5 Ω and 176 ± 6 Ω, respectively ($p<0.05$ and $p<0.01$ v*s.* LPS). BA-SG significantly restored TEER values (BA-SG: 190 ± 6 Ω, $p<0.01$ *vs.* LPS) and showed greater ability than that of the BA ($p<0.01$) and 6-SG ($p<0.05$) alone. Similarly, BA-SG further lowered Evans blue absorbance (0.17 ± 0.02) than that of BA (0.22 ± 0.04) or 6-SG (0.20 ± 0.03) used alone, $p<0.05$ (**Figure 5.3D**).

The impaired tight junction in MVEC cells was further demonstrated by the immunofluorescence staining of ZO-1 upon the stimulation of LPS (**Figure 5.3E-F**). The tight junction protein ZO-1 in the blank tri-culture system was shown as a complete honeycomb structure, but the integrity was damaged after the LPS exposure for 24 hr at 1 µg/mL. The single phytochemicals AN, BA and 6-SG, and the combinations AN-SG and BA-SG combinations increased the yellow honeycomb structure compared with the LPS and single component treatment. However, a prominent improved tight junction was seen after the treatment of AN-SG and BA-SG combinations. Compared with the AN and 6-SG used alone, AN-SG showed increased yellow honeycomb for the ZO-1 protein expression. Similarly, the BA-SG combination showed increased yellow honeycomb for the ZO-1 protein expression compared with the single phytochemicals BA and 6-SG.
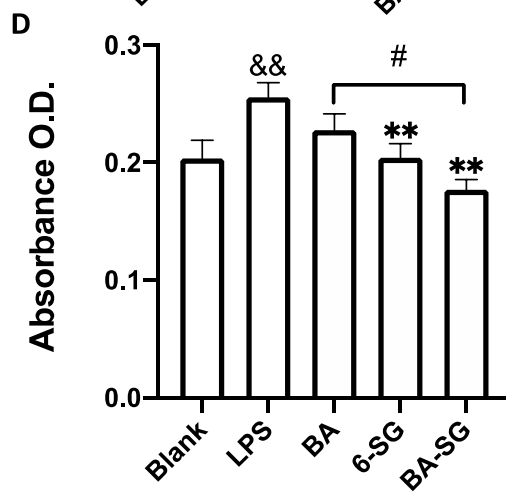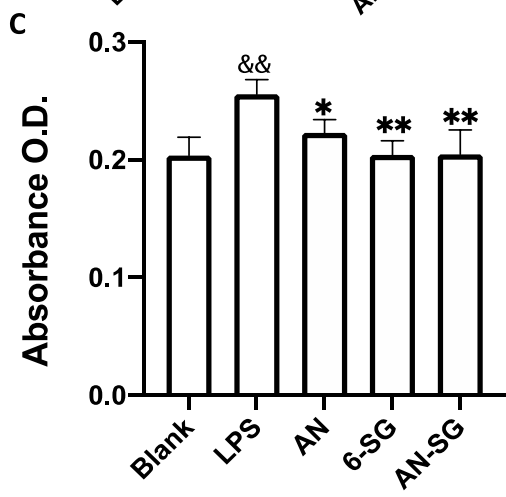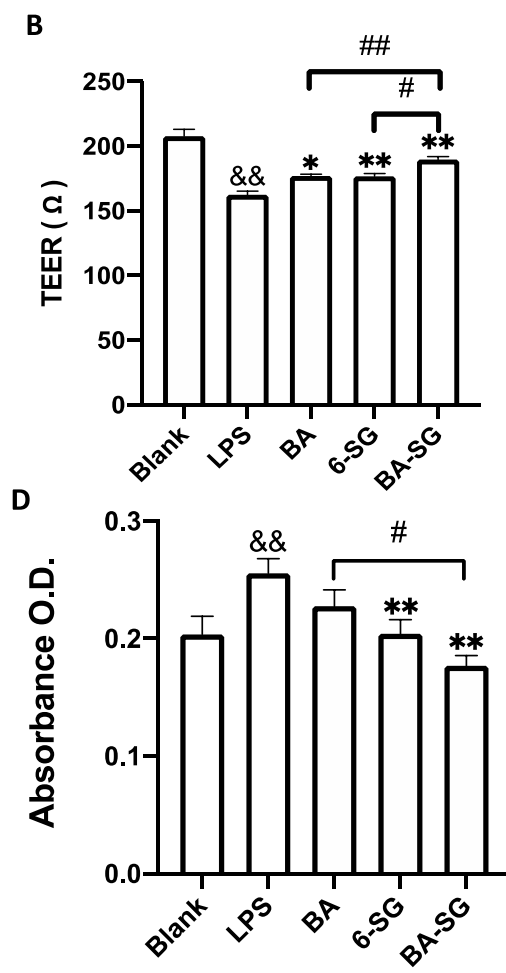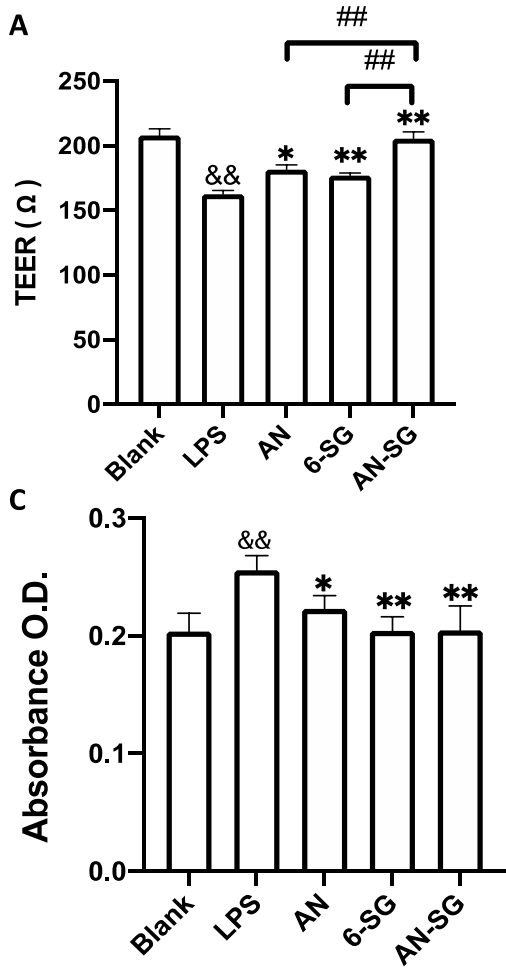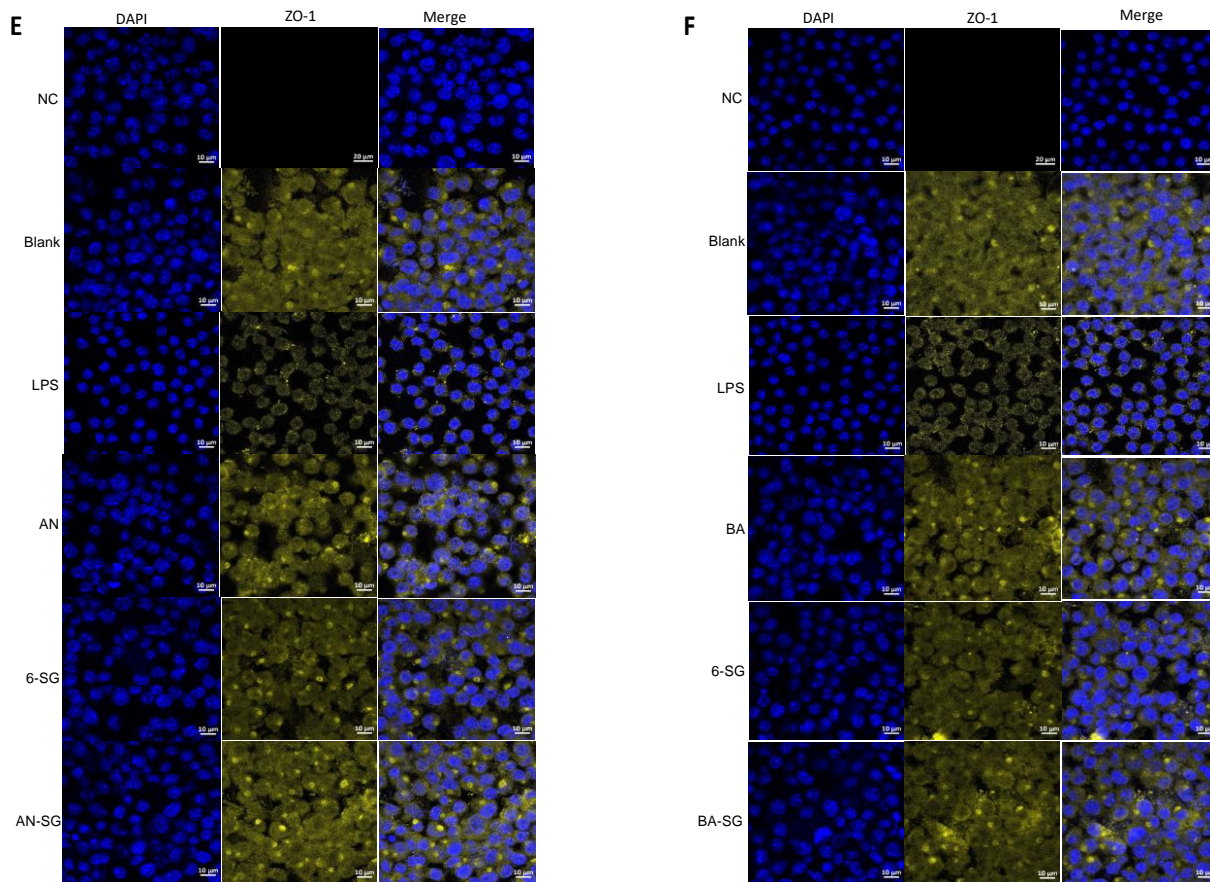
Figure 5.3 AN-SG and BA-SG demonstrated a more prominent effect in protecting the endothelial tight junction of MVEC cells in the tri-culture system against LPS-stimulated neuroinflammation. The measurements of TEER (A), Evans blue absorbance (C) and tight junction protein ZO-1 (E) for AN-SG, and TEER (B), Evans blue absorbance (D) and tight junction protein ZO-1 (F) for BA-SG in the LPS-activated tri-culture model. Immunofluorescence staining of ZO-1 in the MVEC cells of the tri-culture model. Images were taken using a confocal microscope with 63× magnification. Blue: DAPI in the nucleus; yellow: ZO-1 in the microvascular endothelial cells. Scale bar = 10 μm. O.D.: optical density. NC represents the negative tri-culture control group without primary antibody added before immunofluorescence staining. && $p<0.01$ *vs.* Blank, * $p<0.05$, ** $p<0.01$ *vs.* LPS, # $p<0.05$, ## $p<0.01$ *vs.* combination, by one-way ANOVA analysis with Tukey test for group comparison in GraphPad Prism 9.

5.5 Enhanced effects of AN-SG and BA-SG in restoring neuronal survival of N2A cells in tri-culture system

The effects of AN, BA, 6-SG, AN-SG or BA-SG at 25 µM on cell viability of N2A cells in the LPS stimulated-tri-culture system was tested using Alamar blue and MTT assays. In **Figure 5.4A**, the Alamar blue assay demonstrated that the cell viability of N2A cells in the LPS group was significantly reduced compared with the blank group (88.23 ± 1.05% *vs.* Blank=100%, $p<0.0001$) after 24 hr' exposure. All

treatments of AN (95.90 ± 2.20%, $p<0.01$), 6-SG (93.89 ± 1.46%, $p<0.05$) and AN-SG (101.71 ± 3.96%, $p<0.001$) significantly restored the cell viability compared with that of LPS. In particular, AN-SG demonstrated the highest cell viability compared to AN ($p<0.05$) or 6-SG ($p<0.01$) alone. Similarly, in **Figure 5.4B**, all the single phytochemicals BA (92.23 ± 4.22% *vs.* LPS, $p<0.05$), 6-SG (94.12 ± 1.46% *vs.* LPS, $p<0.05$) and combination BA-SG (100.21 ± 1.39% *vs.* LPS, $p<0.001$) significantly restored the cell viability. BA-SG displayed the highest cell viability compared to BA or 6-SG (both $p<0.05$).

MTT assay was conducted to confirm the data obtained from the Alamar blue assay, which showed a similar trend. In **Figure 5.4C**, LPS significantly decreased the cell viability compared with the blank group (87.74 ± 1.19% *vs.* Blank=100%, $p<0.0001$). AN (92.31 ± 2.68%, $p>0.05$), 6-SG (95.55 ± 2.31%, $p<0.01$) and AN-SG (101.83 ± 1.72%, $p<0.0001$) significantly restored the cell viability compared with that of LPS. AN-SG demonstrated a higher cell viability level compared with AN ($p<0.01$) or 6-SG ($p<0.05$) alone. Similarly, in **Figure 5.4D**, BA-SG (102.97 ± 2.26% *vs.* LPS, $p<0.0001$) also showed significantly enhanced cell viability which was greater than that of BA ($p<0.0001$) or 6-SG ($p<0.001$) alone.
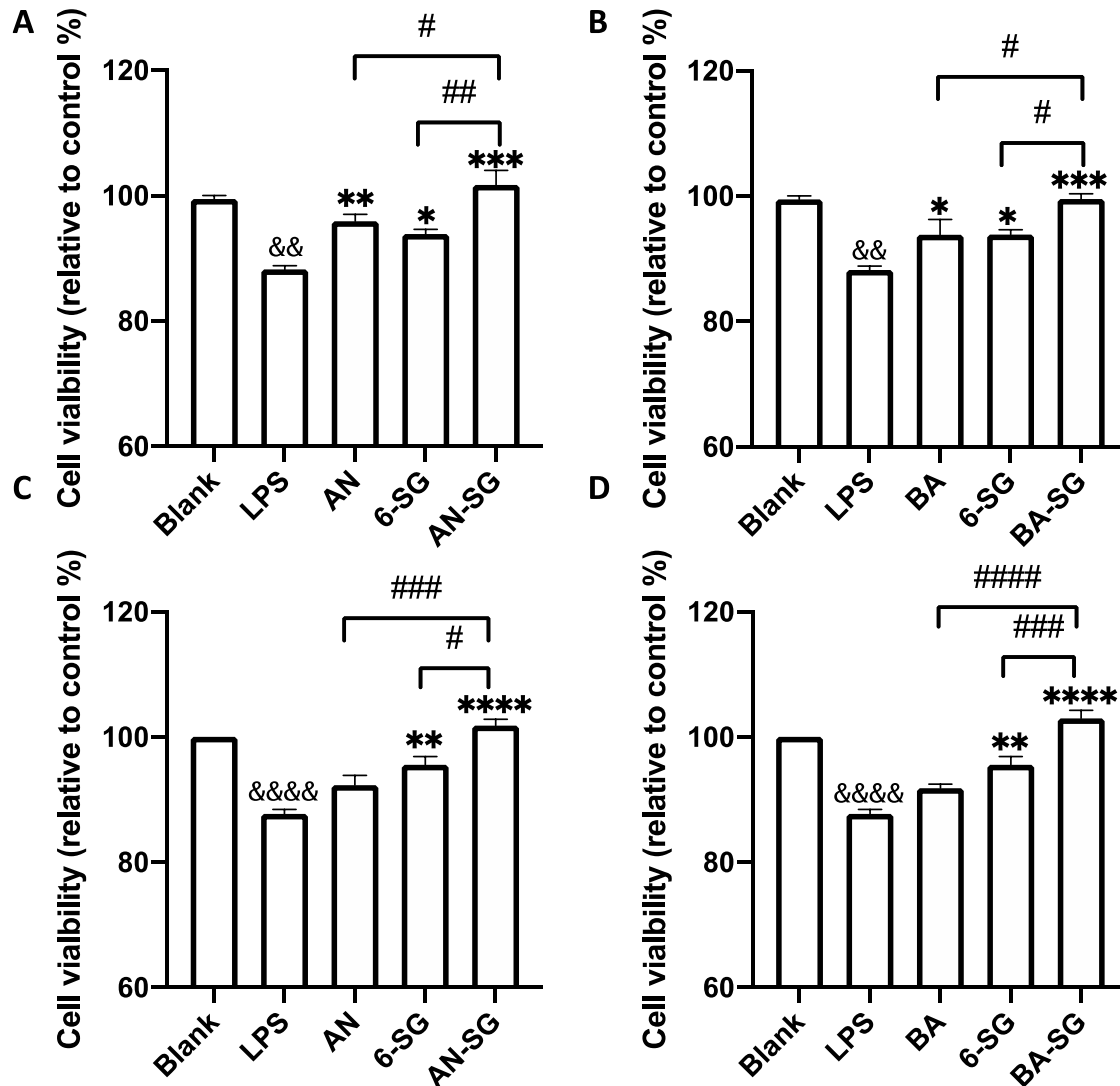
Figure 5.4 AN-SG and BA-SG exhibited greater restored cell viability in N2A cells of the tri-culture system against the LPS stimulation compared with their corresponding individual component. The Alamar blue assay was evaluated for (A) AN-SG and (B) BA-SG, and the MTT assay on (C) AN-SG and (D) BA-SG. Data are shown as mean ± SEM (n > 3). && $p<0.01$, &&&& $p<0.0001$ vs. Blank, * $p<0.05$, ** $p<0.01$, *** $p<0.001$, **** $p<0.0001$ vs. LPS, # $p<0.05$, ## $p<0.01$, ### $p<0.001$, #### $p<0.0001$ vs. combination, by one-way ANOVA analysis with Tukey test for group comparison in GraphPad Prism 9.

5.6 Enhanced effects of AN-SG and BA-SG in reducing tau phosphorylation in N2A cells of tri-culture system

Immunofluorescent staining of p-tau protein in N2A cells was conducted to examine the capacity of AN-SG and BA-SG to attenuate p-tau expression in the LPS-induced neuroinflammation tri-culture system. As

shown in **Figure 5.5**, the phosphorylation of tau protein (red fluorescence) increased significantly in the N2A cells after the LPS exposure for 0.5 hr compared to that of the blank control group (Blank: 1.00 ± 0.08, LPS: 5.70 ± 0.20, $p<0.0001$). AN, 6-SG and AN-SG appeared to decrease the phosphorylation of tau protein compared with the LPS (**Figure 5.5A**). The statistical analysis (**Figure 5.5C**) demonstrated that all the treatments have significantly reduced the p-tau accumulation compared with LPS ($p<0.05$). Particularly, the p-tau accumulation in AN-SG (1.16 ± 0.01) was significantly lower than that of AN (1.62 ± 0.05) or 6-SG (1.53 ± 0.04) individually ($p<0.05$, respectively).

Similarly, it was obvious that BA, 6-SG and BA-SG decreased tau phosphorylation compared with the LPS treatment (BA: 1.55 ± 0.06, 6-SG: 1.53 ± 0.04, BA-SG: 1.14 ± 0.02, $p<0.001$, respectively, **Figure 5.5B** and **5.5D**). However, BA-SG demonstrated a more effective p-tau reduction compared with the BA or 6-SG alone ($p<0.05$, respectively).
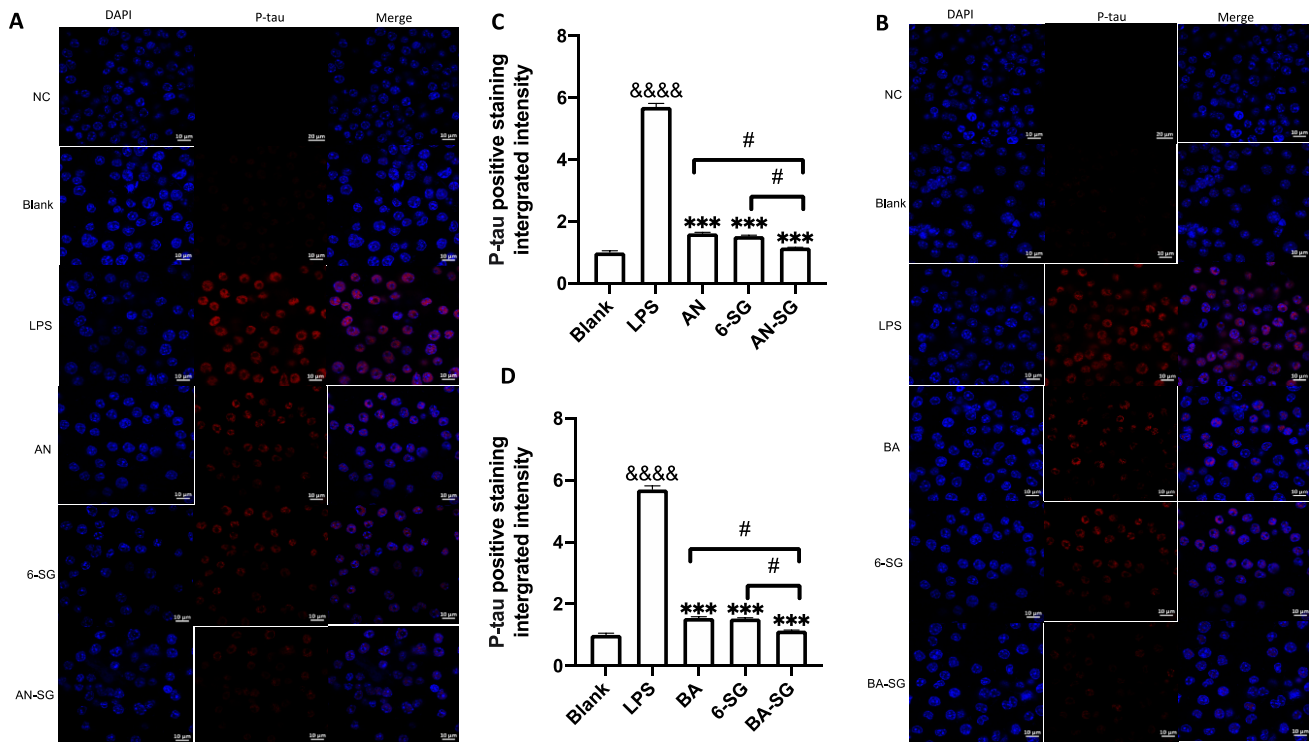
Figure 5.5 AN-SG and BA-SG exhibited greater p-tau reduction in N2A cells of the tri-culture system against the LPS stimulation compared with their corresponding individual component. Immunofluorescence staining of p-tau for (A) AN-SG and (B) BA-SG groups after the exposure of LPS for 0.5 hr. Images were taken by a confocal microscope with 63× magnification. Blue: DAPI in the nucleus. Red: p-tau in tri-cultured N2A cell lines. Scale bar = 10 μm. NC represents the negative tri-culture control group without primary antibody added before immunofluorescence staining. (C: AN-SG; D: BA-SG). Use ImageJ to quantity the tau protein phosphorylation activity. Data are shown as mean ± SEM (n > 3). &&&& $p<0.0001$ *vs.* Blank, *** $p<0.001$ *vs.* LPS, # $p<0.05$ *vs.* combination, by one-way ANOVA analysis with Tukey test for group comparison in GraphPad Prism 9.

5.7 Conclusion

The present study evaluated the combined activities of AN and 6-SG, BA and 6-SG in a neuroinflammatory tri-culture model. Our findings revealed that AN-SG and BA-SG exhibited greater anti-neuroinflammatory activities in the microglia cells compared to their individual components and in turn protected endothelial tight junctions and neuronal survival. Therefore, AN-SG and BA-SG may have a greater potential to be developed as anti-neuroinflammatory and neuroprotective agents than their individual phytochemical alone. Furthermore, it establishes a new framework for drug development in future animal and clinical studies.

Chapter 6: Discussions

Network pharmacology has emerged as a powerful tool for the development of combination therapies (Sakle et al., 2020) and is particularly useful in Chinese herbal medicine research to understand the multi-targeted mechanisms of the bioactive components in complex herbal formulations (Sun Y& Yang, 2019). Herein, network pharmacology has been applied to evaluate the pharmacological actions of eight phytochemicals selected from Chinese medicinal herbs targeting neuroinflammation. Synergistic interactions and the associated mechanisms were also examined and validated through an experimental study. Two paired combinations exhibited synergy in inhibiting LPS-induced NO production in microglia N11 cells, and the mechanisms were found to be associated with the downregulation of iNOS and phosphor-MAPKp38 protein expressions. The data obtained from the experimental study correlates well with that of the network pharmacology and molecular docking analyses.

The highly relevant gene targets for the anti-neuroinflammatory effects of the eight phytochemicals include MAPK14, MAPK8 and NOS3. The top KEGG pathway involved in these actions is the MAPK signaling pathway. MAPKs are a family of serine/threonine protein kinases that regulate key biological processes as well as cellular responses to external stress signals (Satoh T, et al., 2020). MAPKs are vital for intracellular signal transduction and play a critical role in regulating cell proliferation, brain plasticity, inflammatory responses, and other biological functions (Munoz & Ammit, 2010). According to recent preclinical studies, increased MAPK activation is a significant factor in brain inflammation. P38α/MAPK14 and ERK are intracellular signaling regulators (Xing et al., 2011), which mediate the expression of the iNOS and TNF genes in LPS-activated glial cells, suggesting the role of p38MAPK in the activated glial cells (Xing, B., 2011; Bhat, N.R., et al., 2002). Increasing evidence shows that MAPK cascades, including MSK1 and MSK2, were associated with the production of IL-1 in BV-2 mouse microglia cell line and primary rat microglia (Kim, et al., 2013). MAPK14 is ubiquitously expressed and plays an important role in pro-inflammatory signaling, making it an appealing therapeutic target for chronic inflammatory diseases (Madkour, et al., 2021). Anti-neuroinflammatory therapies might be directed by targeting MAPKs kinases, such as MAPK p38 and their role in the transcription and translation of inflammation

mediators, and can lead to an enhanced therapeutic outcome (Qu, et al., 2012). Our network pharmacology findings demonstrated that the MAPK signaling was the common pathway for the anti-neuroinflammatory effects of the phytochemicals, which is in line with the literature.

Nitric oxide synthases (NOS) are the enzymes responsible for NO generation. To date, three distinct NOS isoforms have been identified, including neuronal NOS (nNOS/NOS1), inducible NOS (iNOS/NOS2), and endothelial NOS (eNOS/NOS3) (Schulz, et al., 2005). It has been demonstrated that excessive NO is one of the important neuroinflammatory mediators that trigger neuronal toxicity and death (Liy, et al., 2021). A study by Connelly L. *et al.* (2003) suggested that mice with macrophages NOS3 knock-out revealed downregulated NF-κB signaling and reduced expression of iNOS, which resulted in decreased LPS-induced NO generation and ultimately suppressed neuroinflammatory response (Connelly L, et al., 2003). Thus, these studies supported the results from the current network pharmacology analysis that showed NOS3 is an important mediator in neuroinflammation. Moreover, iNOS generated in activated microglial cells mediates NO synthesis (Pautz et al., 2010). Studies in patients with Parkinson's disease revealed an increased density of iNOS-expressing glial cells in the substantia nigra compared to the control (Brodacki et al., 2008). In addition, iNOS has been linked with microglial activation, inducing an inflammatory response leading to neural cell death (Bachiller et al., 2018). Apart from the most relevant disease proteins targets discussed above, other neuroinflammation targets that are relevant to the anti-neuroinflammatory effects of the eight phytochemicals include EGFR, SRC, CASP3 and PPARG in the compound-gene targets-signaling pathway networks.

Molecular docking is commonly used to model the interactions between small molecules and target proteins (Meng, et al., 2011) and to estimate the binding energy of a ligand and the intensity of the interactions. Thus, molecular docking has the capacity to identify novel phytochemicals of therapeutic interest, predict the ligand−target interactions at protein level, and determine the degree of binding affinity between a phytochemical and its target proteins (Meng et al., 2011). Our results show that all eight phytochemicals were successfully bound with MAPK14 and NOS3 according to intermolecular interactions in the

molecular docking analysis. This result indicates that these phytochemicals have good affinities with the hub targets of neuroinflammation, illustrating the mechanisms of action underlying the therapeutic effects of these phytochemicals (Cui, et al., 2020). Our molecular docking results provide evidence to support the network pharmacology findings at the molecular level.

An *in vitro* experiment was carried out to partly verify the results obtained from the network pharmacology analysis and identify possible synergistic interactions. LPS-induced microglia N11 cells were used to test the individual and combined activities of the eight phytochemicals on NO production. Our results suggest that LU, AN, BA and 6-SG lowered LPS-induced NO expression levels in a dose-dependent manner. Interestingly, although HES and GLY showed high binding affinities to both MAPK14 and NOS3 proteins, they did not show any obvious inhibitory effect in the NO assay, which maybe attributed to their broad and unspecific effects.

Our study demonstrated that the AN-SG and BA-SG combinations exhibited synergistic interactions in reducing NO, IL-6 and TNF-α production. To the best of our knowledge, it is the first study demonstrating synergistic interactions between AN and 6-SG and BA and 6-SG targeting neuroinflammation. Based on the constructed network, the MAPK14 and NOS3 gene targets were highly relevant for the anti-neuroinflammatory actions of the AN-SG and BA-SG combinations, both linking to the downstream production of iNOS protein expression (Mattila, et al., 2014; Bhat N.R, et al., 2002). Our Western blot analysis suggested that the synergistic mechanisms may be associated with the downregulation of phosphor-MAPKp38 and iNOS proteins. These findings are in line with the predictions from our network pharmacology analysis suggesting that the AN-SG and BA-SG combinations have a greater effect on neuroinflammatory than each phytochemical used alone.

Previous studies suggested that AN, BA and 6-SG exhibited anti-neuroinflammatory activity *via* the downregulation of NF-κB and MAPK signaling pathways. AN downregulated the protein levels of iNOS and COX-2 in microglial cells by reduced IκB phosphorylation and attenuated Aβ(1–42)-induced Jun JNK–

MAPK overactivation (Yang R, et al., 2017). BA significantly inhibited the activation of MAPKs and suppressed the transcriptional activity of NF-κB (Zhang X, et al., 2021). Similarly, treatment with 6-SG resulted in the reduction of LPS-induced NF-κB subunit and the dependent transcriptional activity of NF-κB by blocking the phosphorylation of inhibitor κB (IκBα) and subsequent degradation of IκBα (Sharif, et al., 2007). 6-SG also interfered with the activation of PI3K/Akt/IκB kinases and MAPK (Pan et al., 2008). Thus, the common signaling pathways of NF-κB and MAPK may be the key to the synergistic effects of the AN-SG and BA-SG combinations. These combinations may work together to inhibit neuroinflammation pathways, potentially *via* signal transduction and protein expression inhibition.

The anti-neuroinflammatory activities of two combinations, AN-SG and BA-SG were further investigated in the LPS-stimulated tri-culture model in comparison to their individual component. Our results demonstrated that these two combinations exhibited pronounced effects in suppressing neuroinflammation mediated by N11 microglia cells and, in turn, protecting endothelial tight junction and restoring neuronal cell viability. Noticeably, the combined effects were generally greater than the single component used alone.

Neuroinflammation is a complex inflammatory process that occurs in the CNS and is intended to play a vital defensive role against numerous pathogens, toxins, or factors that produce neurodegeneration. Recent research suggests that dysfunctional cell-cell signaling in the NVU is a defining feature of CNS illnesses (Zlokovic, 2005; Benarroch, 2007; Zarekiani, et al., 2022). The CNS's structural and functional integrity is dependent on coordinated activity of the NVU, which regulates transport across the BBB (Erickson, et al., 2020; Pluimer, et al., 2020; Salmina, et al., 2021). Increasing evidence showed that disruption of functional interactions among NVU cells is the early hallmark of Alzheimer's disease (Montagne, et al., 2017; Liebner, et al., 2018; Yu, et al., 2020). Our results suggested that the combinations of AN-SG and BA-SG inhibited NO, IL-6, and TNF-α in mono-cultured N11 and the tri-culture cells. Microglia N11 cells are the resident innate immune cells in the NVU and produce several proinflammatory factors (IL-1, TNF-α, NO, PGE2, superoxide) within the brain (Block & Hong, 2005). Among these, high NO levels can increase neuroinflammation and result in tissue damage and neuronal death (Liy, et al., 2021). IL-6 is a pleiotropic

cytokine that participates in a variety of pathways, including immunological responses, inflammation, hematopoiesis, bone metabolism, and embryonic development (Tanaka, et al., 2014). TNF-α is an inflammatory cytokine that promotes apoptosis and activates NF-κB, resulting in the generation of proinflammatory cytokines and glial activation, which leads to neuroinflammation and neuronal death (Jung, et al., 2019). NF-κB is the key transcription factor that plays a central role in the neuroinflammatory pathways. It is a crucial regulator of cellular gene transcription that can regulate a variety of cytokines and receptors, such as NO, IL-6 and TNF-α (Zhang H & Sun, 2015).

In this study, the single phytochemicals and their combinations effectively inhibited the NF-κB p65 translocation, which at least partly explains the mechanisms underlying their anti-neuroinflammatory activities. Our results showed that compared with the single component, the combinations AN-SG and BA-SG have an advanced effect on many neuroinflammatory mediators, including NO, IL-6 and TNF-α. At present, this is the first study that demonstrated the combined effects of AN and 6-SG for anti-neuroinflammatory activity. Suzuki et al., showed that an aqueous extract of *Scutellaria* root and 6-SG combined together have an advanced effect on cyclic adenosine monophosphate phosphodiesterase inhibitory activity (Suzuki, et al., 1991), which may contribute to attenuated neuroinflammation (Chuang et al., 2017). Since BA is the main active component of *Scutellaria* root, the observed advanced effect of the aqueous fraction of *Scutellaria* root and 6-SG is consistent with the anti-neuroinflammatory activities of the BA and 6-SG combination observed in the current study.

In the NVU, astrocytes, microglia and pericytes are directly localised around the endothelial cells to aid the connection between blood supply and metabolic needs and also release several substances that improve and preserve the BBB integrity (Ronaldson & Davis, 2012). Excessive activation of microglia can have a negative impact on the BBB function. In particular, the excessive release of NO and IL-6 from the activated microglia has been demonstrated to impair the BBB's permeability, enabling potentially toxic chemicals to actively enter the brain (Thiel and Audus, 2001; Mayhan, 2002; Takeshita, et al., 2021). The downregulation of paracellular tight-junction proteins such as claudin-5, occludin, and ZO-1 by reactive

microglia and astrocytes are believed to contribute to the leaky BBB (Morris et al., 2018). Numerous studies demonstrated that increased BBB permeability is observed in a variety of neurological and psychiatric disorders, including stroke, epilepsy, amyotrophic lateral sclerosis, Alzheimer's disease and Parkinson's disease, implying that the compromised BBB plays a role in the pathogenesis and/or severity of brain diseases (Liu, et al., 2015; Patel and Frey, 2015; Małkiewicz, et al., 2019; Hussain, et al., 2021). Thus, therapeutic targets that could minimise the infiltration and invasion of peripheral chemicals or pathogens into the CNS or reduce damage to the NVU that protects the BBB, hold a high promise for treating chronic neurological illnesses and acute CNS traumas. Our present study showed that the AN-SG and BA-SG combinations inhibited the inflammatory mediators of NO, IL-6 and TNF-α, which in turn, led to reduced permeability and restored endothelial tight junction, suggesting their BBB protective effects against cytokine-mediated damage from microglial cells (Haruwaka et al., 2019). This is consistent with the previous studies where AN and BA were shown to protect against BBB damage induced by the production of pro-inflammatory cytokines and increase ZO-1 expression to reduce BBB permeability (Zhu, et al., 2012; Wang, et al., 2022).

Abnormal tau phosphorylation accumulation is a distinguishing characteristic of some neurodegenerative diseases, such as Alzheimer's disease (Wolfe, 2012). Tau proteins are often seen as microtubule-associated proteins in the brain. They are widely distributed throughout the neurons of the CNS and play a large part in preserving the stability of microtubules in axons (Buée, et al., & Hof, 2000). Abnormal phosphorylation of tau proteins results in impaired microtubule stability and the production of potentially neurotoxic aggregates (Johnson & Stoothoff, 2004). An increasing number of studies indicate that the sustained neuroinflammatory process involving microglia and astrocytes activation significantly contributes to the progression of tau pathology and neurodegenerative diseases, reiterating the significance of neuroinflammation as a therapeutic target for neurodegenerative diseases (Laurent, et al., 2018). In addition, inhibiting microglial inflammatory mediator production was shown to protect neurons and reduce p-tau in the tau transgenic mouse model. Previous animal studies have demonstrated that AN and BA used

individually, can reduce p-tau levels (Serrano, et al., 2014; Asai, et al., 2015; Gu, et al., 2016; Patel, et al., 2021; Sonawane, et al., 2021). The mechanism of action of AN and BA were both related to the activation of the Nrf2-mediated p62 signaling pathway (Serrano, et al., 2014; Gu, et al., 2018; Sonawane, et al., 2021; Shengkai and Yazhen, 2022). However, the evidence for the potential effect of 6-SG to inhibit p-tau level is lacking. Thus, the strengthened p-tau inhibition by AN-SG maybe is predominately caused by AN, which is potentiated by 6-SG. However, the potential role of the Nrf2-mediated p62 signaling pathway in the actions of the combination warrants further investigation. Overall, our results suggested that AN-SG and BA-SG reduced cytokines such as NO, IL-6, and TNF-α, which can protect the BBB tight junction and lower the p-tau level. These results provide evidence that AN-SG and BA-SG could provide potential benefits in the treatment of neurodegenerative diseases such as Alzheimer's disease, Parkinson's disease and multiple sclerosis (Laurent, et al., 2018; Singh, et al., 2020; Shengkai and Yazhen, 2022). Further study to explore the effects of these combinations on other Alzheimer's disease-relevant biomarkers, such as Aβeta, which is an early event associated with the onset and progression of neurodegeneration (Roy, et al., 2020), is warranted.

Previously, we have established the LPS-stimulated neuroinflammation tri-culture model as a quick and practical tool for quick drug-screening targeting neuroinflammation (Zheng, et al., 2021). This model was successfully applied in the current study where promising anti-neuroinflammatory, endothelial tight junction protective and neuroprotective effects of three herbal bioactive components and their combinations were demonstrated. Furthermore, we also identified enhanced activities when these bioactive components were combined in pairs. Our study further validates the usefulness of the tri-culture model in the development of therapeutic agents and combination therapy targeting neuroinflammation.

Chapter 7: Conclusion

7.1 General conclusions

Two novel herbal compound combinations targeting neuroinflammation with a synergistic approach have been identified through a series of studies using network pharmacology, molecular docking, and *in vitro* experimental verification. The major research findings are shown as follows:

1) AN-SG and BA-SG synergistically inhibited pro-inflammatory mediators, NO, IL-6 and TNF-α in LPS-induced mono-cultured microglial N11 cells;

2) The observed synergy of AN-SG and BA-SG was associated with downregulation of phosphor-MAPKp38/MAPKp38, iNOS and NF-κB p65 nuclear translocation.

3) AN-SG and BA-SG exhibited enhanced anti-neuroinflammatory activities than their individual component in the neuroinflammation tri-culture model and subsequently restored the endothelial tight junction, protected the neuronal survival and reduced p-tau expression.

Chapter 3 constructed the compound-gene targets-signaling pathway networks, which highlight the hub gene targets and KEGG pathways for eight selected phytochemicals against neuroinflammation. The top five gene targets included MAPK14, MAPK8, NOS3, EGFR and SRC, and the top KEGG pathway was the MAPK signaling pathway. The molecular docking partly verified the network pharmacology results that demonstrated good bind affinities of all phytochemicals with MAPK14 and NOS3.

In Chapter 4, two herbal-compound combinations, AN-SG and BA-SG, were found to exhibit synergistic effects (CI<1) on inhibiting NO, IL-6 and TNF-α productions in LPS-induced N11 cells. Western blot analysis suggested that the observed synergy was associated with downregulation of iNOS and phosphor-MAPKp38/MAPKp38 protein expressions, which were in line with the findings of network pharmacology and molecular docking studies.

In Chapter 5, an LPS-induced neuroinflammation tri-culture model was established to further investigate the anti-neuroinflammatory effects of AN-SG and BA-SG. The LPS-induced neuroinflammation tri-culture model provides an efficient and practical cellular model for a wide range of investigations on neuroinflammation mechanisms and for screening potential compounds or drugs candidates to treat neurodegenerative diseases such as Alzheimer's disease, Parkinson's disease and schizophrenia (Wolfe, 2012). Our results showed that two combinations significantly reduced the NO, IL-6, and TNF-α in the N11 cell in the tri-culture model. They also protected the endothelial tight junction as evidenced by the honeycomb structure of ZO-1 tight junction protein, reduced permeability and restored TEER values in the MVEC cells. Furthermore, the combinations were found to restore the impaired cell viability and reduced p-tau protein expression in N2A cells in the tri-culture model.

7.2 Limitation and future work

There are several limitations in our study. Firstly, the network pharmacology relies primarily on the currently available data from online databases, which may lead to some database selection and detection biases (Zhang, C., et al., 2020). Therefore, it should only be used as a predictive tool for the molecular mechanisms of phytochemical mixtures. In addition, network pharmacology can only reveal the relevant relationship between the phytochemical and gene targets without further information on their down-regulatory or up-regulatory actions, and therefore, further experimental investigation on the involved mechanisms is necessary. Next, the current study only focused on analysing the MAPK pathway based on the network pharmacology results. More in-depth study of NF-κB and their target proteins by the two combinations will be needed in the future. Moreover, it is evident that AN, 6-SG and BA were associated with many other key gene targets and coded proteins as displayed by the compound-gene target network. These gene targets and signaling pathways may also contribute to the synergistic effects of AN-SG and BA-SG against neuroinflammation, which warrants further investigation. The study focused on the NF-κB nuclear translation pathway as an associated mechanism of AN-SG and BA-SG against neuroinflammation. Other pathways or key gene targets that play major roles in modulating microglia-induced

neuroinflammation, such as Nrf-2/HO-1, nucleotide-binding oligomerization domain-like receptor protein three inflammasome, and MAPK pathways, were not investigated (Bernhardi, 2009; S. Chen et al., 2020; Song, et al., 2017; Upadhayay & Mehan, 2021). The combinations demonstrated an enhanced effect on the biomarkers related to neuroinflammation, endothelial tight junction and neuronal survival in the *in vitro* tri-culture system, these effects were not validated in the whole organism. Lastly, the effects of the herbal components and their combinations were investigated at only one concentration (25 µM) in this study due to the time limit. Based on the CI equation (Chapter 1), the synergistic interaction is determined based on the doses of the individual component and their combination when reaching the same effect level (i.e. 50%). Thus, complete dose-response curves of the individual and combined components are required to obtain the dosages at the same effect level (i.e. IC_{50} value). It is obvious that one concentration (25 µM) for an individual and combination would be unlikely to generate the same effect level. Therefore, if there is a synergistic interaction, it could not be efficiently determined. However, the tests we conducted using 25 µM could still serve as an indicator for the initial screening on whether the combination can generate a significantly higher response than that of the individual component used at selected targets (neuronal survival, TNF-α, IL-6, etc.). Further studies are required to generate complete dose-response curves for those two combinations and their components to determine the potential synergy effect in the anti-neuroinflammation and neuroprotective activities. Nonetheless, the enhanced effects of the two herbal combinations against neuroinflammation in our study provide valuable evidence to warrant further investigation of these combinations in animal and human studies as potential therapy options for neurodegenerative diseases.

7.3 Significance of the study

This study provides a systemic approach for exploring the synergistic combination of herbal compounds and associated mechanisms. Network pharmacology and molecular docking were applied to predict the phytochemicals, multi-targets and multi-pathways relevant to the neuroinflammation and provided insight for potential mechanisms underlying the synergistic interactions. A single-cell model was used to test and

screen the synergistic activities among the pair-wised combination. A tri-culture model was used to validate the combinations of anti-neuroinflammation activities.

To the best of our knowledge, this is the first study to investigate the neuroinflammatory effects of phytochemical combinations using the LPS-induced neuroinflammation tri-culture model. It provides scientific evidence for the application of the tri-culture model as a practical neuroinflammatory drug screening tool prior to animal studies.

This study developed two novel herbal combinations that demonstrated promising therapeutic potential through synergistic interactions to address the complex pathological condition of neuroinflammation. These combinations should be further investigated in animal and human studies for the treatment of various neurodegenerative diseases.

References

Adriani, G., Ma, D., Pavesi, A., Kamm, R. D. and Goh, E. L. (2017). A 3D neurovascular microfluidic model consisting of neurons, astrocytes and cerebral endothelial cells as a blood-brain barrier. Lab Chip 17(3), 448-459. doi: 10.1039/c6lc00638h.

An, W., Huang, Y., Chen, S., Teng, T., Shi, Y., Sun, Z., & Xu, Y. (2021). Mechanisms of Rhizoma Coptidis against type 2 diabetes mellitus explored by network pharmacology combined with molecular docking and experimental validation. Sci Rep, 11(1), 20849. doi:10.1038/s41598-021-00293-8

Asai, H., Ikezu, S., Tsunoda, S., Medalla, M., Luebke, J., Haydar, T., et al. (2015). Depletion of microglia and inhibition of exosome synthesis halt tau propagation. Nat Neurosci 18(11), 1584-1593. doi: 10.1038/nn.4132.

Ascierto, P. A., & Marincola, F. M. (2011). Combination therapy: the next opportunity and challenge of medicine. J Transl Med, 9(1), 115. doi: 10.1186/1479-5876-9-115

Bachiller, S., Jiménez-Ferrer, I., Paulus, A., Yang, Y., Swanberg, M., Deierborg, T., & Boza-Serrano, A. (2018). Microglia in Neurological Diseases: A Road Map to Brain-Disease Dependent-Inflammatory Response. Front Cell Neurosci, 12. doi: 10.3389/fncel.2018.00488

Bao, G, Li C, Qi L, Wang N, He B. Tetrandrine protects against oxygen-glucose-serum deprivation/reoxygenation-induced injury via PI3K/AKT/NF-κB signaling pathway in rat spinal cord astrocytes. Biomed Pharmacother. 2016 Dec;84:925-930. doi: 10.1016/j.biopha.2016.10.007.

Benarroch, E. E. (2007). Neurovascular unit dysfunction: A vascular component of Alzheimer disease? Neurology 68(20), 1730-1732. doi: 10.1212/01.wnl.0000264502.92649.ab.

Bernhardi, R. v. (2009). Neurodegenerative Diseases – MAPK Signalling Pathways in Neuroinflammation. In: Binder, M.D., Hirokawa, N., Windhorst, U. (eds) Encyclopedia of Neurosci. Springer, Berlin, Heidelberg. doi: 10.1007/978-3-540-29678-2_3820

Bhat, N. R., Feinstein, D. L., Shen, Q., & Bhat, A. N. (2002). p38 MAPK-mediated transcriptional activation of inducible nitric-oxide synthase in glial cells. Roles of nuclear factors, nuclear factor kappa B, cAMP response element-binding protein, CCAAT/enhancer-binding protein-beta, and activating transcription factor-2. J Biol Chem, 277(33), 29584-29592. doi:10.1074/jbc.M204994200

Block, M. L. and Hong, J. S. (2005). Microglia and inflammation-mediated neurodegeneration: multiple triggers with a common mechanism. Prog Neurobiol 76(2), 77-98. doi: 10.1016/j.pneurobio.2005.06.004.

Blumenfeld, A., Gennings, C., & Cady, R. (2012). Pharmacological Synergy: The Next Frontier on Therapeutic Advancement for Migraine. Headache: J Head and Face Pain, 52(4), 636-647. doi:10.1111/j.1526-4610.2011.02058.x

Bournival, J., Plouffe, M., Renaud, J., Provencher, C., & Martinoli, M. G. (2012). Quercetin and sesamin protect dopaminergic cells from MPP+-induced neuroinflammation in a microglial (N9)-neuronal (PC12) coculture system. Oxid Med Cell Longev, 2012, 921941. doi:10.1155/2012/921941

Brodacki, B., Staszewski, J., Toczyłowska, B., Kozłowska, E., Drela, N., Chalimoniuk, M., & Stępien, A. (2008). Serum interleukin (IL-2, IL-10, IL-6, IL-4), TNFα, and INFγ concentrations are elevated in patients with atypical and idiopathic parkinsonism. Neurosci lett, 441(2), 158-162.

Buée, L., Bussière, T., Buée-Scherrer, V., Delacourte, A. and Hof, P. R. (2000). Tau protein isoforms, phosphorylation and role in neurodegenerative disorders. Brain Res Brain Res Rev 33(1), 95-130. doi: 10.1016/s0165-0173(00)00019-9.

Cai, C., Chen, Y., Zhong, S., Zhang, Y., Jiang, J., Xu, H., & Shi, G. (2016). Synergistic Effect of Compounds from a Chinese Herb: Compatibility and Dose Optimization of Compounds from N-Butanol Extract of Ipomoea stolonifera. Sci Rep, 6(1), 27014. doi:10.1038/srep27014

Chen, S., Peng, J., Sherchan, P., Ma, Y., Xiang, S., Yan, F., et al. (2020). TREM2 activation attenuates neuroinflammation and neuronal apoptosis via PI3K/Akt pathway after intracerebral hemorrhage in mice. J Neuroinflammation 17(1), 168. doi: 10.1186/s12974-020-01853-x.

Chen, J.-J., Dai, L., Zhao, L.-X., Zhu, X., Cao, S., & Gao, Y.-J. (2015). Intrathecal curcumin attenuates pain hypersensitivity and decreases spinal neuroinflammation in rat model of monoarthritis. Sci Rep, 5(1), 10278. doi:10.1038/srep10278

Chou, T.-C. (2018). The combination index (CI < 1) as the definition of synergism and of synergy claims. Synergy (Elsevier), 7, 49-50. doi:10.1016/j.synres.2018.04.001

Chuang, W., Zhen, W., Mengmeng, L., Chenli, L., Hanjie, Y., Dongsheng, Z., & Zhongming, C. (2017). Reducing Neuroinflammation in Psychiatric Disorders: Novel Target of Phosphodiesterase 4 (PDE4) and Developing of the PDE4 Inhibitors. In A. Gonzalo Emiliano Aranda (Ed.), Mechanisms of Neuroinflammation (pp. Ch. 1). Rijeka: IntechOpen. doi: 10.5772/intechopen.69154

Cokol, M., Kuru, N., Bicak, E., Larkins-Ford, J., & Aldridge, B. B. (2017). Efficient measurement and factorization of high-order drug interactions in Mycobacterium tuberculosis. Sci Adv, 3(10), e1701881. doi: 10.1126/sciadv.1701881

Connelly, L, Jacobs AT, Palacios-Callender M, Moncada S, Hobbs AJ. Macrophage endothelial nitric-oxide synthase autoregulates cellular activation and pro-inflammatory protein expression. J Biol Chem. 2003 Jul 18;278(29):26480-7. doi: 10.1074/jbc.M302238200.

Craft, J. M., Watterson, D. M., & Van Eldik, L. J. (2005). Neuroinflammation: a potential therapeutic target. Expert Opin Ther Targets, 9(5), 887-900. doi: 10.2147/CIA.S357558

Cui, S., Chen, S., Wu, Q., Chen, T., & Li, S. (2020). A network pharmacology approach to investigate the anti-inflammatory mechanism of effective ingredients from Salvia miltiorrhiza. Int Immunopharmacol, 81, 106040. doi: 10.1016/j.intimp.2019.106040

Dainiak, N., Feinendegen, L. E., Hyer, R. N., Locke, P. A., & Waltar, A. E. (2018). Synergies resulting from a systems biology approach: integrating radiation epidemiology and radiobiology to optimize protection of the public after exposure to low doses of ionizing radiation. Int J Radiat biol, 94(1), 2-7. doi: 10.1080/09553002.2018.1407461

Dang, Y., Xu, Y., Wu, W., Li, W., Sun, Y., Yang, J., . . . Zhang, C. (2014). Tetrandrine Suppresses Lipopolysaccharide-Induced Microglial Activation by Inhibiting NF-κB and ERK Signaling Pathways in BV2 Cells. PLoS One, 9(8), e102522. doi:10.1371/journal.pone.0102522

De la Fuente, M. (2008). Role of Neuroimmunomodulation in Aging. Neuroimmunomodulation 15(4-6), 213-223. doi: 10.1159/000156465

Dey, A., Bhattacharya, R., Mukherjee, A., & Pandey, D. K. (2017). Natural products against Alzheimer's disease: Pharmaco-therapeutics and biotechnological interventions. Biotechnol Adv, 35(2), 178-216. doi:10.1016/j.biotechadv.2016.12.005

DiSabato, D.J., N. Quan, and J.P. Godbout, Neuroinflammation: the devil is in the details. J Neurochem, 2016. 139 Suppl 2(Suppl 2): p. 136-153. doi: 10.1111/jnc.13607

Doncheva, N. T., Morris, J. H., Gorodkin, J., & Jensen, L. J. (2019). Cytoscape StringApp: Network Analysis and Visualization of Proteomics Data. J Proteome Res, 18(2), 623-632. doi:10.1021/acs.jproteome.8b00702

El Hassouni, B., Mantini, G., Li Petri, G., Capula, M., Boyd, L., Weinstein, H. N. W., et al. (2019). To Combine or Not Combine: Drug Interactions and Tools for Their Analysis. Reflections from the EORTC-PAMM Course on Preclinical and Early-phase Clinical Pharmacology. Anticancer Res 39(7), 3303-3309. doi: 10.21873/anticanres.13472.

Elizabeth, D. (2017). Dementia Summit presents strategies. Knight-Ridder/Tribune Business News.

Erickson, M. A., Wilson, M. L. and Banks, W. A. (2020). In vitro modeling of blood–brain barrier and interface functions in neuroimmune communication. Fluids and Barriers CNS 17(1), 26. doi: 10.1186/s12987-020-00187-3.

Fernández, J. A., Rojo, L., Kuljis, R. O. and Maccioni, R. B. (2008). The Damage Signals Hypothesis of Alzheimer's Disease Pathogenesis. J Alzheimer's Dis14, 329-333. doi: 10.3233/JAD-2008-14307.

Foucquier, J. and Guedj, M. (2015). Analysis of drug combinations: current methodological landscape. Pharmacol Res Perspect 3(3), e00149. doi: 10.1002/prp2.149.

Glass, G. (2004). Cardiovascular combinations. Nat Rev Drug Discov, 3(9), 731-732. doi:10.1038/nrd1501

Gordon, R., & Woodruff, T. M. (2017). Chapter 3 - Neuroinflammation as a therapeutic target in neurodegenerative diseases. In V. Baekelandt & E. Lobbestael (Eds.), Disease-Modifying Targets in Neurodegenerative Disorders (pp. 49-80): Academic Press. doi: 10.1016/B978-0-12-805120-7.00003-8

Gu, L., Yu, Q., Li, Q., Zhang, L., Lu, H. and Zhang, X. (2018). Andrographolide Protects PC12 Cells Against β-Amyloid-Induced Autophagy-Associated Cell Death Through Activation of the Nrf2-Mediated p62 Signaling Pathway. Int J Mol Sci 19(9). doi: 10.3390/ijms19092844.

Gu, X.-H., Xu, L.-J., Liu, Z.-Q., Wei, B., Yang, Y.-J., Xu, G.-G., et al. (2016). The flavonoid baicalein rescues synaptic plasticity and memory deficits in a mouse model of Alzheimer's disease. Behav Brain Res 311, 309-321. doi: 10.1016/j.bbr.2016.05.052.

Guzman-Martinez, L., Maccioni, R. B., Andrade, V., Navarrete, L. P., Pastor, M. G. and Ramos-Escobar, N. (2019). Neuroinflammation as a Common Feature of Neurodegenerative Disorders. Front Pharmacol 10. doi: 10.3389/fphar.2019.01008.

Ha, S. K., Moon, E., Ju, M. S., Kim, D. H., Ryu, J. H., Oh, M. S., et al. (2012). 6-Shogaol, a ginger product, modulates neuroinflammation: A new approach to neuroprotection. Neuropharmacology 63(2), 211-223. doi: 10.1016/j.neuropharm.2012.03.016.

Haruwaka, K., Ikegami, A., Tachibana, Y., Ohno, N., Konishi, H., Hashimoto, A., et al. (2019). Dual microglia effects on blood brain barrier permeability induced by systemic inflammation. Nat Commun 10(1), 5816. doi: 10.1038/s41467-019-13812-z.

Hashimoto, M., Yamamoto, S., Iwasa, K., Yamashina, K., Ishikawa, M., Maruyama, K., . . . Yoshikawa, K. (2017). The flavonoid Baicalein attenuates cuprizone-induced demyelination via suppression of neuroinflammation. Brain Res Bull, 135, 47-52. doi:10.1016/j.brainresbull.2017.09.007

He, D, Huang JH, Zhang ZY, Du Q, Peng WJ, Yu R, Zhang SF, Zhang SH, Qin YH. A Network Pharmacology-Based Strategy For Predicting Active Ingredients And Potential Targets Of LiuWei DiHuang Pill In Treating Type 2 Diabetes Mellitus. Drug Des Devel Ther. 2019 Nov 28;13:3989-4005. doi: 10.2147/DDDT.S216644.

He, F. Q., Qiu, B. Y., Li, T. K., Xie, Q., Cui, D. J., Huang, X. L., & Gan, H. T. (2011). Tetrandrine suppresses amyloid-β-induced inflammatory cytokines by inhibiting NF-κB pathway in murine BV2 microglial cells. Int Immunopharmacol, 11(9), 1220-1225. doi:10.1016/j.intimp.2011.03.023

Heo, S.-D., Kim, J., Choi, Y., Ekanayake, P., Ahn, M., & Shin, T. (2020). Hesperidin improves motor disability in rat spinal cord injury through anti-inflammatory and antioxidant mechanism via Nrf-2/HO-1 pathway. Neurosci lett, 715, 134619. doi: 10.1016/j.neulet.2019.134619

Hussain, B., Fang, C. and Chang, J. (2021). Blood-Brain Barrier Breakdown: An Emerging Biomarker of Cognitive Impairment in Normal Aging and Dementia. Front Neurosci 15, 688090. doi: 10.3389/fnins.2021.688090.

Javed, H., Vaibhav, K., Ahmed, M. E., Khan, A., Tabassum, R., Islam, F., . . . Islam, F. (2015). Effect of hesperidin on neurobehavioral, neuroinflammation, oxidative stress and lipid alteration in intracerebroventricular streptozotocin induced cognitive impairment in mice. J neurol sci, 348(1), 51-59. doi: 10.1016/j.jns.2014.10.044

Jin, M., Park, S. Y., Shen, Q., Lai, Y., Ou, X., Mao, Z., . . . Zhang, W. (2018). Anti-neuroinflammatory effect of curcumin on Pam3CSK4-stimulated microglial cells. Int J Mol Med, 41(1), 521-530. doi:10.3892/ijmm.2017.3217

Johnson, G. V. and Stoothoff, W. H. (2004). Tau phosphorylation in neuronal cell function and dysfunction. J Cell Sci 117(Pt 24), 5721-5729. doi: 10.1242/jcs.01558.

Jung, Y. J., Tweedie, D., Scerba, M. T. and Greig, N. H. (2019). Neuroinflammation as a Factor of Neurodegenerative Disease: Thalidomide Analogs as Treatments. Front Cell Dev Biol 7, 313. doi: 10.3389/fcell.2019.00313.

Justin Thenmozhi, A., Dhivya Bharathi, M., Kiruthika, R., Manivasagam, T., Borah, A., & Essa, M. M. (2018). Attenuation of Aluminum Chloride-Induced Neuroinflammation and Caspase Activation Through the AKT/GSK-3β Pathway by Hesperidin in Wistar Rats. Neurotox Res, 34(3), 463-476. doi:10.1007/s12640-018-9904-4

Katzir, I., Cokol, M., Aldridge, B. B., & Alon, U. (2019). Prediction of ultra-high-order antibiotic combinations based on pairwise interactions. PLoS computational biology, 15(1), e1006774-e1006774. doi:10.1371/journal.pcbi.100677

Kempuraj, D., Thangavel, R., Natteru, P. A., Selvakumar, G. P., Saeed, D., Zahoor, H., et al. (2016). Neuroinflammation Induces Neurodegeneration. J Neurol Neurosurg Spine 1(1).

Khan, M. S., Muhammad, T., Ikram, M., & Kim, M. O. (2019). Dietary Supplementation of the Antioxidant Curcumin Halts Systemic LPS-Induced Neuroinflammation-Associated Neurodegeneration and Memory/Synaptic Impairment via the JNK/NF-κB/Akt Signaling Pathway in Adult Rats. Oxid Med Cell Longev, 2019, 7860650. doi:10.1155/2019/7860650

Kim, BW, Koppula S, Hong SS, Jeon SB, Kwon JH, Hwang BY, Park EJ, Choi DK. Regulation of microglia activity by glaucocalyxin-A: attenuation of lipopolysaccharide-stimulated neuroinflammation through NF-κB and p38 MAPK signaling pathways. PLoS One. 2013;8(2):e55792. doi: 10.1371/journal.pone.0055792.

Kong, ZH., Chen, X., Hua, H.-P., Liang, L., & Liu, L.-J. (2017). The Oral Pretreatment of Glycyrrhizin Prevents Surgery-Induced Cognitive Impairment in Aged Mice by Reducing Neuroinflammation and Alzheimer's-Related Pathology via HMGB1 Inhibition. J Mol Neurosci, 63(3), 385-395. doi:10.1007/s12031-017-0989-7

Kou, JJ, Shi JZ, He YY, Hao JJ, Zhang HY, Luo DM, Song JK, Yan Y, Xie XM, Du GH, Pang XB. Luteolin alleviates cognitive impairment in Alzheimer's disease mouse model via inhibiting endoplasmic reticulum stress-dependent neuroinflammation. Acta Pharmacol Sin. 2022 Apr;43(4):840-849. doi: 10.1038/s41401-021-00702-8.

Kovacs, GG. Concepts and classification of neurodegenerative diseases. Handb Clin Neurol. 2017;145:301-307. doi: 10.1016/B978-0-12-802395-2.00021-3.

Kwon, H. S., & Koh, S.-H. (2020). Neuroinflammation in neurodegenerative disorders: the roles of microglia and astrocytes. Transl Neurodegener, 9(1), 42. doi:10.1186/s40035-020-00221-2

Laurent, C., Buée, L. and Blum, D. (2018). Tau and neuroinflammation: What impact for Alzheimer's Disease and Tauopathies? Biomedi J 41(1), 21-33. doi: 10.1016/j.bj.2018.01.003.

Leroi, I., Collins, D. and Marsh, L. (2006). Non-dopaminergic treatment of cognitive impairment and dementia in Parkinson's disease: a review. J Neurol Sci 248(1-2), 104-114. doi: 10.1016/j.jns.2006.05.021.

Li, X, Wu L, Liu W, Jin Y, Chen Q, et al. (2014) A Network Pharmacology Study of Chinese Medicine QiShenYiQi to Reveal Its Underlying Multi-Compound, Multi-Target, Multi-Pathway Mode of Action. PLOS ONE 9(5): e95004. doi: 10.1371/journal.pone.0095004

Li, M., Shao, H., Zhang, X., & Qin, B. (2016). Hesperidin Alleviates Lipopolysaccharide-Induced Neuroinflammation in Mice by Promoting the miRNA-132 Pathway. Inflammation, 39(5), 1681-1689. doi:10.1007/s10753-016-0402-7

Li, Q., & Barres, B. A. (2018). Microglia and macrophages in brain homeostasis and disease. Nat Rev Immunol, 18(4), 225-242. doi:10.1038/nri.2017.125

Li, X., Wang, T., Zhang, D., Li, H., Shen, H., Ding, X., et al. (2018). Andrographolide ameliorates intracerebral hemorrhage induced secondary brain injury by inhibiting neuroinflammation induction. Neuropharmacology 141, 305-315. doi: 10.1016/j.neuropharm.2018.09.015.

Li, Z., Wang, Q., Zhang, Z., Zhang, X., Wu, X., Li, L., . . . Yu, Y. (2022). A20, as a downstream factor of Nrf2, is involved in the anti-neuroinflammatory and antidepressant-like effects of luteolin. J Funct Foods, 99, 105305. doi: 10.1016/j.jff.2022.105305

Lian, F., Wu, L., Tian, J., Jin, M., Zhou, S., Zhao, M., . . . Tong, X. (2015). The effectiveness and safety of a danshen-containing Chinese herbal medicine for diabetic retinopathy: a randomized, double-blind, placebo-controlled multicenter clinical trial. J Ethnopharmacol, 164, 71-77. doi:10.1016/j.jep.2015.01.048

Liang, B, Gao L, Wang F, Li Z, Li Y, Tan S, Chen A, Shao J, Zhang Z, Sun L, Zhang F, Zheng S. The mechanism research on the anti-liver fibrosis of emodin based on network pharmacology. IUBMB Life. 2021 Sep;73(9):1166-1179. doi: 10.1002/iub.2523.

106

Liebner, S., Dijkhuizen, R. M., Reiss, Y., Plate, K. H., Agalliu, D. and Constantin, G. (2018). Functional morphology of the blood–brain barrier in health and disease. Acta Neuropathologica 135(3), 311-336. doi: 10.1007/s00401-018-1815-1.

Liu, J., Zhu, J., Xue, J., Qin, Z., Shen, F., Liu, J., et al. (2017). In silico-based screen synergistic drug combinations from herb medicines: a case using Cistanche tubulosa. Sci Rep 7(1), 16364. doi: 10.1038/s41598-017-16571-3.

Liu, P., Wang, Y., Sun, Y., & Peng, G. (2022). Neuroinflammation as a Potential Therapeutic Target in Alzheimer's Disease. Clin Interv Aging, 17, 665-674. doi:10.2147/cia.S357558

Liu, W., Huang, S., Li, Y., Zhang, K., & Zheng, X. (2019). Suppressive effect of glycyrrhizic acid against lipopolysaccharide-induced neuroinflammation and cognitive impairment in C57 mice via toll-like receptor 4 signaling pathway. Food Nutr Res, 63. doi:10.29219/fnr.v63.1516

Liu, W. Y., Wang, Z. B., Wang, Y., Tong, L. C., Li, Y., Wei, X., et al. (2015). Increasing the Permeability of the Blood-brain Barrier in Three Different Models in vivo. CNS Neurosci Ther 21(7), 568-574. doi: 10.1111/cns.12405.

Liu, Y., Grimm, M., Dai, W.-T., Hou, M.-C., Xiao, Z.-X., & Cao, Y. (2020). CB-Dock: a web server for cavity detection-guided protein-ligand blind docking. Acta Pharmacol Sin, 41(1), 138-144. doi:10.1038/s41401-019-0228-6

Liu, Z.-J., Li, Z.-H., Liu, L., Tang, W.-X., Wang, Y., Dong, M.-R., & Xiao, C. (2016). Curcumin Attenuates Beta-Amyloid-Induced Neuroinflammation via Activation of Peroxisome Proliferator-Activated Receptor-Gamma Function in a Rat Model of Alzheimer's Disease. Front Pharmacol, 7. doi:10.3389/fphar.2016.00261

Liy, P. M., Puzi, N. N. A., Jose, S. and Vidyadaran, S. (2021). Nitric oxide modulation in neuroinflammation and the role of mesenchymal stem cells. Exp Biol Med (Maywood) 246(22), 2399-2406. doi: 10.1177/1535370221997052.

Maccioni, R. B., González, A., Andrade, V., Cortés, N., Tapia, J. P. and Guzmán-Martínez, L. (2018). Alzheimer´s Disease in the Perspective of Neuroimmunology. Open Neurol J 12, 50-56. doi: 10.2174/1874205x01812010050.

Maccioni, R. B., Rojo, L. E., Fernández, J. A. and Kuljis, R. O. (2009). The Role of Neuroimmunomodulation in Alzheimer's Disease. A N Y Acade Sci 1153(1), 240-246. doi: 10.1111/j.1749-6632.2008.03972.x.

Madkour, M.M., H.S. Anbar, and M.I. El-Gamal, Current status and future prospects of p38α/MAPK14 kinase and its inhibitors. Eur J Med Chem, 2021. 213: p. 113216-113216. doi: 10.1016/j.ejmech.2021.113216

Małkiewicz, M. A., Szarmach, A., Sabisz, A., Cubała, W. J., Szurowska, E. and Winklewski, P. J. (2019). Blood-brain barrier permeability and physical exercise. J Neuroinflammation 16(1), 15. doi: 10.1186/s12974-019-1403-x.

Mattila, J.T. and A.C. Thomas, Nitric oxide synthase: non-canonical expression patterns. Front Immunol, 2014. 5: p. 478. doi: 10.3389/fimmu.2014.00478

Mayhan, W. G. (2002). Cellular mechanisms by which tumor necrosis factor-alpha produces disruption of the blood-brain barrier. Brain Res 927(2), 144-152. doi: 10.1016/s0006-8993(01)03348-0.

McNutt, A. T., Francoeur, P., Aggarwal, R., Masuda, T., Meli, R., Ragoza, M., . . . Koes, D. R. (2021). GNINA 1.0: molecular docking with deep learning. J Cheminformatics, 13(1), 43. doi:10.1186/s13321-021-00522-2

Meng, X. Y., Zhang, H. X., Mezei, M., & Cui, M. (2011). Molecular docking: a powerful approach for structure-based drug discovery. Curr Comput Aided Drug Des, 7(2), 146-157. doi:10.2174/157340911795677602

Milatovic, D., Zaja-Milatovic, S., Breyer, R. M., Aschner, M., & Montine, T. J. (2017). Neuroinflammation and oxidative injury in developmental neurotoxicity. In Reprod Dev Toxicol (pp. 1051-1061). Elsevier. https://doi.org/10.1016/B978-0-12-804239-7.00055-X

Mohd Sairazi, N. S. and Sirajudeen, K. N. S. (2020). Natural Products and Their Bioactive Compounds: Neuroprotective Potentials against Neurodegenerative Diseases. Evid Based Complement Alternat Med 2020, 6565396. doi: 10.1155/2020/6565396.

Montagne, A., Zhao, Z. and Zlokovic, B. V. (2017). Alzheimer's disease: A matter of blood-brain barrier dysfunction? J Exp Med 214(11), 3151-3169. doi: 10.1084/jem.20171406.

Moon, M., Kim, H. G., Choi, J. G., Oh, H., Lee, P. K. J., Ha, S. K., . . . Oh, M. S. (2014). 6-Shogaol, an active constituent of ginger, attenuates neuroinflammation and cognitive deficits in animal models of dementia. Biochem Biophys Res Commun, 449(1), 8-13. doi: 10.1016/j.bbrc.2014.04.121

Morales, I., Guzmán-Martínez, L., Cerda-Troncoso, C., Farías, G. A. and Maccioni, R. B. (2014). Neuroinflammation in the pathogenesis of Alzheimer's disease. A rational framework for the search of novel therapeutic approaches. Front cell neurosci 8, 112. doi: 10.3389/fncel.2014.00112

Morris, G., Fernandes, B. S., Puri, B. K., Walker, A. J., Carvalho, A. F. and Berk, M. (2018). Leaky brain in neurological and psychiatric disorders: Drivers and consequences. Aust N Z J Psychiatry 52(10), 924-948. doi: 10.1177/0004867418796955.

Munoz, L., & Ammit, A. J. (2010). Targeting p38 MAPK pathway for the treatment of Alzheimer's disease. Neuropharmacology, 58(3), 561-568. doi:10.1016/j.neuropharm.2009.11.010

Ojha, S., Javed, H., Azimullah, S., Abul Khair, S. B., & Haque, M. E. (2016). Glycyrrhizic acid Attenuates Neuroinflammation and Oxidative Stress in Rotenone Model of Parkinson's Disease. Neurotox Res, 29(2), 275-287. doi:10.1007/s12640-015-9579-z

Pan, M.-H., Hsieh, M.-C., Hsu, P.-C., Ho, S.-Y., Lai, C.-S., Wu, H., . . . Ho, C.-T. (2008). 6-Shogaol suppressed lipopolysaccharide-induced up-expression of iNOS and COX-2 in murine macrophages. Mol Nutr Food Res, 52(12), 1467-1477. doi: 10.1002/mnfr.200700515

Park, G., Kim, H. G., Ju, M. S., Ha, S. K., Park, Y., Kim, S. Y., et al. (2013). 6-Shogaol, an active compound of ginger, protects dopaminergic neurons in Parkinson's disease models via anti-neuroinflammation. Acta Pharmacologica Sinica 34(9), 1131-1139. doi: 10.1038/aps.2013.57.

Park, J., Wetzel, I., Marriott, I., Dréau, D., D'Avanzo, C., Kim, D. Y., et al. (2018). A 3D human triculture system modeling neurodegeneration and neuroinflammation in Alzheimer's disease. Nat Neurosci 21(7), 941-951. doi: 10.1038/s41593-018-0175-4.

Patel, J. P. and Frey, B. N. (2015). Disruption in the Blood-Brain Barrier: The Missing Link between Brain and Body Inflammation in Bipolar Disorder? Neural Plast 2015, 708306. doi: 10.1155/2015/708306

Patel, R., Kaur, K. and Singh, S. (2021). Protective effect of andrographolide against STZ induced Alzheimer's disease in experimental rats: possible neuromodulation and Aβ((1-42)) analysis. Inflammopharmacology 29(4), 1157-1168. doi: 10.1007/s10787-021-00843-6.

Pautz, A., Art, J., Hahn, S., Nowag, S., Voss, C., & Kleinert, H. (2010). Regulation of the expression of inducible nitric oxide synthase. Nitric Oxide, 23(2), 75-93. doi: 10.1016/j.niox.2010.04.007

Pippi, B, Lana AJ, Moraes RC, Güez CM, Machado M, de Oliveira LF, Lino von Poser G, Fuentefria AM. In vitro evaluation of the acquisition of resistance, antifungal activity and synergism of Brazilian red propolis with antifungal drugs on Candida spp. J Appl Microbiol. 2015 Apr;118(4):839-50. doi: 10.1111/jam.12746.

Pluimer, B. R., Colt, M. and Zhao, Z. (2020). G Protein-Coupled Receptors in the Mammalian Blood-Brain Barrier. Front Cell Neurosci 14. doi: 10.3389/fncel.2020.00139

Pohl, F. and P. Kong Thoo Lin, The Potential Use of Plant Natural Products and Plant Extracts with Antioxidant Properties for the Prevention/Treatment of Neurodegenerative Diseases: In Vitro, In Vivo and Clinical Trials. Molecules (Basel, Switzerland), 2018. 23(12): p. 3283. doi: 10.3390/molecules23123283

Qu, WS, Tian DS, Guo ZB, Fang J, Zhang Q, Yu ZY, Xie MJ, Zhang HQ, Lü JG, Wang W. Inhibition of EGFR/MAPK signaling reduces microglial inflammatory response and the associated secondary damage in rats after spinal cord injury. J Neuroinflammation. 2012 Jul 23;9:178. doi: 10.1186/1742-2094-9-178.

Raza, S. S., Khan, M. M., Ahmad, A., Ashafaq, M., Khuwaja, G., Tabassum, R., . . . Islam, F. (2011). Hesperidin ameliorates functional and histological outcome and reduces neuroinflammation in experimental stroke. Brain Res, 1420, 93-105. doi: 10.1016/j.brainres.2011.08.047

Ren, D., Fu, Y., Wang, L., Liu, J., Zhong, X., Yuan, J., . . . Li, Z. (2021). Tetrandrine ameliorated Alzheimer's disease through suppressing microglial inflammatory activation and neurotoxicity in the 5XFAD mouse. Phytomedicine, 90, 153627. doi: 10.1016/j.phymed.2021.153627

Ronaldson, P. T. and Davis, T. P. (2012). Blood-brain barrier integrity and glial support: mechanisms that can be targeted for novel therapeutic approaches in stroke. Curr Pharm Des 18(25), 3624-3644. doi: 10.2174/138161212802002625.

Roy, E. R., Wang, B., Wan, Y. W., Chiu, G., Cole, A., Yin, Z., et al. (2020). Type I interferon response drives neuroinflammation and synapse loss in Alzheimer disease. J Clin Invest 130(4), 1912-1930. doi: 10.1172/jci133737.

Rui, W., Li, S., Xiao, H., Xiao, M., & Shi, J. (2020). Baicalein Attenuates Neuroinflammation by Inhibiting NLRP3/Caspase-1/GSDMD Pathway in MPTP-Induced Mice Model of Parkinson's Disease. Int J Neuropsychopharmacol, 23(11), 762-773. doi:10.1093/ijnp/pyaa060

Sakle, N. S., More, S. A., & Mokale, S. N. (2020). A network pharmacology-based approach to explore potential targets of Caesalpinia pulcherima: an updated prototype in drug discovery. Sci Rep, 10(1), 17217. doi:10.1038/s41598-020-74251-1

Salmina, A. B., Kharitonova, E. V., Gorina, Y. V., Teplyashina, E. A., Malinovskaya, N. A., Khilazheva, E. D., et al. (2021). Blood-Brain Barrier and Neurovascular Unit In Vitro Models for Studying Mitochondria-Driven Molecular Mechanisms of Neurodegeneration. Int J Mol Sci 22(9). doi: 10.3390/ijms22094661.

Satoh, T, Nakatsuka D, Watanabe Y, Nagata I, Kikuchi H, Namura S. Neuroprotection by MAPK/ERK kinase inhibition with U0126 against oxidative stress in a mouse neuronal cell line and rat primary cultured cortical neurons. Neurosci Lett. 2000 Jul 14;288(2):163-6. doi: 10.1016/s0304-3940(00)01229-5.

Schain, M., & Kreisl, W. C. (2017). Neuroinflammation in Neurodegenerative Disorders—a Review. Curr Neurol Neurosci Rep, 17(3), 25. doi:10.1007/s11910-017-0733-2

Schnöder, L., Hao, W., Qin, Y., Liu, S., Tomic, I., Liu, X., . . . Liu, Y. (2016). Deficiency of Neuronal p38α MAPK Attenuates Amyloid Pathology in Alzheimer Disease Mouse and Cell Models through Facilitating Lysosomal Degradation of BACE1*. J Biol Chem, 291(5), 2067-2079. doi: 10.1074/jbc.M115.695916

Schober, J., Polina, J., Walters, F., Scott, N., Lodholz, E., Crider, A., et al. (2021). NNC 26-9100 increases Aβ1-42 phagocytosis, inhibits nitric oxide production and decreases calcium in BV2 microglia cells. PLoS One 16(7), e0254242. doi: 10.1371/journal.pone.0254242.

Schulz, R., Rassaf, T., Massion, P., Kelm, M., & Balligand, J.-L. (2005). Recent advances in the understanding of the role of nitric oxide in cardiovascular homeostasis. Pharmacol Ther, 108(3), 225-256. doi: 10.1016/j.pharmthera.2005.04.005

Serrano, F. G., Tapia-Rojas, C., Carvajal, F. J., Hancke, J., Cerpa, W. and Inestrosa, N. C. (2014). Andrographolide reduces cognitive impairment in young and mature AβPPswe/PS-1 mice. Mol Neurodegener 9(1), 61. doi: 10.1186/1750-1326-9-61.

Sharif, O., Bolshakov, V. N., Raines, S., Newham, P., & Perkins, N. D. (2007). Transcriptional profiling of the LPS induced NF-κB response in macrophages. BMC Immunol, 8(1), 1. doi:10.1186/1471-2172-8

Shengkai, D. and Yazhen, S. (2022). Flavonoids from Stems and Leaves of Scutellaria baicalensis Georgi Regulate the Brain Tau Hyperphosphorylation at Multiple Sites Induced by Composited Aβ in Rats. CNS Neurol Disord Drug Targets 21(4), 367-374. doi: 10.2174/1871527320666210827112609.

Shi, Y., Chen, M., Zhao, Z., Pan, J., & Huang, S. (2021). Network Pharmacology and Molecular Docking Analyses of Mechanisms Underlying Effects of the Cyperi Rhizoma Chuanxiong Rhizoma Herb Pair on Depression. Evid Based Complement Alternat Med, 2021. doi: 10.1155/2021/5704578

Singh, S. S., Rai, S. N., Birla, H., Zahra, W., Rathore, A. S. and Singh, S. P. (2020). NF-κB-Mediated Neuroinflammation in Parkinson's Disease and Potential Therapeutic Effect of Polyphenols. Neurotox Res 37(3), 491-507. doi: 10.1007/s12640-019-00147-2.

Shyr, Z. A., Cheng, Y.-S., Lo, D. C., & Zheng, W. (2021). Drug combination therapy for emerging viral diseases. Drug Discovery Today, 26(10), 2367-2376. doi: 10.1016/j.drudis.2021.05.008

Sonawane, S. K., Uversky, V. N. and Chinnathambi, S. (2021). Baicalein inhibits heparin-induced Tau aggregation by initializing non-toxic Tau oligomer formation. Cell Commun Signal 19(1), 16. doi: 10.1186/s12964-021-00704-3.

Song, J.-H., Lee, J.-W., Shim, B., Lee, C.-Y., Choi, S., Kang, C., . . . Shin, J.-W. (2013). Glycyrrhizin Alleviates Neuroinflammation and Memory Deficit Induced by Systemic Lipopolysaccharide Treatment in Mice. Molecules, 18(12), 15788-15803. doi: 1420-3049/18/12/15788

Song, L., Pei, L., Yao, S., Wu, Y. and Shang, Y. (2017). NLRP3 Inflammasome in Neurological Diseases, from Functions to Therapies. Front Cell Neurosci 11. doi: 10.3389/fncel.2017.00063.

Sorrenti, V., Contarini, G., Sut, S., Dall'Acqua, S., Confortin, F., Pagetta, A., . . . Zusso, M. (2018). Curcumin Prevents Acute Neuroinflammation and Long-Term Memory Impairment Induced by Systemic Lipopolysaccharide in Mice. Front Pharmacol, 9. doi:10.3389/fphar.2018.00183

Souza, L. C., Andrade, M. K., Azevedo, E. M., Ramos, D. C., Bail, E. L., & Vital, M. A. B. F. (2022). Andrographolide Attenuates Short-Term Spatial and Recognition Memory Impairment and Neuroinflammation Induced by a Streptozotocin Rat Model of Alzheimer's Disease. Neurotox Res, 40(5), 1440-1454. doi:10.1007/s12640-022-00569-5

Stanzione F, Giangreco I, Cole JC. Use of molecular docking computational tools in drug discovery. Prog Med Chem. 2021;60:273-343. doi: 10.1016/bs.pmch.2021.01.004

Sun, H., Guo, Z., Li, L., Yan, X., Wu, N., & Yan, K. (2018). The Pharmacological and Clinical Evidences of a Multi-herbal Drug Product - Dantonic (T89) Indicated for the Prevention and Treatment of Chronic Stable Angina - for FDA Registration. 日本薬理学会年会要旨集, WCP2018, SY41-42. doi:10.1254/jpssuppl.WCP2018.0_SY41-2

Sun, R., Xu, G., Gao, D., Ding, Q., & Shi, Y. (2021). To Predict Anti-Inflammatory and Immunomodulatory Targets of Guizhi Decoction in Treating Asthma Based on Network Pharmacology, Molecular Docking, and Experimental Validation. Evid Based Complement Alternat Med, 2021, 9033842-9033817. doi:10.1155/2021/9033842

Sun, X., Zeng, H., Wang, Q., Yu, Q., Wu, J., Feng, Y., . . . Zhang, H. (2018). Glycyrrhizin ameliorates inflammatory pain by inhibiting microglial activation-mediated inflammatory response via blockage of the HMGB1-TLR4-NF-kB pathway. Exp Cell Res, 369(1), 112-119. doi: 10.1016/j.yexcr.2018.05.012

Sun, Y., & Yang, J. (2019). A bioinformatics investigation into the pharmacological mechanisms of the effect of Fufang Danshen on pain based on methodologies of network pharmacology. Sci Rep, 9(1), 5913-5913. doi:10.1038/s41598-019-40694-4

Sun, Y., Zhao, R., Liu, R., Li, T., Ni, S., Wu, H., . . . Sun, Y. (2021). Integrated Screening of Effective Anti-Insomnia Fractions of Zhi-Zi-Hou-Po Decoction via Drosophila melanogaster and Network Pharmacology Analysis of the Underlying Pharmacodynamic Material and Mechanism. ACS omega, 6(13), 9176-9187. doi:10.1021/acsomega.1c00445

Suzuki, M., Nikaido, T. and Ohmoto, T. (1991). The Study of Chinese Herbal Medicinal Prescription with Enzyme Inhibitory Activity. V. The Study of Hange-shashin-to, Kanzo-shashin-to, Shokyo-shashin-to with Adenosine 3', 5'-Cyclic Monophosphate Phosphodiesterase. Yakugaku zasshi 111(11), 695-701. doi: 10.1248/yakushi1947.111.11_695.

Takata, F., Nakagawa, S., Matsumoto, J. and Dohgu, S. (2021). Blood-Brain Barrier Dysfunction Amplifies the Development of Neuroinflammation: Understanding of Cellular Events in Brain Microvascular Endothelial Cells for Prevention and Treatment of BBB Dysfunction. Front cell neurosci 15. doi: 10.3389/fncel.2021.661838.

Takeshita, Y., Fujikawa, S., Serizawa, K., Fujisawa, M., Matsuo, K., Nemoto, J., et al. (2021). New BBB Model Reveals That IL-6 Blockade Suppressed the BBB Disorder, Preventing Onset of NMOSD. Neurol-Neuroimmunol 8(6), e1076. doi: 10.1212/nxi.0000000000001076.

Tao, L., Zhang, L., Gao, R., Jiang, F., Cao, J., & Liu, H. (2018). Andrographolide Alleviates Acute Brain Injury in a Rat Model of Traumatic Brain Injury: Possible Involvement of Inflammatory Signaling. Front Neurosci, 12. doi:10.3389/fnins.2018.00657

Tanaka, T., Narazaki, M. and Kishimoto, T. (2014). IL-6 in inflammation, immunity, and disease. Cold Spring Harb Perspect Biol 6(10), a016295. doi: 10.1101/cshperspect.a016295

Tegenge, M. A., Rajbhandari, L., Shrestha, S., Mithal, A., Hosmane, S., & Venkatesan, A. (2014). Curcumin protects axons from degeneration in the setting of local neuroinflammation. Exp. neurol, 253, 102-110. doi: 10.1016/j.expneurol.2013.12.016

Tiwari, V., & Chopra, K. (2012). Attenuation of oxidative stress, neuroinflammation, and apoptosis by curcumin prevents cognitive deficits in rats postnatally exposed to ethanol. Psychopharmacology, 224(4), 519-535. doi:10.1007/s00213-012-2779-9

Tiwari, V., & Chopra, K. (2013). Protective effect of curcumin against chronic alcohol-induced cognitive deficits and neuroinflammation in the adult rat brain. Neurosci, 244, 147-158. doi: 10.1016/j.neuroscience.2013.03.042

Thiel, V. E. and Audus, K. L. (2001). Nitric oxide and blood-brain barrier integrity. Antioxid Redox Signal 3(2), 273-278. doi: 10.1089/152308601300185223.

Tsikas, D. (2007). Analysis of nitrite and nitrate in biological fluids by assays based on the Griess reaction: Appraisal of the Griess reaction in the l-arginine/nitric oxide area of research. J Chromatogr B 851(1), 51-70. doi: 10.1016/j.jchromb.2006.07.054.

Upadhayay, S. and Mehan, S. (2021). Targeting Nrf2/HO-1 anti-oxidant signaling pathway in the progression of multiple sclerosis and influences on neurological dysfunctions. Brain Disorders 3, 100019. doi: 10.1016/j.dscb.2021.100019.

Van Bulck, M., Sierra-Magro, A., Alarcon-Gil, J., Perez-Castillo, A. and Morales-Garcia, J. A. (2019). Novel Approaches for the Treatment of Alzheimer's and Parkinson's Disease. Int J Mol Sci 20(3). doi: 10.3390/ijms20030719.

Wang, D. P., Kang, K., Sun, J., Lin, Q., Lv, Q. L. and Hai, J. (2022). URB597 and Andrographolide Improve Brain Microvascular Endothelial Cell Permeability and Apoptosis by Reducing Oxidative Stress and Inflammation Associated with Activation of Nrf2 Signaling in Oxygen-Glucose Deprivation. Oxid Med Cell Longev 2022, 4139330. doi: 10.1155/2022/4139330.

Wimett, Lynn RN, ANP, EdD; Laustsen, Gary RN, PhDc, CFNP. Caduet Treats Two Cardiovascular Conditions at Once. Nurse Pract 29(6):p 56-57, June 2004.

Wolfe, M. S. (2012). The role of tau in neurodegenerative diseases and its potential as a therapeutic target. Scientifica (Cairo) 2012, 796024. doi: 10.6064/2012/796024.

World Health Organization (2022). Dementia [Online]. Available: https://www.who.int/news-room/fact-sheets/detail/dementia [Accessed].

Wyss-Coray, T. and Mucke, L. (2002). Inflammation in neurodegenerative disease—a double-edged sword. Neuron 35(3), 419-432. doi: 10.1016/S0896-6273(02)00794-8

Xiao, L., Ding, M., Fernandez, A., Zhao, P., Jin, L., & Li, X. (2017). Curcumin alleviates lumbar radiculopathy by reducing neuroinflammation, oxidative stress and nociceptive factors. Eur Cell Mater, 33, 279-293. doi:10.22203/eCM.v033a21

Xin, W., Jing, M., Yang, J., Wang, M., Hou, G., Wang, Q., . . . Wang, C. (2021). Baicalein Exerts Anti-Neuroinflammatory Effects by Inhibiting the TLR4-ROS /NF-κB-NLRP3 Inflammasome. Nat Prod Commun, 16(4), 1934578X211011385. doi:10.1177/1934578X211011385

Xing, B., Bachstetter, A. D., & Van Eldik, L. J. (2011). Microglial p38α MAPK is critical for LPS-induced neuron degeneration, through a mechanism involving TNFα. Mol Neurodegener, 6, 84. doi:10.1186/1750-1326-6-84

Yan, J. J., Du, G. H., Qin, X. M., & Gao, L. (2020). Baicalein attenuates the neuroinflammation in LPS-activated BV-2 microglial cells through suppression of pro-inflammatory cytokines, COX2/NF-κB

expressions and regulation of metabolic abnormality. Int Immunopharmacol, 79, 106092. doi:10.1016/j.intimp.2019.106092

Yang, R., Chang, L., Guo, B. Y., Wang, Y. W., Wang, Y. L., Jin, X., . . . Li, Y. J. (2014). Compound danshen dripping pill pretreatment to prevent contrast-induced nephropathy in patients with acute coronary syndrome undergoing percutaneous coronary intervention. Evid Based Complement Alternat Med, 2014, 256268. doi:10.1155/2014/256268

Yang, R., Liu, S., Zhou, J., Bu, S., & Zhang, J. (2017). Andrographolide attenuates microglia-mediated Aβ neurotoxicity partially through inhibiting NF-κB and JNK MAPK signaling pathway. Immunopharmacol Immunotoxicol, 39(5), 276-284. doi:10.1080/08923973.2017.1344989

Yang, S., Wang, H., Yang, Y., Wang, R., Wang, Y., Wu, C., et al. (2019). Baicalein administered in the subacute phase ameliorates ischemia-reperfusion-induced brain injury by reducing neuroinflammation and neuronal damage. Biomed Pharmacother 117, 109102. doi: 10.1016/j.biopha.2019.109102.

Yang, S., Yang, Y., Chen, C., Wang, H., Ai, Q., Lin, M., et al. (2021). The Anti-Neuroinflammatory Effect of Fuzi and Ganjiang Extraction on LPS-Induced BV2 Microglia and Its Intervention Function on Depression-Like Behavior of Cancer-Related Fatigue Model Mice. Front Pharmacol 12, 670586. doi: 10.3389/fphar.2021.670586.

Yang, Y., Tan, X., Xu, J., Wang, T., Liang, T., Xu, X., . . . Chen, G. (2020). Luteolin alleviates neuroinflammation via downregulating the TLR4/TRAF6/NF-κB pathway after intracerebral hemorrhage. Biomed Pharmacother, 126, 110044. doi: 10.1016/j.biopha.2020.110044

Yang, Z., Zhao, T., Zou, Y., Zhang, J. H., & Feng, H. (2014). Curcumin inhibits microglia inflammation and confers neuroprotection in intracerebral hemorrhage. Immunol. Lett., 160(1), 89-95. doi:10.1016/j.imlet.2014.03.005

Yao, Z.-H., Yao, X.-l., Zhang, Y., Zhang, S.-f., & Hu, J.-c. (2018). Luteolin Could Improve Cognitive Dysfunction by Inhibiting Neuroinflammation. Neurochem. Res., 43(4), 806-820. doi:10.1007/s11064-018-2482-2

Yoon, W. J., Lee, N. H. and Hyun, C. G. (2010). Limonene suppresses lipopolysaccharide-induced production of nitric oxide, prostaglandin E2, and pro-inflammatory cytokines in RAW 264.7 macrophages. J Oleo Sci 59(8), 415-421. doi: 10.5650/jos.59.415.

Yıldız, M. O., Çelik, H., Caglayan, C., Kandemir, F. M., Gür, C., Bayav, İ., . . . Kandemir, Ö. (2022). Neuromodulatory effects of hesperidin against sodium fluoride-induced neurotoxicity in rats: Involvement of neuroinflammation, endoplasmic reticulum stress, apoptosis and autophagy. Neurotoxicology, 90, 197-204. doi: 10.1016/j.neuro.2022.04.002

Yu, R.-J., Liu, H.-B., Yu, Y., Liang, L., Xu, R., Liang, C., . . . Yao, X.-S. (2016). Anticancer activities of proanthocyanidins from the plant Urceola huaitingii and their synergistic effects in combination with chemotherapeutics. Fitoterapia, 112, 175-182. doi:10.1016/j.fitote.2016.05.015

Yu, X., Ji, C. and Shao, A. (2020). Neurovascular Unit Dysfunction and Neurodegenerative Disorders. Front in Neurosci 14. doi: 10.3389/fnins.2020.00334.

Zarekiani, P., Nogueira Pinto, H., Hol, E. M., Bugiani, M. and de Vries, H. E. (2022). The neurovascular unit in leukodystrophies: towards solving the puzzle. Fluids Barriers CNS 19(1), 18. doi: 10.1186/s12987-022-00316-0.

Zhao, H., Wang, S.-L., Qian, L., Jin, J.-L., Li, H., Xu, Y., & Zhu, X.-L. (2013). Diammonium Glycyrrhizinate Attenuates Aβ1–42-Induced Neuroinflammation and Regulates MAPK and NF-κB Pathways In Vitro and In Vivo. CNS Neurosci Ther, 19(2), 117-124. doi:10.1111/cns.12043

Zhao, X., Kong, D., Zhou, Q., Wei, G., Song, J., Liang, Y., & Du, G. (2021). Baicalein alleviates depression-like behavior in rotenone- induced Parkinson's disease model in mice through activating the BDNF/TrkB/CREB pathway. Biomed. Pharmacother, 140, 111556. doi: 10.1016/j.biopha.2021.111556

Zhang, C., et al., A Network Pharmacology Approach to Investigate the Active Compounds and Mechanisms of Musk for Ischemic Stroke. Evid Based Complement Alternat Med, 2020. doi: 10.1155/2020/4063180

Zhang, H. and Sun, S.-C. (2015). NF-κB in inflammation and renal diseases. Cell Biosci 5(1), 63. doi: 10.1186/s13578-015-0056-4.

Zhang, J., Zheng, Y., Zhao, Y., Zhang, Y., Liu, Y., Ma, F., et al. (2021). Andrographolide ameliorates neuroinflammation in APP/PS1 transgenic mice. Int Immunopharmacol 96, 107808. doi: 10.1016/j.intimp.2021.107808.

Zhang, J., Zheng, Y., Luo, Y., Du, Y., Zhang, X., & Fu, J. (2019). Curcumin inhibits LPS-induced neuroinflammation by promoting microglial M2 polarization via TREM2/ TLR4/ NF-κB pathways in BV2 cells. Mol. Immunol., 116, 29-37. doi: 10.1016/j.molimm.2019.09.020

Zhang, R., Zhu, X., Bai, H., & Ning, K. (2019). Network Pharmacology Databases for Traditional Chinese Medicine: Review and Assessment. Front. Pharmacol, 10. doi:10.3389/fphar.2019.00123

Zhang, X., Yang, Y., Du, L., Zhang, W. and Du, G. (2017). Baicalein exerts anti-neuroinflammatory effects to protect against rotenone-induced brain injury in rats. Int Immunopharmacol 50, 38-47. doi: 10.1016/j.intimp.2017.06.007.

Zhang, X, Qin Y, Ruan W, Wan X, Lv C, He L, Lu L, Guo X. Targeting inflammation-associated AMPK//Mfn-2/MAPKs signaling pathways by baicalein exerts anti-atherosclerotic action. Phytother Res. 2021 Aug;35(8):4442-4455. doi: 10.1002/ptr.7149.

Zheng, Y. F., Zhou, X., Chang, D., Bhuyan, D. J., Zhang, J. P., Yu, W. Z., et al. (2021). A novel tri-culture model for neuroinflammation. J Neurochem 156(2), 249-261. doi: 10.1111/jnc.15171.

Zhou, W., Hu, M., Hu, J., Du, Z., Su, Q., & Xiang, Z. (2021). Luteolin Suppresses Microglia Neuroinflammatory Responses and Relieves Inflammation-Induced Cognitive Impairments. Neurotox. Res., 39(6), 1800-1811. doi:10.1007/s12640-021-00426-x

Zhou, X., Münch, G., Wohlmuth, H., Afzal, S., Kao, M.-H., Al-Khazaleh, A., . . . Li, C. G. (2022). Synergistic Inhibition of Pro-Inflammatory Pathways by Ginger and Turmeric Extracts in RAW 264.7 Cells. Front. Pharmacol, 13. doi:10.3389/fphar.2022.818166

Zhou, X., Razmovski-Naumovski, V., Kam, A., Chang, D., Li, C. G., Chan, K., & Bensoussan, A. (2019). Synergistic study of a Danshen (Salvia Miltiorrhizae Radix et Rhizoma) and Sanqi (Notoginseng Radix et Rhizoma) combination on cell survival in EA.hy926 cells. BMC Complement Altern Med, 19(1), 50. doi:10.1186/s12906-019-2458-z

Zhou, X., Seto, S. W., Chang, D., Kiat, H., Razmovski-Naumovski, V., Chan, K., & Bensoussan, A. (2016). Synergistic Effects of Chinese Herbal Medicine: A Comprehensive Review of Methodology and Current Research. Front. Pharmacol, 7(201). doi:10.3389/fphar.2016.00201

Zhou, Y., Xu, J., Hou, Y. et al. Network medicine links SARS-CoV-2/COVID-19 infection to brain microvascular injury and neuroinflammation in dementia-like cognitive impairment. Alz Res Therapy **13**, 110 (2021). doi: 10.1186/s13195-021-00850-3

Zhu, H., Wang, Z., Xing, Y., Gao, Y., Ma, T., Lou, L., et al. (2012). Baicalin reduces the permeability of the blood-brain barrier during hypoxia in vitro by increasing the expression of tight junction proteins in brain microvascular endothelial cells. J Ethnopharmacol 141(2), 714-720. doi: 10.1016/j.jep.2011.08.063.

Zhu, K., Zhu, X., Liu, S., Yu, J., Wu, S., & Hei, M. (2022). Glycyrrhizin Attenuates Hypoxic-Ischemic Brain Damage by Inhibiting Ferroptosis and Neuroinflammation in Neonatal Rats via the HMGB1/GPX4 Pathway. Oxid. Med. Cell. Longev, 2022, 8438528. doi:10.1155/2022/8438528

Zhu, L.-H., Bi, W., Qi, R.-b., Wang, H.-d., & Lu, D.-x. (2011). Luteolin Inhibits Microglial Inflammation and Improves Neuron Survival Against Inflammation. Int. J. Neurosci, 121(6), 329-336. doi:10.3109/00207454.2011.569040

Zhu, L.-H., Bi, W., Qi, R.-B., Wang, H.-D., Wang, Z.-G., Zeng, Q., . . . Lu, D.-X. (2011). Luteolin reduces primary hippocampal neurons death induced by neuroinflammation. Neuro. Res., 33(9), 927-934. doi:10.1179/1743132811Y.0000000023

Zlokovic, B. V. (2005). Neurovascular mechanisms of Alzheimer's neurodegeneration. TINS 28(4), 202-208. doi: 10.1016/j.tins.2005.02.001.

Zotova, E., Bharambe, V., Cheaveau, M., Morgan, W., Holmes, C., Harris, S., . . . Boche, D. (2013). Inflammatory components in human Alzheimer's disease and after active amyloid-β42 immunization. Brain, 136(Pt 9), 2677-2696. doi:10.1093/brain/awt210

Appendix

Appendix 1. HPLC analysis of the isolated phytochemicals used in the study (Chengdu BioPurify Pty Co., China). (A) LU purity: 98.62%, retention time: 10.29 min. (B) BA purity: 98.63%, retention time: 11.91 min, (C) AN purity: 99.33%, retention time: 4.73 min, (D) SG purity: 98.70%, retention time: 4.00 min, (E) CU purity: 99.95%, retention time: 10.79 min, (F) HES purity: 99.20%, retention time: 7.78 min, (G) TE purity: 99.20%, retention time: 5.68 min, (H) GLY purity: 99.70%, retention time:7.62 min.

A
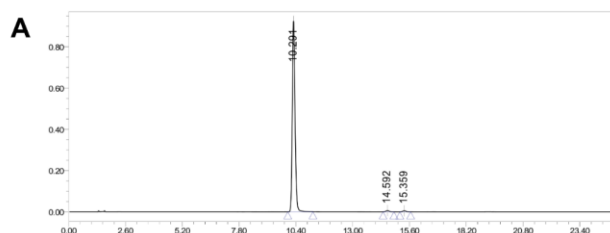
Peaks	Retention (min)	Peak area (mAU*s)	Peak height (µV)	Peak are (%)
1	10.291	8037396	98.62	924369
2	14.592	61611	0.76	6045
3	15.359	51237	0.63	4986

B
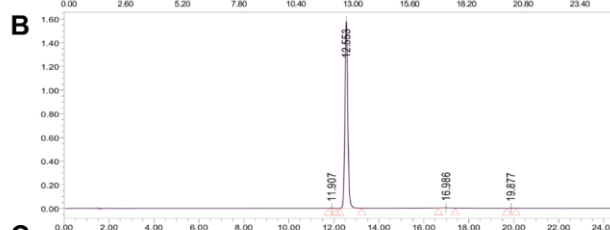
Peaks	Retention (min)	Peak area (mAU*s)	Peak height (µV)	Peak are (%)
1	11.907	15070		0.11
2	12.553	14016843		99.33
3	16.986	65681		0.47
4	19.877	14248		0.1

C
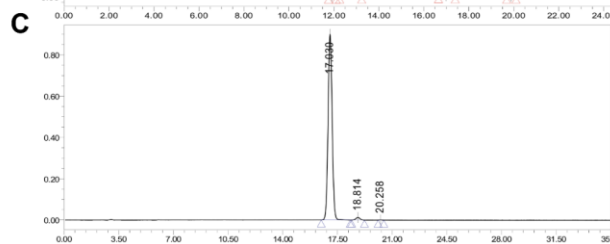
Peaks	Retention (min)	Peak area (mAU*s)	Peak height (µV)	Peak are (%)
1	4.732	9788	0.09	1624
2	5.898	22093	0.21	3453
3	12.981	13427	0.13	984
4	13.651	10351271	98.63	1052992
5	21.685	8895	0.08	620
6	22.593	15742	0.15	1076
7	24.334	73520	0.7	4204

D
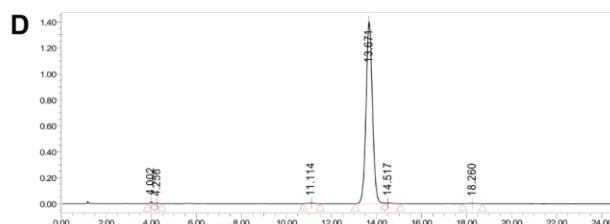
Peaks	Retention (min)	Peak area (mAU*s)	Peak height (µV)	Peak are (%)
1	4.002	84421	14096	0.3
2	4.256	25213	0.09	3935
3	11.114	96920	0.34	5031
4	13.671	27854508	98.7	1401299
5	14.517	108216	0.38	5293
6	18.26	52082	0.18	2143

E
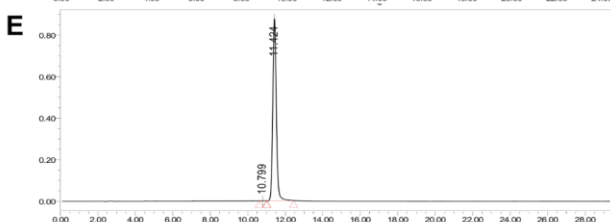
Peaks	Retention (min)	Peak area (mAU*s)	Peak height (µV)	Peak are (%)
1	10.799	5255	0.05	513
2	11.424	11500817	99.95	875514

F
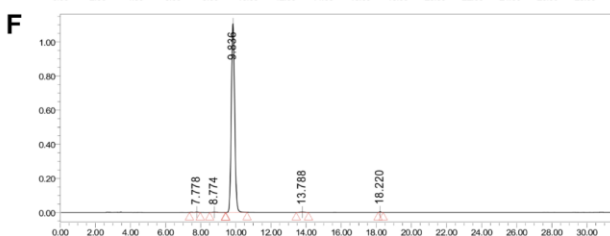
Peaks	Retention (min)	Peak area (mAU*s)	Peak height (µV)	Peak are (%)
1	7.778	28443	0.19	2175
2	8.774	30987	0.21	1737
3	9.836	14827095	99.2	1106757
4	13.788	39748	0.27	2262
5	18.22	21073	0.14	4390

G
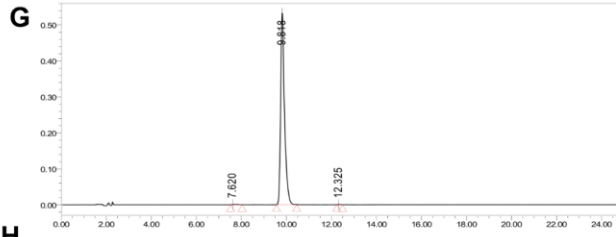
Peaks	Retention (min)	Peak area (mAU*s)	Peak height (μV)	Peak are (%)
1	5.681	22291	0.12	1827
2	5.952	72204	0.4	4104
3	6.46	41236	0.23	2813
4	8.359	3533	0.02	332
5	9.643	2684	0.01	403
6	10.159	17768865	99.21	708728

H
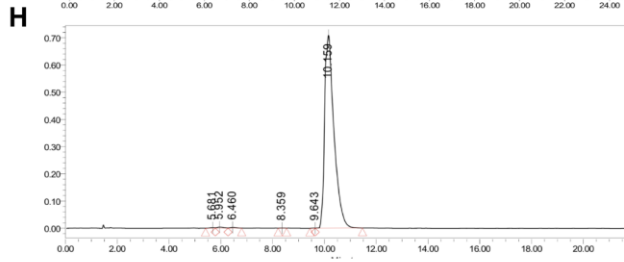
Peaks	Retention (min)	Peak area (mAU*s)	Peak height (μV)	Peak are (%)
1	7.62	12917	0.2	686
2	9.818	6376972	99.74	532828
3	12.325	3893	0.06	393

117

Appendix 2. GO enrichment analysis of BP, CC and MF for eight phytochemicals related to neuroinflammation.
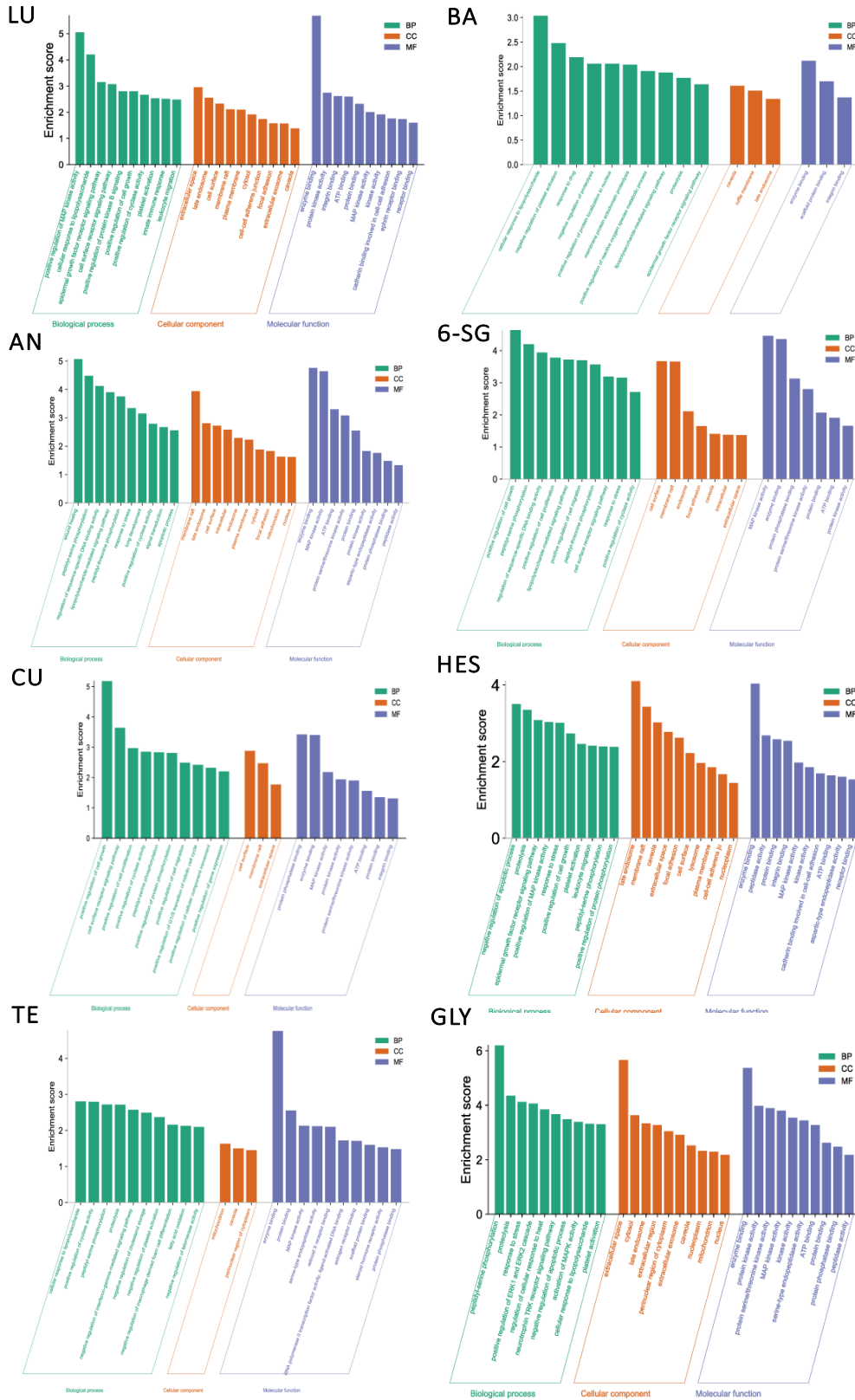
Appendix 3. KEGG pathway analysis of potential targets in eight phytochemicals. The size of the bubbles reflects the gene counts of the phytochemical from low to high, and the scale of 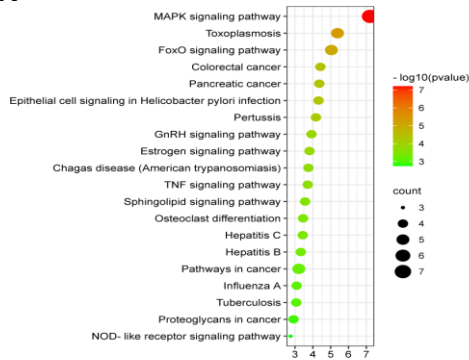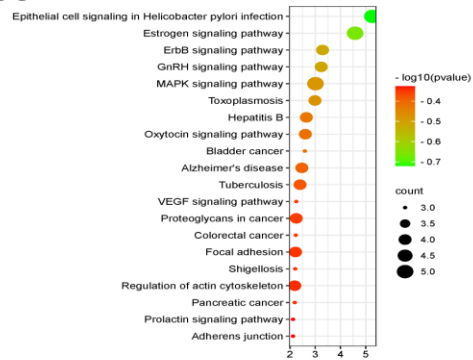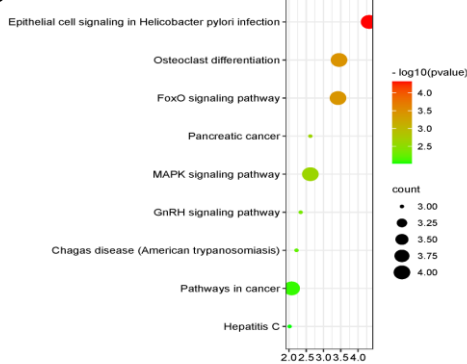colours refers to the *p* values from large to small.